

## ATTACHMENT I

The Excel spreadsheets and MCNP input and output files are provided on a compact disk and are listed in Table I.1. Each file is identified by its name, size (in bytes), and the date and time of last access. It should be noted that for files transferred from the HP workstation to the personal computer, the date and time reflect the time of transfer. The actual date and time of run completion can be found in the file.

Table I.1. File Attributes for the Contents of Attachment II

File Name	Description	File Size (bytes)	File Date	File Time
a-h.i	MCNP input file for the asymmetric configuration with hematite degradation product	46,938	09/24/2001	4:02 p.m.
a-h.io	MCNP output file for the asymmetric configuration with hematite degradation product	1,311,887	09/24/2001	4:02 p.m.
a-hd.i	MCNP input file for the asymmetric configuration with hematite and diaspore degradation products	46,896	09/24/2001	4:02 p.m.
a_hd.io	MCNP output file for the asymmetric configuration with hematite and diaspore degradation products	1,318,225	09/24/2001	4:02 p.m.
s-h.i	MCNP input file for the symmetric configuration with hematite degradation product	49,077	09/24/2001	9:56 a.m.
s-h.io	MCNP output file for the symmetric configuration with hematite degradation product	1,691,217	09/24/2001	9:56 a.m.
s_hd.i	MCNP input file for the symmetric configuration with hematite and diaspore degradation products	49,075	09/24/2001	4:02 p.m.
s_hd.io	MCNP output file for the symmetric configuration with hematite and diaspore degradation products	1,729,002	09/24/2001	4:02 p.m.
fuel_comp.xls	Spreadsheet to calculate fuel atom densities	19,456	09/26/2001	1:39 p.m.
deg_comp.xls	Spreadsheet to calculate degradation product number densities	22,016	09/26/2001	7:57 a.m.
21-PWR-EDAll-A-0914_cor.xls	Spreadsheets to calculate WP and fuel assembly geometry, composition, critical water height, number densities, and radiolytic specie production	286,208	09/27/2001	3:56 p.m.

## **ATTACHMENT II**

Attachment II is a CD-ROM containing the files listed in Attachment I.

### **ATTACHMENT III**

Attachment III contains the text of the white paper documenting the initial scoping calculation of the potential for radiolytic generation of nitric acid during a static criticality in a CSNF WP and estimation of the consequences of such production with respect to possible corrosion enhancement of Zircaloy cladding.

## Summary

Accelerated corrosion rates due to radiolytic chemical specie generation (primarily nitric acid) have been considered in the repository degradation models and, for the most part, eliminated from further consideration due to the low specie generation from radionuclide decay. However, the radiation dose from a criticality event may generate significantly greater quantities of nitric acid than from radionuclide decay that could result in a low pH within the WP. A low pH, coupled with an increase in fluoride concentration, could accelerate cladding corrosion rates.

A scoping calculation performed to estimate the range of possible quantities that could be generated from an internal waste package steady-state criticality resulted in 40-200 moles. This amount of nitric acid could result in low pH values ( $< 2$ ) in the WP. This estimate does not account for possible mitigating reactions, such as with the Hematite, that scavenge the nitric acid. Calculations with EQ6 are proposed to investigate the effects on the evolution of the chemical environment in the WP when nitric acid is added to the mixture.

## Scoping Calculation of Potential for Enhanced Corrosion in a 21 PWR Waste Package from Chemical Species Generated by Radiolysis Effects during a Criticality Event

January 19, 2001

### I. Introduction

The effects of radiation on the corrosion of various metals and alloys, particularly with respect to in-reactor processes, has been discussed by a number of authors (Shoesmith and King 1999, p. 1). Shoesmith and King (1999) additionally discuss the effects of radiation on proposed Monitored Geologic Repository (MGR) Waste Package (WP) materials. Radiation effects on the corrosion of metals and alloys include, among other things, radiolysis of the local gaseous and aqueous environment to produce oxidizing and reducing radicals. In particular, radiolysis processes in moist air environments lead to the fixation of nitrogen as NO, NO<sub>2</sub>, and especially HNO<sub>3</sub> (Reed and Van Konynenburg 1988, pp. 393-404). The nitric acid is produced in an irradiated air-water vapor system when the hydroxyl radicals generated from the water vapor convert nitrogen dioxides, which are formed by the radiolytic reaction between nitrogen and oxygen, to nitric acids.

Chemical species produced by radiolysis have been identified as a mechanism for accelerating corrosion of the MGR engineered barrier system (EBS), in the Disposal Criticality Analysis Methodology Topical Report (DCTR) (CRWMS M&O 2000a, p. 2-2). Radiolytic sources of corrosion have also been considered in the screening of processes and issues in the drip shield and WP degradation (CRWMS M&O 2000b, Section 6.2.27), Yucca Mountain Project (YMP) FEP (features, events, and processes) No. 2.1.13.01.00. The latter reference dealt specifically with radiolytic effects of gamma radiation on the WP and drip shield, excluding them from

further consideration because of low consequence. The potential for chemical interactions within the WP from radiolytic effects was considered insignificant in the Waste Form Degradation Process Model Report (CRWMS M&O 2000c, p. 3-21) and therefore neglected except as a possible perforation mechanism for the Zircaloy cladding (CRWMS M&O 2000c, p. 3-40). The rationale is that although Zircaloy has excellent corrosion resistance to nitric acid and hydrogen peroxide, the concentration of these species can be enhanced by radiolysis during an internal waste package criticality, potentially accelerating the corrosion effects in the cladding material.

Radiolysis producing local depression of pH resulting in localized corrosion of cladding material is included in the localized corrosion model as a special feature, YMP FEP NO. 2.1.02.15.00 (CRWMS M&O 2000d, Section 6.2.5). Neutron and gamma doses considered in the screening decision for this FEP were representative of the residual radionuclide decay only and did not consider the dose from an internal criticality. Although the Zircaloy cladding is resistant to direct attack by nitric acid, cladding destabilization may occur allowing the buildup of metal-halide complexes in solutions that can promote corrosion (CRWMS M&O 2000e, p. II-1). Screening arguments for this corrosion mechanism show that environments conducive to the accumulation of the necessary chemical species are unlikely.

The NRC has also raised a question concerning effects on criticality consequence evaluations due to radiation from the criticality event (CRWMS M&O 2000i, p. 6) that was to be resolved by appropriate calculations. Nitric acid is assumed to be the principal corrosive radiolytic chemical specie. Accordingly, a scoping calculation of the possible quantity of  $\text{HNO}_3$  produced by radiolysis during a criticality has been made with the MCNP code (CRWMS M&O 1998a) in response to this issue. The calculational method, model input description, and results from this calculation are given in the following sections.

## II. Computational Method

Radiolytic production of particular chemical species depends upon the radiation environment, the chemical components present, and the physical environment where the radiolytic reactions are occurring. However, the yield of any given chemical species is characterized by a single parameter, "G", identified as the G-factor (Reed and Van Konynenburg 1991, pp. 1396-1403). The "G" value represents the number of molecules of a chemical species produced per 100 eV of absorbed radiation energy in the volume containing the irradiated environment. Measurements of the "G" factor for production of nitric acid from gamma radiation range from approximately 0.5 to 2.5 molecules/100 eV. The value used in this calculation is 1.0 and this value is also assumed to apply to neutron irradiation. The acid production rate scales linearly with the "G" factor and the uncertainty in the factor expressed in Section IV as range of possible molar quantities of nitric acid generated. The "G" value of 1.0 was chosen for this calculation to be consistent with other radiolytic acid production calculations discussed in Section IV.

For this calculation, a 21-pressurized water reactor (PWR) waste package, containing B&W 15x15 commercial spent nuclear fuel (CSNF) assemblies, was assumed to have failed and subsequently partially filled with water. The steel basket structure was assumed to have fully

degraded with the degradation products settling to the bottom of the WP. Hematite ( $\text{Fe}_2\text{O}_3$ ) is assumed to be the only degradation product remaining from the basket. This is consistent with previous studies that showed that replacement of hematite by goethite had little effect on criticality. The packing fraction of the hematite was assumed to be 0.58 (CRWMS M&O 1998b, p. 15) with the remaining space filled with water. Hematite was assumed to be present outside the fuel pins in assemblies within the hematite-water mixture level but not within the guide tube spaces of those assemblies. The water level was assumed to extend to the top of the fourth row of assemblies, leaving three assemblies in the air-water vapor space at the top of the WP. The radiant energy deposition in the air-water vapor space was calculated with the MCNP code (CRWMS M&O 1998a) using the KCODE option and tracking both neutron and gamma particles. The gamma interactions include photon and electron processes.

### III. Model Description

The MCNP model for the radiolysis calculation was adapted from the model developed to calculate the neutron current external to a 21-PWR waste package due to an internal criticality event (CRWMS M&O 2000f). The PWR assembly used in the referenced calculation was a Babcock and Wilcox (B&W) 15 x 15 PWR CSNF assembly. Each assembly was composed of 4 regions: the bottom end-fitting region, the active fuel region, the plenum region, and the top end-fitting region. The content of each assembly region in this model was homogenized within the region volume. Volumes and masses of material in the bottom end-fitting region, the plenum region, and the top end-fitting region were obtained from a prior shielding calculation (CRWMS M&O 2000g). Modification to this model included placing a water-Hematite mixture external to the assemblies in the lower part of the WP, adding a water moderated region above the water-Hematite mixture with an air space above the water level, and explicitly defining the fuel pins and guide tubes of assemblies in the active fuel region. As was explained above, the water-Hematite mixture was assumed to fill the region external to the fuel pins but was excluded from guide tube cells. Based on the volume of Fe in the assembly basket structure and assuming a packing fraction of 0.58 for the Hematite, the water-Hematite level has an elevation of 76.27 cm that covers the 11<sup>th</sup> row of fuel pins in the 3<sup>rd</sup> assembly row. The water moderator extends to an elevation of 120.32 cm at the top of the 4<sup>th</sup> assembly row. This level was estimated (without iteration) to be at or slightly above the level necessary to achieve a critical configuration providing a basis for estimating the void space available for radiolytic specie production. The remaining space is filled with air at a conservative density of  $1.225 \text{ kg/m}^3$ . Use of dry air rather than an air-water vapor mixture is conservative for radiant energy deposition since the deposition depends upon the mass present and dry air maximizes the material density in the that region. The effect of including water vapor could be evaluated with additional analysis. Cross sectional views of the WP model are shown in Figures 1 and 2. Data preparation was performed with Excel spreadsheets in the file "o:\wpd\mclure\radiolysis\21-PWR-EDAII.xls". Geometry calculations are done in the sheets "VOL-MASS" and "EDA-II.WP.rev1.dat2". Cell identifiers where the radiant energy deposition is tallied are given as follows: cell 275, external region to the three assemblies in the air space, cell 283, region external to fuel pins in the three assemblies, and cell 284, the guide tube region in the three assemblies (indicated by the white dots in Figure 2).

The energy deposition in the air filled region calculated by MCNP is given in units of MeV per gram per fission neutron. This energy must be multiplied by the mass in the deposition region, nuubar (number of neutrons per fission), and number of fission events occurring in the criticality to obtain the total energy deposition from a criticality. A secondary check on the energy tallies was made by estimating the energy deposition in the specified region from the average (neutron and gamma) flux in each region multiplied by flux to dose conversion factors. These conversion factors introduce additional uncertainties and the tallies are listed for reference only.

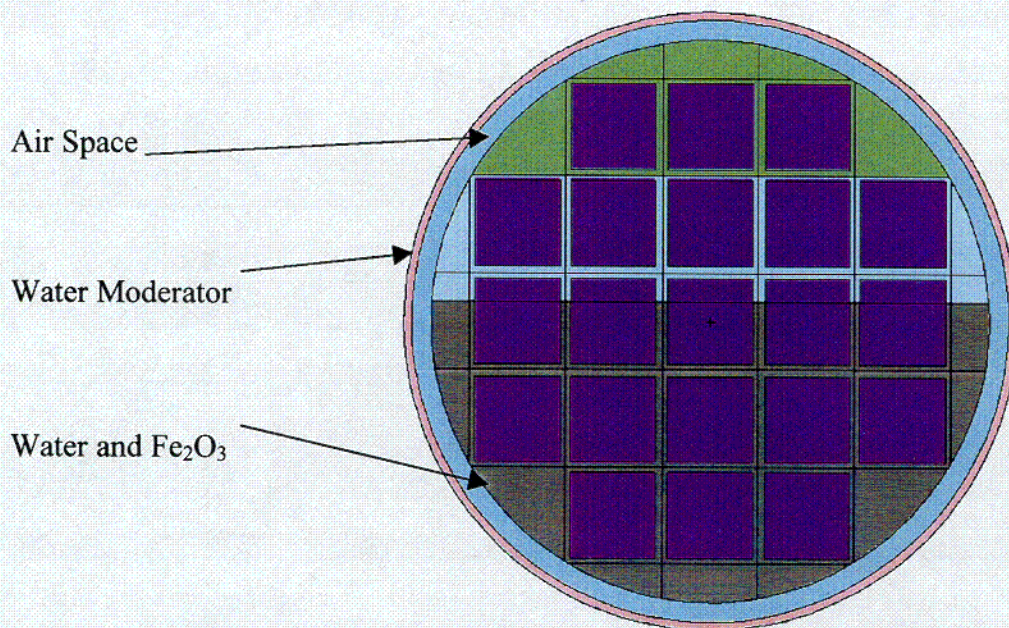


Figure 1. Cross Sectional View of 21-PWR Waste Package with Homogenized Assembly Regions

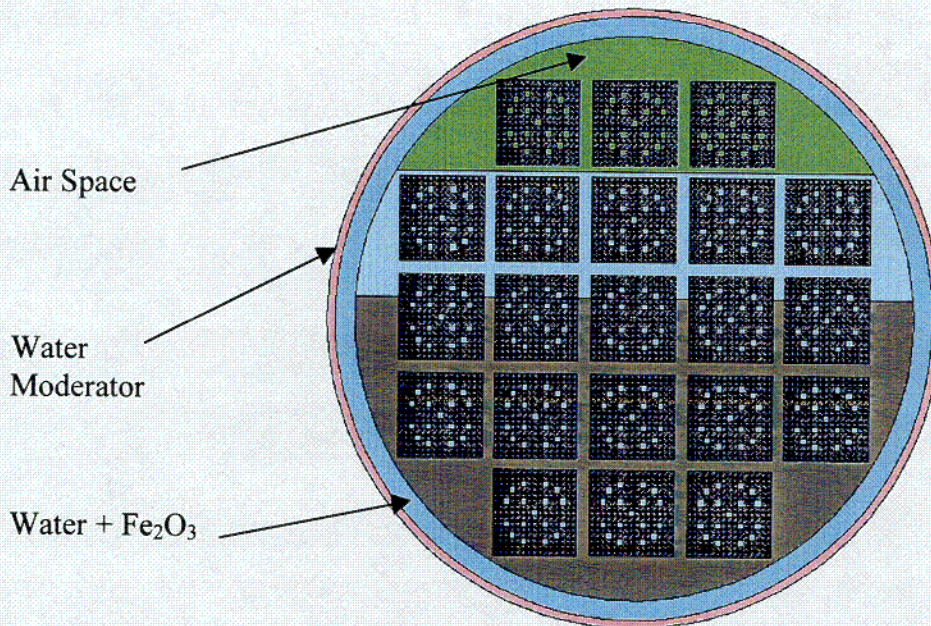


Figure 2. Cross Sectional View of the Fuel Pin Region of Assemblies in the 21-PWR Waste Package

#### IV. Energy Deposition Results

The radiolysis case run with the MCNP model described in Section III resulted in a  $k_{\text{eff}}$  of  $\sim 1.026$ . Since this case was an initial scoping one to determine if significant production of nitric acid was possible, parameters in the system were adjusted to assure that the system was critical but were not optimized further. Model revisions to better optimize the system (to a  $k_{\text{eff}} \cong 1.0$  or other suitably prescribed value) for a more detailed calculation include removing the gaps between the fuel assemblies, positioning the assemblies to be in contact with the WP as appropriate for support, and specifying the end fittings explicitly rather than as homogenized regions. The radiant energy depositions in the air filled region from both the energy and flux tallies are listed in Table 1 for each cell and also the combined region (Sheet "Tally-result"). Energy tallies involve the mass in each region as compared to flux tallies that involve the volumes. Tallies are given in units of MeV per fission neutron (Total Tally Value in Table 1) for the flux tallies and in MeV per gram per fission neutron (Mean Tally Value in Table 1) for energy deposition tallies.

Table 1. Radiant Energy Deposition in Air Filled Region Within A 21-PWR WP

Cell No.	Tally type	Multiplier (Total/Mean)	Total Tally Value	Mean Tally Value	statistical error	Energy Deposition	Comparison
		Vol (cm <sup>3</sup> ) /mass (g)	MeV/fissio n neutron	MeV/g/fissio n neutron		MeV/fission neutron	Flux to Deposition
275	n-flux	560637.5637	5.4665E-04		2.6000E-03		1.0033E+01
263	n-energy	4.970014863		2.0186E-08	3.1600E-02	1.0033E-07	
162	n-energy	14.3374776		1.6375E-08	2.9800E-02	2.3477E-07	
263, 162	n-energy	19.30749247		1.7356E-08	2.4900E-02	3.3510E-07	
284	n-flux	38233.51513	5.1276E-05		3.1000E-03		1.1019E+01
275	n-energy	686.7810156		7.9334E-08	3.0000E-03	5.4485E-05	
284	n-energy	46.83605604		9.9357E-08	3.9000E-02	4.6535E-06	
283	n-energy	315.1092646		1.0235E-07	2.9000E-03	3.2253E-05	
275, 284, 283	n-energy	1048.726336		8.7145E-08	2.7000E-03	9.1391E-05	
283	n-flux	257232.0527	3.4436E-04		2.5000E-03		1.0677E+01
289	n-energy	14.76094414		1.6950E-08	2.5700E-02	2.5020E-07	
387	n-energy	42.58230848		1.2881E-08	2.3800E-02	5.4849E-07	
289, 387	n-energy	57.34325263		1.3928E-08	2.0800E-02	7.9869E-07	
294	n-energy	9.871692022		9.2691E-09	3.7700E-02	9.1502E-08	
392	n-energy	28.47781489		7.5430E-09	3.4600E-02	2.1481E-07	
294, 392	n-energy	38.34950691		7.9873E-09	2.9800E-02	3.0631E-07	
96	n-energy	137.1801781		3.9847E-09	3.5100E-02	5.4663E-07	
263	gamma-energy	4.970014863		3.8617E-08	3.5800E-02	1.9193E-07	
162	gamma-energy	14.3374776		2.5225E-08	3.8700E-02	3.6166E-07	
263, 162	gamma-energy	19.30749247		2.8672E-08	3.0100E-02	5.5359E-07	
275	gamma-energy	686.7810156		9.4934E-08	4.1000E-03	6.5199E-05	
284	gamma-energy	46.83605604		7.7581E-08	6.2000E-03	3.6336E-06	
283	gamma-energy	315.1092646		8.9838E-08	3.6000E-03	2.8309E-05	
275, 284, 283	gamma-energy	1048.726336		9.2628E-08	3.4000E-03	9.7141E-05	
275	gamma-flux	560637.5637	8.1476E-05		4.0000E-03		1.2496E+00
289	gamma-energy	14.76094414		2.0635E-08	3.5400E-02	3.0459E-07	
387	gamma-energy	42.58230848		1.8423E-08	3.1900E-02	7.8450E-07	
289, 387	gamma-energy	57.34325263		1.8993E-08	2.8100E-02	1.0891E-06	
284	gamma-flux	46.83605604	4.5233E-06		6.0000E-03		1.2448E+00
294	gamma-energy	9.871692022		1.4607E-08	4.5800E-02	1.4419E-07	

Cell No.	Tally type	Multiplier (Total/Mean)	Total Tally Value	Mean Tally Value	statistical error	Energy Deposition	Comparison
		Vol (cm <sup>3</sup> ) /mass (g)	MeV/fission n neutron	MeV/g/fission n neutron		MeV/fission neutron	Flux to Deposition
392	gamma- energy	28.47781489		1.3864E-08	4.2000E-02	3.9483E-07	
294, 392	gamma- energy	38.34950691		1.4056E-08	3.6800E-02	5.3902E-07	
283	gamma- flux	315.1092646	3.5267E-05		3.6000E-03		1.2458E+00
96	gamma- energy	137.1801781		8.0346E-09	3.8000E-02	1.1022E-06	
				Total		1.9380E-04	
				Neutron		9.3378E-05	
				Gamma		1.0043E-04	

The energy depositions from the flux tallies were higher than the direct energy tallies, approximately a factor of 11 for neutron and 1.25 for photons. These tallies include dose conversion factors given by

$$\text{Factor} = [(\text{rem/hour})/(\#/\text{cm}^2 - \text{second})] \times [(\text{MeV/gram})/(\text{rad/hour})] \times \text{grams}/(\text{rem/rad})$$

where the rem/rad term is spectrally dependent for neutrons and unity for photons. This term is a "quality" parameter for neutron radiation that relates the rem dose in phantoms to the rad value of the dose and ranges from 2 to 11. Since the void region composition differs from that of phantoms, the flux based evaluation provides only a bounding estimate of the energy deposition. The flux based energy deposition estimates were consistently higher by the factors given in the last column of Table 1 than the direct energy tallies.

The quality factors and flux-to-dose conversion are given in Table H.1 for neutrons and Table H.2 for photons (Briesmeister 1997) by energy spectra. The spectral distributions of the total conversion factors for both neutron and photons are listed in Sheet "Tally Multipliers".

The total nitric acid production in the prescribed air space from an internal WP criticality is determined by multiplying the deposition energy per fission neutron by the number of fission neutrons in the event and the specie "G" factor. Values calculated for a transient and steady state criticality are listed in Table 2. The steady state values assumed a 1000 W power level for 1 year. These values can be linearly scaled for different powers, criticality duration times, and "G" factors.

Table 2. Radiolytic Generation of Nitric Acid from Criticality Events

Criticality Event	Energy Generated (J)	# Fissions	Radiolysis Energy (eV)	Moles HNO <sub>3</sub>	HNO <sub>3</sub> (kg)
Transient Event	9.5800E+07	3.30352E+18	1.6006E+21	2.6578E-05	1.675e-06
1000 W Steady State Event (per year)	3.1558E+10	1.05896E+21	5.1308E+23	8.5198E-03	5.369e-04

The specie production rate scales as the number of fissions per unit interval and, thus, linearly for steady-state events. For a 1.0 kW steady-state criticality event extending over 10,000 years (maximum steady state duration assumed for consequence analyses), approximately 85 moles or 5.4 kg of HNO<sub>3</sub> could possibly be produced, assuming a "G" factor of 1.0. Uncertainty in the "G" factor results in a range of approximately 40 to 200 moles for the total acid production from the referenced steady-state criticality.

The 85-mole quantity of HNO<sub>3</sub> from the steady-state criticality calculation compares to approximately 13 moles or 0.82 kg of HNO<sub>3</sub> produced over 90,000 years at < 4 rad/hr from radionuclide decay (CRWMS M&O 2000h, Section 6.3). A second calculation of the radiolytic production of HNO<sub>3</sub> (CRWMS M&O 2000e, Attachment II) resulted in approximately 22.7 moles or 1.4 kg at an irradiation level of 5.0 rad/hour over 90,000 years. These latter two calculations are equivalent when adjusted for dose and air mass in the WP volume.

#### V. Estimated Consequences of Nitric Acid Production

The nominal value for uniform corrosion of Zircalloy-2 and -4 given in the clad degradation-localized corrosion analysis model report (AMR) (CRWMS M&O 2000j, p. 48) is approximately 8.8e-08 μm/y assuming the corrosion product is ZrO<sub>2</sub>. The AMR provides an assessment of conditions under which zirconium and its alloys might experience enhanced corrosion rates above the nominal value. This analysis indicates that accelerated corrosion rates of zirconium are bounded by the rate derived from the fluoride concentration. The nominal corrosion rate can be enhanced in environments where the pH is less than 3.18 and the fluoride ion concentration exceeds 5 ppm (CRWMS M&O 2000j, p. 49). The fluoride concentration in J-13 water is given as 2.18 ppm (CRWMS M&O 2000c, Table 3-2.1). Fluoride concentrations in degraded waste packages containing CSNF have been estimated to range from 1.148e-04 mol/l to 9.114e-04 mol/l (CRWMS M&O 2000k, Section 6.4.3) which translate to approximately 2.2-17 ppm, thus spanning the range where accelerated zirconium corrosion could occur.

Assuming, conservatively, that the water level is maintained in the WP by equivalence between the influx drip rate and evaporation and that the nitric acid remains in the aqueous state, the concentration of HNO<sub>3</sub> will gradually increase by the end of the criticality to about 0.03 molar having a pH ≈ 1.5. In terms of a volume percent, the 85 moles occupy 3.57 l out of a total liquid volume of 2716 l, resulting in a 0.13 volume percent.

A mitigating factor affecting enhanced corrosion from nitric acid production during a criticality event is that its production occurs in the air space allowing dispersal outside the WP, particularly since water vapor is assumed to exit the WP to maintain the critical water level. Other factors include dilution in the water volume, dispersal by outflow from the WP, and scavenging by other materials. With respect to scavenging (likely the most important factor), nitric acid reacting with the Hematite would result in approximately 28 moles or 6.77 kg of Fe(NO<sub>3</sub>)<sub>3</sub> based on the chemical balance



This mass constitutes less than 0.03% of the Hematite in the WP.

## VI. References

- Shoesmith, D.W. and King, F. 1999. *The Effects of Gamma Radiation on the Corrosion of Candidate Materials for the Fabrication of Nuclear Waste Packages*. AECL-11999. AECL Technologies, Inc. Pinawa, Manitoba, Canada.
- Reed, D.T. and Van Konynenburg, R.A. 1988. *Effect of Ionizing Radiation on Moist Air Systems*. Materials Research Society Symposium Proceedings, Vol. 112. Materials Research Society, Pittsburgh, Pennsylvania.
- CRWMS M&O 2000a. *Disposal Criticality Analysis Methodology Topical Report Revision 01*. YMP/TR-004Q. CRWMS M&O. Las Vegas, Nevada. ACC: MOL.20001117.0221.
- CRWMS M&O 2000b. *FEPs Screening of Processes and Issues in Drip Shield and Waste Package Degradation*. ANL-EBS-PA-000002 REV 00 ICN 01. CRWMS M&O. Las Vegas, Nevada: ACC: MOL.20001211.0004.
- CRWMS M&O 2000c. *Waste Form Degradation Process Model Report*. TDS-WIS-MD-000001 REV 00 ICN 01. Las Vegas, Nevada: CRWMS M&O. ACC: MOL. 20000713.0362.
- CRWMS M&O 1998a. *Software Qualification Report for MCNP Version 4B2, A General Monte Carlo N-Particle Transport Code*. CSCI: 30033 V4B2LV. 30033-2003 Rev. 01. Las Vegas, Nevada: CRWMS M&O. ACC: MOL.19980622.0637.
- Reed, D.T. and Van Konynenburg, R.A. 1991. *Effect of Ionizing Radiation on the Waste Package Environment*. High Level Radioactive Waste Management, Proceeding of the Second Annual International Conference. Las Vegas, Nevada. April 28-May 3, 1991. American Nuclear Society. LaGrange Park, Illinois. TIC: 204272.
- CRWMS M&O 2000d. *Clad Degradation - FEPs Screening Arguments*. ANL-WIS-MD-000008 REV 00 ICN 01. Las Vegas, Nevada. CRWMS M&O. ACC: MOL.20001208.0061.
- CRWMS M&O 2000e. *Summary of In-Package Chemistry for Waste Forms*. ANL-EBS-MD-000050 REV 01E. Las Vegas, Nevada. CRWMS M&O.
- CRWMS M&O 2000f. *Neutron Current in a Neighboring WP due to Criticality of a Degraded 21-PWR WP*. CAL-EBS-NU-000015 REV 00A. Las Vegas, Nevada. CRWMS M&O.
- CRWMS M&O 2000g. *Dose Rate Calculation for the 21-PWR UCF Waste Package*. CAL-UDC-NU-000002 REV 00. Las Vegas, Nevada: CRWMS M&O. ACC: MOL.20000223.0507.
- CRWMS M&O 1998b. *Supplemental Criticality Calculations for Degraded Internal Configurations of a 21 PWR WP*. BBA000000-01717-0210-00022 REV 00. Las Vegas, Nevada: CRWMS M&O. ACC: MOL.19980919.0086.

Title: Radiolytic Specie Generation from Internal Waste Package Criticality

Document Identifier: CAL-EBS-NU-000017 REV 00 ATTACHMENT III Page III-12 of III-12

---

Briesmeister, J.F., ed. 1997. *MCNP-A General Monte Carlo N-Particle Transport Code*. LA-12625-M, Version 4B. Los Alamos, New Mexico: Los Alamos National Laboratory. ACC: MOL.19980624.0328.

CRWMS M&O 2000h. *Gamma and Neutron Radiolysis in a 21-PWR Waste Package*. CAL-MGR-NU-000006 REV 00A. Las Vegas, Nevada: CRWMS M&O.

CRWMS M&O 2000i. Summary Highlights of NRC/DOE Technical Exchange and Management Meeting on Subissues Related to Criticality, October 23-25, 2000. Las Vegas, Nevada: CRWMS M&O.

CRWMS M&O 2000j. *Clad Degradation-Local Corrosion of Zirconium and its Alloys under Repository Conditions*. ANL-EBS-MD-000012 REV 00. Las Vegas, Nevada. CRWMS M&O. ACC: MOL.20000405.0479.

CRWMS M&O 2000k. *In-Package Chemistry Abstraction*. ANL-EBS-MD-000037 REV 00. Las Vegas, Nevada. CRWMS M&O. ACC: MOL.20000418.0818.

ANALYSIS/MODEL COVER SHEET

Complete Only Applicable Items

2.  Analysis Check all that apply

Type of Analysis	<input type="checkbox"/> Engineering
	<input type="checkbox"/> Performance Assessment
	<input type="checkbox"/> Scientific
Intended Use of Analysis	<input type="checkbox"/> Input to Calculation
	<input type="checkbox"/> Input to another Analysis or Model
	<input type="checkbox"/> Input to Technical Document
	<input type="checkbox"/> Input to other Technical Products
Describe use:	

3.  Model Check all that apply

Type of Model	<input type="checkbox"/> Conceptual Model	<input type="checkbox"/> Abstraction Model
	<input type="checkbox"/> Mathematical Model	<input type="checkbox"/> System Model
	<input checked="" type="checkbox"/> Process Model	
Intended Use of Model	<input checked="" type="checkbox"/> Input to Calculation	
	<input checked="" type="checkbox"/> Input to another Model or Analysis	
	<input checked="" type="checkbox"/> Input to Technical Document	
	<input checked="" type="checkbox"/> Input to other Technical Products	
Describe use:		
To estimate the quantities of external accumulation of fissile material for use in external criticality risk assessments.		

4. Title:  
Geochemistry Model Validation Report: External Accumulation Model

5. Document Identifier (including Rev. No. and Change No., if applicable):  
ANL-EBS-GS-000002 REV 00

6. Total Attachments: 2	7. Attachment Numbers - No. of Pages in Each: I(5), II(CDROM)
----------------------------	--

	Printed Name	Signature	Date
8. Originator	Kaveh Zarrabi, Jean-Philippe Nicot, Harlan Stockman, and Susan LeStrange	<i>Susan LeStrange</i>	9/27/01
9. Checker	Sara Arthur (technical) S. F. Alex Deng (compliance)	<i>Sara Arthur FOR SARA ARTHUR</i> <i>SFD</i>	9/27/01 9/27/01
10. Lead/Supervisor	Susan LeStrange	<i>Susan LeStrange</i>	9/27/01
11. Responsible Manager	Daniel Thomas	<i>D.A. Thomas</i>	09/27/2001

12. Remarks:

OFFICE OF CIVILIAN RADIOACTIVE WASTE MANAGEMENT  
ANALYSIS/MODEL REVISION RECORD

*Complete Only Applicable Items*

1. Page: 2 of 72

2. Analysis or Model Title:

Geochemistry Model Validation Report: External Accumulation Model

3. Document Identifier (including Rev. No. and Change No., if applicable):

ANL-EBS-GS-000002 REV 00

4. Revision/Change No.

5. Description of Revision/Change

Rev 00

Initial Issue

## CONTENTS

	Page
1. PURPOSE.....	8
2. QUALITY ASSURANCE.....	9
3. COMPUTER SOFTWARE AND MODEL USAGE.....	10
3.1 SOFTWARE APPROVED FOR QA WORK.....	10
3.1.1 EQ3/6.....	10
3.1.2 PHREEQC.....	10
3.1.3 C Program "transl" Version 2.0.....	11
3.1.4 Microsoft Excel Visual Basic Macro "SeepageFlow_macro".....	11
3.1.5 Microsoft Excel Visual Basic Macro "Acc_with_decay".....	12
3.2 MODELS.....	12
4. INPUTS.....	12
4.1 DATA AND PARAMETERS.....	12
4.2 CRITERIA.....	13
4.3 CODES AND STANDARDS.....	13
5. ASSUMPTIONS.....	13
6. MODEL.....	16
6.1 THE CONCEPTUAL MODEL.....	16
6.1.1 Fractures-Only Geometry and Fractures-with-Lithophysae Geometry.....	16
6.1.2 Large Stand-Alone Lithophysae Geometry.....	17
6.2 DEVELOPMENT OF THE MODEL.....	18
6.2.1 Mixing Loci.....	18
6.2.1.1 Sources of Dilution in the Drift.....	18
6.2.1.2 Fracture System.....	19
6.2.1.3 Lithophysae.....	19
6.3 GEOMETRIC CHARACTERISTICS OF FRACTURES AND LITHOPHYSAE.....	20
6.3.1 Fracture Aperture.....	21
6.3.2 Lithophysae Porosity.....	21
6.3.3 Probability of High Fracture Intensity.....	21
6.3.4 Equivalent Fracture Intensity.....	25
6.4 GEOMETRIC CHARACTERISTICS OF THE DILUTION-MIXING ZONE.....	29
6.4.1 Size of the Dilution-Mixing Zone.....	30
6.4.2 Dilution.....	30
6.4.2.1 Infiltration and Seepage Rates.....	30
6.4.2.2 Thorough Mixing.....	33

## CONTENTS (Continued)

	Page
6.4.3 Fracture Saturation.....	33
6.4.3.1 Homogeneity by Layer Permeability Model.....	34
6.4.3.2 Stochastic Permeability Model.....	35
6.4.3.3 Probability of a Given Saturation.....	35
6.5 STAND-ALONE LITHOPHYSAE .....	37
6.6 PHREEQC POSTPROCESSING .....	38
6.7 MODEL IMPLEMENTATION.....	38
6.7.1 Step-By-Step Model Description.....	38
6.7.1.1 Fractures-Only and Fractures-With-Small-Lithophysae Geometries..	38
6.7.1.2 Large Stand-Alone Lithophysae.....	51
6.7.1.3 Example Results.....	55
6.7.2 WP Source Terms.....	55
6.7.3 Water Composition.....	56
6.7.4 Drip Rates.....	56
6.7.5 Mineral Dissolution at the Fracture Surface.....	56
6.7.6 Precipitation of Minerals.....	57
6.7.7 Thermodynamic Database.....	57
6.7.8 Number of PHREEQC Time Steps.....	57
6.7.9 Number of Cells in Mixing-Dilution Zone .....	57
6.7.10 Stand-Alone Lithophysae Runs.....	58
6.8 MODEL VALIDATION .....	58
6.8.1 Comparison of PHREEQC Performance with Experimental Results .....	59
6.8.2 Description of the Fracture System .....	62
6.8.3 Evaluation of Mechanisms for Fissile Accumulation.....	62
6.8.3.1 Bio-accumulation .....	62
6.8.3.2 Reducing Zone .....	63
6.8.3.3 Colloidal transport and filtering .....	64
6.8.3.4 Sorption.....	66
7. CONCLUSIONS.....	67
8. INPUTS AND REFERENCES.....	68
8.1 DOCUMENTS CITED .....	68
8.2 CODES, STANDARDS, REGULATIONS, AND PROCEDURES .....	71
8.3 SOURCE DATA.....	71
ATTACHMENT I. LIST OF FILES ON ATTACHED COMPACT DISK (CD).....	I-1
ATTACHMENT II. TWO CDS CONTAINING INPUT FILES, OUTPUT FILES, AND SPREADSHEETS.....	N/A

## FIGURES

	<b>Page</b>
1. Representation of External Accumulation Model (not to scale).....	9
2. Far-Field Representation (not to scale) .....	17
3. Sketch of the Drift Dilution Loci.....	19
4. Conceptual Model of Flow Through a Lithophysae .....	20
5. Fracture Saturation around the Drift at Different Infiltration Rates .....	34
6. Saturation Response to a Flux Increase in Fractures .....	35
7. Source Term for Run p52rLx41 From EQ6 .....	39
8. Moles U Accumulated per Cell in One Year.....	43
9. Moles Pu Accumulated in One Year Versus Cell Number .....	44
10. Cumulative Mass of Solids at 23,000 Years After Breach (No Decay).....	46
11. Cumulative Molar Density at Final Time for Fractures Only .....	50
12. Cumulative Molar Density at Final Time for Fractures with Small Lithophysae .....	50
13. Accumulation in a Large Stand-Alone Lithophysae at 10,000 Years After Breach.....	52
14. Case s5: Minerals and Aqueous U and Pu.....	64
15. Schematic Representation of Iron-(Hydro)oxide Colloid Stability as a Function of pH and Ionic Strength.....	65

## TABLES

	<b>Page</b>
1. Summary List of Input .....	12
2. Miscellaneous Parameters .....	13
3. Fracture and Lithophysae Porosity in the Repository Units.....	20
4. CCDF of the Average Number of Fractures >1 m per meter .....	22
5. Correction Factor for Fracture Intensity for Fractures > 1 m.....	22
6. CCDF of Uncorrected Fracture Intensity for Fractures with Length between 0.3 and 1 m (TSw34 unit).....	23
7. CCDF of Uncorrected Fracture Intensity of Fractures with Length < 1 m (TSw35 unit) .....	24
8. Correction Factor for Fracture Intensity for Fractures < 1 m.....	24
9. Summary of Fracture Intensity for Stochastic Sampling .....	25
10. Equivalent Fracture Intensity (that includes lithophysae).....	29
11. Distribution of Seepage Versus Infiltration Flux.....	31
12. Average Infiltration Rates .....	31
13. Flow Focusing Multipliers.....	32
14. Probability of Seepage Rate into Drift Being Between 1 and 20 liter/year .....	32
15. Percentiles of Dilution Factor for the 3 Climates (seepage rate between 1 and 20 liter/year)	32
16. Correspondence between Local Infiltration Rate and Dilution Factor .....	33
17. Fracture Intensity needed for Thorough Mixing under Different Conditions .....	33
18. CCDF of High Dilution Factors .....	36
19. Parameters for Equation 12 .....	37
20. CCDF for the Number of Composite Fracture Intersections for Selected Lithophysal Cavity Size.....	37
21. Example Results for Four Source Terms .....	55
22. Accumulation in 1 meter-Diameter Lithophysal Cavity with High Fracture Intensity .....	55
23. Comparison of Experimentally Observed and Predicted Precipitates in Reaction of DWPF Glass with J-13 Well Water at 90°C .....	60
24. Comparison of Experimentally Observed and Predicted Precipitates in Reaction of West Valley Glass with J-13 Well Water at 90°C .....	61
25. Sorption Coefficient Distributions for UZ Unit.....	66

## ACRONYMS AND ABBREVIATIONS

AMR	Analysis and Modeling Report
CCDF	complementary cumulative distribution function
CD-ROM	compact disc-read-only memory
CRWMS	Civilian Radioactive Waste Management System
DOE	U.S. Department of Energy
DLS	Detailed Line Survey
DS	drip shield
DTN	Data Tracking Number
DWPF	Defense Waste Product Facility
EBS	Engineered Barrier System
ECRB	Enhanced Characterization of the Repository Block
HLW	high-level waste
M&O	Management and Operating Contractor
QA	quality assurance
STN	Software Tracking Number
TBV	to be verified
THC	Thermal Hydrological Chemical (model)
TPO	technical product output
TST	Transition State Theory
UZ	unsaturated zone
WP	waste package

## 1. PURPOSE

The purpose of this Analysis and Modeling Report (AMR) is to validate the External Accumulation Model that predicts accumulation of fissile materials in fractures and lithophysae in the rock beneath a degrading waste package (WP) in the potential monitored geologic repository at Yucca Mountain. (Lithophysae are voids in the rock having concentric shells of finely crystalline alkali feldspar, quartz, and other materials that were formed due to entrapped gas that later escaped, DOE 1998, p. A-25.)

The intended use of this model is to estimate the quantities of external accumulation of fissile material for use in external criticality risk assessments for different types of degrading WPs: U.S. Department of Energy (DOE) Spent Nuclear Fuel (SNF) codisposed with High Level Waste (HLW) glass, commercial SNF, and Immobilized Plutonium Ceramic (Pu-ceramic) codisposed with HLW glass.

The scope of the model validation is to (1) describe the model and the parameters used to develop the model, (2) provide rationale for selection of the parameters by comparisons with measured values, and (3) demonstrate that the parameters chosen are the most conservative selection for external criticality risk calculations. To demonstrate the applicability of the model, a Pu-ceramic WP is used as an example.

The model begins with a source term from separately documented EQ6 calculations; where the source term is defined as the composition versus time of the water flowing out of a breached waste package (WP). Next, PHREEQC, is used to simulate the transport and interaction of the source term with the resident water and fractured tuff below the repository. In these simulations the primary mechanism for accumulation is mixing of the high pH, actinide-laden source term with resident water; thus lowering the pH values sufficiently for fissile minerals to become insoluble and precipitate. In the final section of the model, the outputs from PHREEQC, are processed to produce mass of accumulation, density of accumulation, and the geometry of the accumulation zone. The density of accumulation and the geometry of the accumulation zone are calculated using a characterization of the fracture system based on field measurements made in the proposed repository (BSC 2001k). The model predicts that accumulation would spread out in a conical accumulation volume. The accumulation volume is represented with layers as shown in Figure 1.

This model does not directly feed the assessment of system performance. The output from this model is used by several other models, such as the configuration generator, criticality, and criticality consequence models, prior to the evaluation of system performance.

This document has been prepared according to AP-3.10Q, *Analyses and Models* and prepared in accordance with the technical work plan (BSC 2001d).

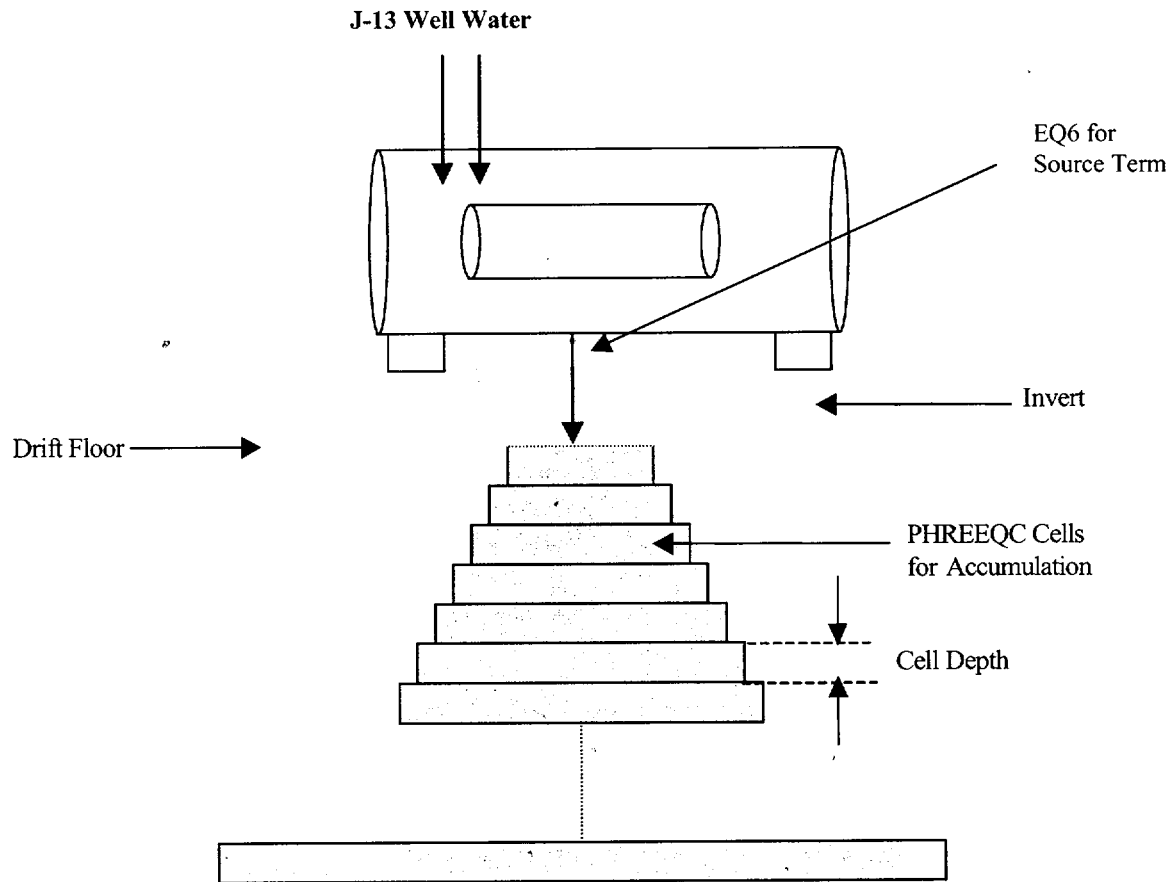


Figure 1. Representation of External Accumulation Model (not to scale)

## 2. QUALITY ASSURANCE

An activity evaluation (BSC 2001d, Addendum A), which was prepared per AP-2.21Q, *Quality Determinations and Planning for Scientific, Engineering, and Regulatory Compliance Activities*, determined that the Quality Assurance (QA) program (DOE 2000) applies to the activity under which this analysis was developed.

With regard to the development of this document, the control of the electronic management of data was evaluated in accordance with AP-SV.1Q, *Control of the Electronic Management of Information*. The evaluation determined that current work processes and procedures are in accordance with the controls specified in the technical work plan (BSC 2001d).

### 3. COMPUTER SOFTWARE AND MODEL USAGE

#### 3.1 SOFTWARE APPROVED FOR QA WORK

This document includes the results from software codes used in the supporting calculations, but these software products were not used in the development of this report (except for PHREEQC as noted in Section 3.1.2). The following statements regarding these software products are made for information only.

##### 3.1.1 EQ3/6

The software package, "EQ3/6 V7.2b" (CRWMS M&O 1998) and "EQ6 Version 7.2bLV", (CRWMS M&O 1999e) were qualified under the AP-SI.1Q procedure. The software was obtained through Configuration Management. The software is appropriate for use in the calculations summarized in this report and has been used within the range of parameters for which the software has been validated.

The major components of the EQ3/6 package include EQ3NR, a speciation-solubility code; EQ6, a reaction path code which represents water/rock interaction or fluid mixing in either a pure reaction progress mode or a time mode; EQPT, a data file; EQLIB, a supporting software library; and several (> 5) supporting thermodynamic data files preprocessor (Daveler and Wolery 1992). EQ6 7.2bLV was validated (CRWMS M&O 2000e) and is the only version of EQ6 capable of incorporating radioactive decay (CRWMS M&O 1999d).

The EQ3/6 programs have been used within the range of parameters for which they were validated and are, therefore, appropriate for the application. The software was used within its range of validation. However, some runs simulated periods of high ionic strength (1 to ~4). While EQ6 is capable of handling high ionic strengths, there is no Yucca Mountain Project qualified thermodynamic database with corrections for high ionic strength. To address this issue, several sensitivity tests were performed using other thermodynamic databases that have corrections for high ionic strength (CRWMS M&O 2000g, Section 5.1.2). The results of calculations relating to these tests have shown that calculations at high ionic strength, using the "data0.ymp" database (DTN: MO0009THRMODYN.001), overestimate the solubility of Pu and U, which is conservative with respect to release from the waste package and external accumulations of these elements. This program was employed to produce input information for PHREEQC runs.

##### 3.1.2 PHREEQC

This model validation uses the software package, "PHREEQC V2.0", STN: 10068-2.0-00 (CRWMS M&O 1999c), which has been qualified under the AP-SI.1Q procedure under the Software Activity Number LV-1999-002 (CRWMS M&O 1999c). The Validation Test Report (VTR) (CRWMS M&O 1999b) that has been reviewed and approved. The software was obtained through Configuration Management. It is appropriate for use in the calculations summarized in this report and has been used within the range of parameters for which the software was validated. PHREEQC runs were performed on a Duke Engineering & Services Dell Pentium II computer (CPU# U998E, DE&S, 9111 Research Boulevard, Austin, TX).

The PHREEQC family of software products originated in the late 1970's and was developed by the U.S. Geological Survey. However, PHREEQC is a totally new, integrated version rewritten in the C language (CRWMS M&O 1999a). PHREEQC Version 2.0 PC contains capabilities such as speciation-solubility and kinetically controlled reaction pathway features, similar to many geochemical software packages, but also includes surface complexation, ion exchange, absorption and solid solutions, and a versatile treatment of rate laws. In addition, PHREEQC models 1D-transport and dispersion and diffusion in a double-porosity medium. PHREEQC supports only the use of the Davies or B-dot equations for activity coefficients, and the thermodynamic database used by PHREEQC is a direct transcription of the EQ6 data0.ymp (DTN: MO0009THERMODYN.001), translated into a PHREEQC-readable format.

PHREEQC models reactions of an aqueous solution with a set of reactants according to thermodynamic laws. It can also include very complex kinetics laws through a BASIC interpreter coupled to the program. PHREEQC handles advective transport by moving aqueous solutions from one cell to the next, allowing the contents of each cell to react with the solids and surface features present in the cell (CRWMS M&O 1999a). Diffusion and dispersion are handled by mixing the contents of cells in proportion to the diffusion (or dispersion) parameters. PHREEQC uses a finite-difference scheme and is therefore subject to numerical dispersion. PHREEQC uses a hybrid Newton-Raphson technique to solve a set of differential equations at each time step, and it is restricted to a constant time step, unlike EQ6 dynamic time stepping.

The input and output files for the PHREEQC runs discussed in Section 6.8.1 are provided in Attachment I, folder "Glass Valid".

### **3.1.3 C Program "transl" Version 2.0**

The transl Version 2.0 software has been qualified under AP-SI.1Q, *Software Management*, as level 3 software under the Software Tracking Number 10251-2.0-00 (BSC 2001e). Transl runs were performed on a Duke Engineering & Services Dell Pentium II computer (CPU# U998E, DE&S, 9111 Research Boulevard, Austin, TX). The software was obtained through Configuration Management. The software is appropriate for use in this AMR and has been used within the range of parameters for which the software was validated. The program transl is written in C language. It translates the EQ6 thermodynamic database from the EQ6 format to the PHREEQC format. The database that resulted from the translation process was submitted to the Technical Data Management System during development of BSC 20011 (Data Tracking Number (DTN): MO0105SPATHE04.005).

### **3.1.4 Microsoft Excel Visual Basic Macro "SeepageFlow\_macro"**

The SeepageFlow\_macro Version 1.0 software has been qualified under AP-SI.1Q, *Software Management*, as a level 3 software under the Software Tracking Number 10497-1.0-00 (BSC 2001f). SeepageFlow\_macro runs were performed on a Duke Engineering & Services Dell Pentium II computer (CPU# U998E, DE&S, 9111 Research Boulevard, Austin, TX). The software was obtained through Configuration Management. The software is appropriate for use in this AMR and has been used within the range of parameters for which the software has been validated. SeepageFlow\_macro is a Microsoft Excel macro written in Visual Basic that combines all the distributions involved in the seepage of water into the drift into a single distribution.

### 3.1.5 Microsoft Excel Visual Basic Macro "Acc\_with\_decay"

The Acc\_with\_decay Version 1.0 software has been qualified under AP-SI.1Q, *Software Management*, as level 3 software under Software Tracking Number 10499-1.0-00 (BSC 2001a). Acc\_with\_decay runs were performed on a Duke Engineering & Services Dell Pentium II computer (CPU# U998E, DE&S, 9111 Research Boulevard, Austin, TX). The software was obtained through Configuration Management. The software is appropriate for use in this AMR and has been used within the range of parameters for which the software has been validated. Acc\_with\_decay is an Microsoft Excel macro written in Visual basic that postprocesses PHREEQC runs to include radioactive decay. The software "Acc\_with\_decay" V.1.0 is used in the spreadsheet "XXX\_CritIn.xls" in Attachment II, where XXX stands for the source term name.

## 3.2 MODELS

None used.

## 4. INPUTS

### 4.1 DATA AND PARAMETERS

This section presents inputs that were used to develop the model and specific inputs that were used to model external accumulation of fissile materials from WPs containing Pu ceramic waste forms for the example case. The inputs are appropriate for the model because they have been developed or measured specifically for use in modeling processes at the potential repository.

Table 1 summarizes DTNs and other inputs.

Table 1. Summary List of Input

Source	Content
GS990408314224.001	ECRB <sup>a</sup> DLS <sup>a</sup> , Stations 00+00.89 to 14+95.18, Rev.00
GS990408314224.002	ECRB DLS, Stations 15+00.85 to 26+63.85, Rev.00
MO0006J13WTRCM.000	J13-well water composition
LB0101DSTTHCR1.001	Current pore water composition
BSC 2001c (Section 6.8.2)	Effluent (source term) composition
MO0009THERMODYN.001	Thermodynamic Database Molar volumes
BSC 2001k (Sections 6 and 7)	Fracture and lithophysae geometry characteristics
MO0109SPAFIE10.006.	Fracture intensity
LB990861233129.001	Fracture Van Genuchten parameters
LB990861233129.002	
LB990861233129.003	
LB991200DSTTHC.002	THC model fracture saturation
CRWMS M&O 2000b (Table 12-14)	Water Velocity
CRWMS M&O 2000h (Table 3.5-4)	Average net infiltration rates
SN0012T0511599.003	Drift seepage Rates

NOTES: <sup>a</sup> ECRB: Enhanced Characterization of the Repository Block; DLS: Detailed Line Survey

A few specific parameters were also used in the validation of the model (Table 2):

Table 2. Miscellaneous Parameters

Parameter	Value	Source
<sup>239</sup> Pu half-life (years)	24110	Parrington et al. (1996, p. 48)
21PWR WP length (m)	5.165	CRWMS M&O 2000d, Att. I - SK-0175 Rev.02 S1
44BWR WP length (m)	5.165	CRWMS M&O 2000d, Att. II - SK-0192 Rev.00 S1
Nominal WP Interval (cm)	10	BSC 2001h, Section 4.2.1.4
Emplacement Drift Diameter (m)	5.5	BSC 2001h, Section 4.2.1.3
Repository Elevation (m above sea level)	1100	BSC 2001h, Section 4.1.5.2
Water Table Elevation (m above sea level)	760	CRWMS M&O 2000h, Section 3.2.2.6
Average Distance to the Water Table (m)	340	Difference between the two previous values

## 4.2 CRITERIA

None used.

## 4.3 CODES AND STANDARDS

None used

## 5. ASSUMPTIONS

The following assumptions are used in the course of this report:

- 5.1 *It is assumed that the effluent from the WP is not chemically affected by its contact with the invert when precipitation in the fracture system is considered.* The rationale for this assumption is that it is conservative for fracture precipitation because no fissile material is lost in the invert and all of the fissile material is available to be precipitated in the fractures underneath the drift. This assumption is used in Section 6.2.1.1.
- 5.2 *It is assumed that advective transport occurs in the vertical direction.* The rationale for this assumption is that most of the fractures are vertical (BSC 2001k, Section 6.5). This assumption is used throughout. A corollary of this assumption is that vertical permeabilities are used. This assumption is used in Section 6.1.1.
- 5.3 *It is assumed that all the fractures within the tuff beneath the WP (as depicted in Figure 2) are conductive to water.* The rationale for this assumption is that the connectivity of fractures is high (BSC 2001k, Section 6.10) and that it is conservative for mineralization. This assumption is used in Section 6.1.1.
- 5.4 *It is assumed that all of the fractures have the same average aperture.* The rationale for this assumption is the following: if it were not the case, the largest fracture(s) would take most of the flow according to the cubic law (Domenico and Schwartz 1990, pp. 86-87). This assumption is then conservative because it leads to a more compact mineralization

shape. Aperture variability would favor the widest fractures and would lead to a more elongated mineralization that is less conservative for criticality. This assumption is used in Section 6.1.1.

- 5.5 *It is assumed that the fracture aperture is constant within a single fracture.* The rationale for this assumption is that it is conservative. In reality, apertures vary within the same fracture. However, this assumption is conservative because it leads to a more compact mineralization shape. Aperture variability would favor a few sections of the fractures and lead to a more elongated mineralization that is less conservative for criticality. This assumption is used in Section 6.1.1.
- 5.6 *It is assumed that there is no channeling in the fracture planes.* No part of the fracture is restricted from flow and from the accompanying precipitation and dissolution. The rationale for this assumption is that it is conservative because it increases the surface area available for tuff dissolution and leads to a more compact mineralization shape. This assumption is used in Section 6.1.1.
- 5.7 *It is assumed that the fracture surface area is independent of fracture aperture.* The fracture surface area is calculated as the surface area of parallel plates; the distance between them has no effect on the surface area. The rationale for this assumption is that the increase in surface area resulting from a different model would be difficult to ascertain and can be addressed by sensitivity studies. This assumption is used in Sections 6.1.1 and 6.7.5.
- 5.8 *It is assumed that the accumulation envelope is cone-shaped and that the actinide density is constant by layer.* The basis for this assumption is that as dilution progresses, the reactive domain encompasses more and more rock volume because of conservation of mass. Because of the linear dimension of the drift, a wedge-shaped accumulation could have been promoted. It is, however, more appropriate to use the more conservative cone-shaped accumulation because the water deflected by the WP/Drip Shield (DS) system brings dilution in the third dimension parallel to the drift. This assumption is used in Sections 6.1.1, 6.4, and 6.8.3.1.
- 5.9 *It is assumed that, in the equivalent fracture system, mineral accumulation occurs evenly over the surface area open to deposition.* This assumption applies both to lithophysal cavities and to fractures, where only large fractures are likely to receive some mineralization. The rationale is that it is conservative from a criticality standpoint. This assumption is not applied when a single lithophysae is considered. This assumption is used in Section 6.1.1.
- 5.10 *It is assumed that the depth of dilution is 10 meters in all cases independently of infiltration rate, focusing multiplier (defined in Section 6.4.2), or fracture saturation.* The basis for this assumption is that it is conservative to choose a low value so that accumulation occurs in a small volume, as close to the drift as possible. A value of 10 is significantly lower than the lowest analytical calculated value (22 m) or than the numerical model results, as described in Section 6.4.1. This assumption is used throughout the document.

- 5.11 *It is assumed that solutes do not diffuse into the rock matrix.* The rationale for this assumption is that deposits are likely to plug small pores responsible for matrix diffusion. This will happen at early times preventing a significant quantity of radionuclides from diffusing into the matrix. This assumption is used throughout the document.
- 5.12 *It is assumed that the surface area and volume of fractures do not change as the tuff dissolves.* The rationale for the first part of this assumption is that it is conservative because it maximizes the amount of chemical elements released, such as Si, needed for actinide precipitation. The tuff surface area would probably decrease because of the precipitation of alteration products or new minerals. The second part of the assumption is conservative as well because it leaves a larger surface area per liter of water available for precipitation of radionuclides (BSC 2001I, Figure 6-9). This assumption is used in Section 6.7.5.
- 5.13 *It is assumed that all the drift seepage flows from the crown area.* The basis for this assumption is that very little water enters the drift outside of the crown area. The crown area is the top of the drift as shown in Figure 3. This assumption is used in Section 6.4.2.1.
- 5.14 *It is assumed that only drift seepage rates between 1 and 20 liter/year are relevant to this analysis.* The basis for this assumption is that only those cases with low flux through a WP may increase the probability of criticality. The range takes into account the fact that not all the drift seepage flux may flow into a WP but some may be deflected by the DS of the WP system. This assumption is used in Section 6.4.2.1.
- 5.15 *It is assumed that longitudinal dispersivity is about 10% of the characteristic length of the system for a fractured saturated medium with good connectivity and the same as the system characteristic length for a fractured unsaturated medium.* In this work, the characteristic length of the system is equivalent to the length of the dilution zone (as given in Assumption 5.10). CRWMS M&O 2000f (Attachment II) details the rationale for this assumption. This assumption is used in Section 6.4.2.2. *It is further assumed that transverse dispersivity is approximately 10% of the longitudinal dispersivity.* The rationale for this assumption is justified in CRWMS M&O 2000f (Attachment II). This assumption is used in Section 6.4.2.2.
- 5.16 *It is assumed that all solids that are deposited remain in place; no solids are entrained or otherwise re-mobilized, except possibly by dissolving later.* The rationale for this assumption is that it is conservative because it precludes the loss of fissile material from the mineralization region as suspended solids. This assumption is used in Section 6.1.1.
- 5.17 *It is assumed in the equivalent fracture intensity model that a lithophysae is intersected by only one fracture and that all lithophysae have the same size.* (Fracture intensity is defined in Section 6.3 as the total length of fracture per unit area.) To achieve that effect which maximizes the equivalent fracture intensity, the longest dimension of a lithophysal cavity is taken as  $\frac{1}{4}$  of the fracture spacing (average distance between two successive parallel fractures). The basis for this assumption is that it maximizes the accumulation density and is, thus, conservative. The implication of this model is that the higher the fracture intensity, the smaller the lithophysae. This assumption is used in Section 6.3.4.

- 5.18 *It is assumed that in the stand-alone lithophysae model, the dilution of the effluent WP water by the resident water is directly and linearly a function of the local fracture intensity. The basis for the assumption is that, on average, the amount of water seeping into a lithophysal cavity increases with the fracture intensity. Because all fractures are assumed to have the same aperture (Assumption 5.4), they carry the same water flux. Dilution is then a linear function of the fracture intensity. This assumption is used throughout the document.*
- 5.19 *It is assumed that the relationship between fracture saturation and relative permeability follows the Van Genuchten formulation. The rationale for this assumption is that it is reliable except at very low water saturation. At very low water saturation, whether or not the assumption holds is unimportant because low water saturation systems are less prone to critical mineral deposition. This assumption is used in Section 6.4.1.*
- 5.20 *It is assumed that 25°C thermodynamic data can be used for the calculations. The rationale for this assumption is that although the initial breach of the WP may occur at 10,000 years, when the WP contents are at temperatures ~50°C (CRWMS M&O 2000a, Figure 4.6-2, p. F4-49), at times > 25,000 years, the WP temperatures are likely to be close to 25°C. This assumption is used in Section 6.8.1.*

## 6. ANALYSIS / MODEL

### 6.1 THE CONCEPTUAL MODEL

Based on the screening criteria provided in AP-3.15Q, Managing Technical Product Inputs, this AMR does not include estimates of any "Principal factors" or "Other Factors" and is thus assigned an importance level of 3 per AP-3.10Q.

The external accumulation model considers accumulation in three different geometries within the tuff: (1) fractures only, (2) fractures with small lithophysae, and (3) large stand-alone lithophysae only. Figure 2 shows the waste package and an idealized representation of lithophysae and fractures in the tuff immediately beneath. The first step in the model for all three geometries is running PHREEQC to determine the amount of U and Pu minerals that precipitate in the rock. The subsequent steps involve using Microsoft Excel to make further calculations to yield results of total accumulation (moles) and accumulation density ( $\text{mol}/\text{m}^3$ ). The steps involved in running the model for the fractures-only geometry and the fractures-with-lithophysae geometry are summarized first, followed by the steps to run the model for the stand-alone lithophysae.

#### 6.1.1 Fractures-Only Geometry and Fractures-with-Lithophysae Geometry

**Step 1**—Run PHREEQC to determine the transport and accumulation of U and Pu in a system containing minerals similar to those found in the tuff at Yucca Mountain. The advective transport is assumed to occur mainly in the vertical direction (Assumption 5.2). It is also assumed that all fractures are conductive to water (Assumption 5.3) and have the same aperture (Assumptions 5.4 and 5.5). It is also assumed that there is no channeling in the fracture planes

(Assumption 5.6), and the fracture surface area is independent of fracture aperture (Assumption 5.7). It is assumed that inputs include the WP effluent water compositions generated by EQ6, drip rate, description of the minerals composing the tuff, composition of water mixing with WP effluent, and mixing ratio of WP effluent to mixing water.

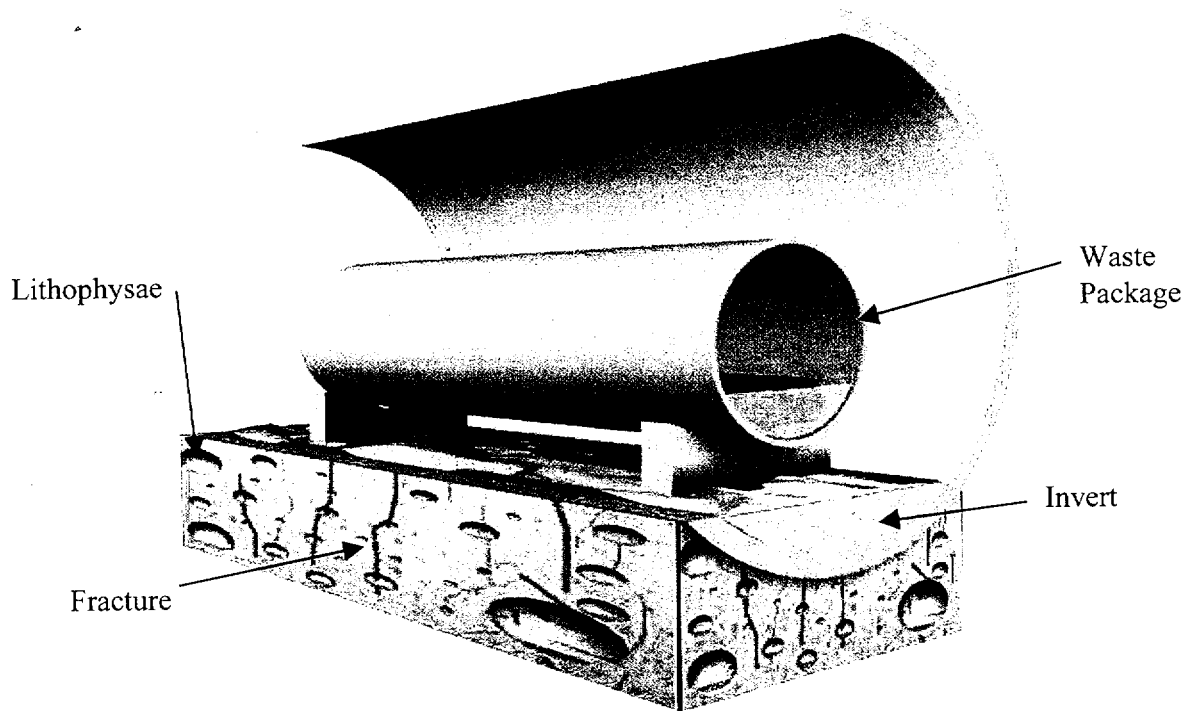


Figure 2. Far-Field Representation (not to scale)

**Steps 2-9**—Using Microsoft Excel, calculate the total accumulation in the tuff. Calculate the dimensions of the precipitation zone. It is assumed that the accumulation envelope is cone-shaped and that the actinide density is constant by layer (Assumption 5.8). In all cases it was assumed that mineralization is uniformly distributed over all the fractures (Assumption 5.9) and lithophysae (Assumption 5.9 - except in the stand-alone lithophysae cavity case). In addition, it was assumed that no solid precipitates in the matrix (Assumption 5.11); and there is no remobilization of precipitated minerals (Assumption 5.16). Inputs include fracture porosity, fracture saturation, fracture aperture, local infiltration rate, shadow zone (the depth of the mixing zone below the WP), and output from Step 1.

### 6.1.2 Large Stand-Alone Lithophysae Geometry

**Step 1**—Run PHREEQC to calculate the accumulation in a large lithophysae (Assumption 5.18). Inputs include the WP effluent water compositions generated by EQ6, water composition of water mixing with WP effluent, and volumes of mixing water that is mixed with 1 liter of WP effluent.

**Steps 2-5**—Calculate the total accumulation of U and Pu. Calculate the percentage of the lithophysae filled with the Pu and U minerals for different volumes of mixing water that is mixed with 1 liter WP effluent. Inputs include molar volumes ( $\text{cm}^3/\text{mole}$ ) of minerals formed, diameter of lithophysae, and outputs from Step 1.

## **6.2 DEVELOPMENT OF THE MODEL**

There are three types of open spaces where actinide deposition can occur (Figure 2):

1. Fractures
2. Matrix pores (the rock between the fractures)
3. Lithophysae.

The matrix pores are not treated in this document (Assumption 5.11). Lithophysae are treated in two ways: as a stand-alone lithophysal cavity for large size lithophysae (Section 6.5) or part of the fracture network for a large number of smaller lithophysae (Section 6.3.4). Section 6.3.3 presents statistics and extrapolation of the different types of porosity.

The main mode for maximizing actinide precipitation is dilution under unsaturated conditions. The driving force is the decrease in pH. CRWMS M&O 2000f (Section 2.1.4) details the dilution mechanism. Alternative mechanisms for actinide accumulation are discussed in Section 6.8.3.

### **6.2.1 Mixing Loci**

Actinide precipitation can occur as the result of mixing waters with different properties (in particular with different pH values). It then becomes important to understand the details of the flow patterns leading to mixing.

#### **6.2.1.1 Sources of Dilution in the Drift**

A sketch of an emplacement drift (Figure 3) reveals that there are three sources of dilution of the actinide-laden effluent water in the invert:

- Water flowing along the outside wall of the WP but not through the WP
- Water diverted by both the outside surface and the underside of the DS
- Water diverted along the drift wall or seeping from the drift sides.

This model currently assumes that the invert is bypassed (Assumption 5.1) and that most of the drift seepage water flows through the WP.

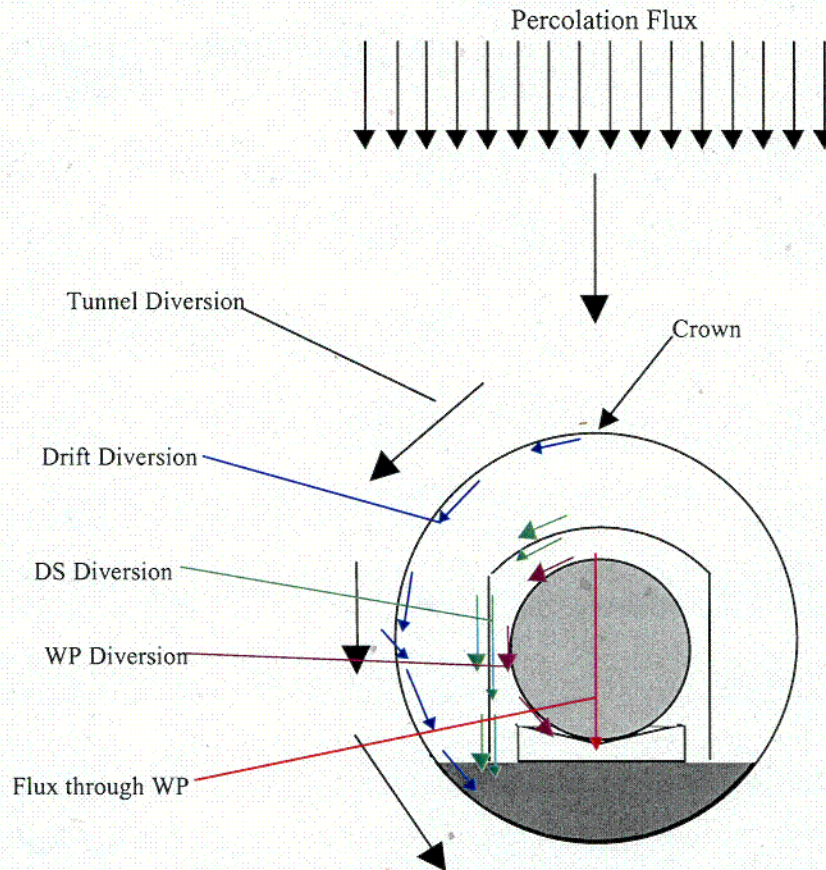


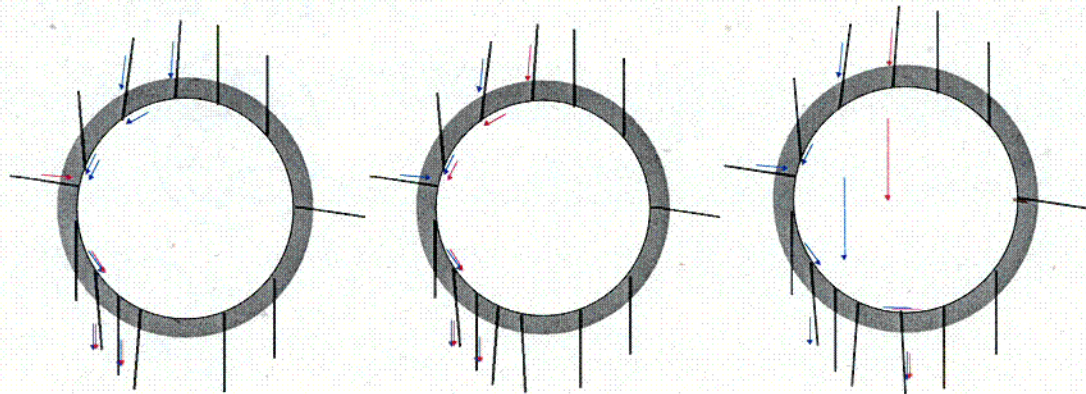
Figure 3. Sketch of the Drift Dilution Loci

### 6.2.1.2 Fracture System

The fracture system beneath the drift receives both water diverted by the emplacement drift tunnel (Figure 3) and water flowing through the invert to the rock. Within the rock, mixing can occur in the plane of a single fracture where channels of different origin meet and at the connection between two fractures.

### 6.2.1.3 Lithophysae

Mixing can occur on the walls or at the bottom of the lithophysae (Figure 3). For large lithophysae, the water flows through the fractures and into the lithophysae where mixing occurs. The number of fractures carrying the resident water is assumed to relate directly to the volume of resident water involved in the mixing (Assumption 5.18). A lithophysae with a large number of fractures carrying resident water indicates a large volume of resident water mixing with the WP effluent.



(a) Flow along the cavity walls and mixing only at the bottom of the cavity  
 (b) Flow along the cavity walls and mixing over the whole internal surface of the cavity  
 (c) Dripping flow and mixing only at the bottom of the cavity  
 NOTE: Blue and red arrows denote WP effluent water and resident water, respectively.

Figure 4. Conceptual Model of Flow Through a Lithophysae

### 6.3 GEOMETRIC CHARACTERISTICS OF FRACTURES AND LITHOPHYSAE

Fracture systems in the host rock and lithophysae in the vicinity of the proposed repository determine the density of the accumulation of fissile material. Accumulation in the fracture network depends on the fracture porosity, which is the product of two terms: the average fracture aperture ( $[L]$ ) and the fracture intensity ( $[L^{-1}]$ ). The fracture intensity (in  $m/m^2$  or  $m^2/m^3$ ) for accumulation purposes is better described by the total length of fracture per unit area (2D fracture intensity) or by the total surface area per unit volume (3D fracture intensity) than by the fracture frequency (number of fractures in a unit distance in  $1/m$  or 1D fracture intensity). Fracture frequency results from direct field measurements and is the simplest measure of fracture intensity. However, 2D or 3D fracture intensity measures are more appropriate for accumulation purposes because they truly describe the void space due to fractures. Because most fractures are almost vertical, 2D and 3D fracture intensity measurements are equivalent, the unit of  $m/m^2$  (2D fracture intensity) will be used in this document to distinguish it from fracture frequency expressed in  $1/m$ . The following porosity values (Table 3) summarize the relevant results of BSC 2001k for typical and extreme values found in the ECRB cross-drift. Extrapolated values to very high fracture intensity are presented in Section 6.3.3. Those very high values are needed to approach the threshold for criticality (McClure and Alsaed 2001).

Table 3. Fracture and Lithophysae Porosity in the Repository Units

Formation	Worst Case	95% Confidence Interval	Median
TSw34	2.7%	1.2%	0.4%
TSw35(1)	2.0% + 27%L <sup>a</sup>	1.2% + 18%L <sup>a</sup>	0.9% + 7.1%L <sup>a</sup>
TSw35(2)	4.1%	N/A	N/A
TSw36	6.5%	2.8%	0.8%

Source: BSC 2001k, Table 7-1

NOTE: <sup>a</sup>L = Percent porosity of lithophysae, for example, 27%L indicates an additional 27% porosity is due to small lithophysae.

COY

### 6.3.1 Fracture Aperture

The median of the aperture is approximately 740  $\mu\text{m}$  (DTN: MO0109SPAFIE10.006; worksheet "Transport Aperture"). The distribution is lognormal and the fracture aperture at 2 standard deviations is 2 mm or more. However, the largest aperture cannot be sustained for all fractures when the fracture intensity is high. DTN: MO0109SPAFIE10.006 (worksheet "Transport Aperture") presents the average aperture at 95% and 99.5% confidence interval in a fracture set of up to 80 fractures (for 80 fractures: ~840  $\mu\text{m}$  and 870  $\mu\text{m}$ , respectively). Table 10 provides values of fracture aperture for the 50<sup>th</sup> percentile, 95<sup>th</sup> percentile, and worst case.

### 6.3.2 Lithophysae Porosity

Lithophysae vary in size from a fraction of a cm to over 1.0 m in diameter within the TSw35 unit (average diameter is about 18 cm). Lithophysae porosity and size distributions were derived in BSC 2001k (Section 6.4) and are given in DTN: MO0102SPALIT10.001.

### 6.3.3 Probability of High Fracture Intensity

The goal of this section is to determine the probability of high fracture intensity areas. The high fracture intensity areas cannot be sustained for long in the horizontal direction because geostatistical analyses have determined that the correlation length is small in this direction (BSC 2001k, Section 6.9.3). Semi-variograms of fracture spacing are almost flat suggesting that 2 or 3 fractures tightly clustered with a small spacing do not infer that the next fracture is also closely attached to the same group (in other words the correlation length is small). However, high fracture intensity in the vertical direction is more common as it is one of the main fracture directions. Since most fracture surveys use a minimum fracture length cutoff of 1 m, the fracture frequency for fractures > 1 m is well known. This parameter, however, gives an incomplete picture of the total space open for accumulation. Since the connectivity of the fracture network is good (BSC 2001k, Section 6.10), even the tiniest fracture can not be excluded from mineralization.

In this section the probability of high fracture intensity is presented for each hydrologic unit. Because of the way the measurements were made, it is convenient to categorize the fractures according to their length: fractures greater than 1.0 m, fractures between 1.0 and 0.3 m, and fractures smaller than 0.3 m. The starting point of the procedure (explained in more details in Section 6.9 of BSC 2001k) uses the extensive fracture frequency data sets for fractures > 1.0 m. The probability of fracture frequency for fractures > 1.0 m can then be extrapolated to any number of fractures according to the Complementary Cumulative Distribution Function (CCDF) extrapolation as given in Table 4.

Table 4. CCDF of the Average Number of Fractures >1 m per meter

Fracture Frequency for Fractures > 1 m (1/m)	Unit TSw34	Unit TSw35	Unit TSw36
1	5.781E-01	2.344E-01	1.874E-01
2	3.324E-01	4.807E-02	9.490E-02
3	1.469E-01	1.650E-02	4.982E-02
4	4.623E-02	3.697E-03	1.305E-02
5	1.638E-02	1.138E-03	7.117E-03
6	4.096E-03	2.649E-04	1.186E-03
7	2.320E-03	6.837E-05	9.040E-04
8	1.014E-03	1.764E-05	3.485E-04
9	4.436E-04	4.553E-06	1.343E-04
10	1.940E-04	1.175E-06	5.178E-05
11	8.482E-05	3.032E-07	1.996E-05

Source: DTN: MO0109SPAFIE10.006

NOTE: Values in italics are extrapolated, values in regular prints are from actual field measurements.

Fracture intensity due to fractures > 1.0 m can then be computed (see below) by applying correction factors (Table 5) on the fracture frequency. The correction for non-verticality accounts for the dip of the fractures which is on average not quite vertical. For the same fracture frequency and the same aperture, the less vertical the fractures, the more material can accumulate in the same rock volume. This correction is obtained by noting that an overwhelming number of fractures have a dip larger than 65° and the extra-length added by nonverticality is 1/sin(65°)~1.1 (BSC 2001k, Section 6.9.6). The correction for survey bias takes into account the measurement artifact that fracture azimuth and drift bearing where the measurements are made is not always orthogonal. This correction is made by averaging fracture orientation and local drift bearing. The smaller fractures correction adds those fractures < 0.3 m that have not been thoroughly studied but are always present. This correction is obtained from small scale survey data. More details about its origin are given later in this section.

Table 5. Correction Factor for Fracture Intensity for Fractures > 1 m

	TSw34	TSw35	TSw36
Non-verticality	1.1	1.1	1.1
Survey bias	1.18	1.12	1.18
Smaller fractures (<0.3 m)	1.33	N/A (=1.0)	1.40
<b>U<sub>ACC1</sub></b> (product of individual correction factors)	<b>1.726</b>	<b>1.232</b>	<b>1.817</b>

Source: DTN: MO0109SPAFIE10.006

The second step is to add the fracture intensity due to fractures < 1 m (uncorrected fracture intensity in Table 6 and Table 7 with correction factors in Table 8. ). There are few measurements for these fractures. They are made mainly in the small scale survey in the ECRB.

By comparing data for fractures > 1.0 m and fractures < 1.0 m at the same location, one can infer their relationship. There is a difference in treatment for fractures whose length is between 1 and 0.3 m in lithophysal (TSw35) and non-lithophysal (TSw34 and TSw36) units. It has been determined for non-lithophysal units that the total number of fractures for with lengths between 0.3 and 1 m is independent of the fracture frequency at a 1-meter scale (BSC 2001k, Section 6.9.8). Because the distribution already takes into account fractures < 0.3 m, the correction factors  $u_{ACC1}$  and  $u_{ACC2}$  for unit TSw35 do not include a correction for small fractures.

Table 6. CCDF of Uncorrected Fracture Intensity for Fractures with Length between 0.3 and 1 m (TSw34 unit)

Uncorrected Fracture Intensity (m/m <sup>2</sup> )	CCDF
1	5.5440E-01
2.1	2.1848E-01
3	7.5993E-02
4	2.6770E-02
5.04	7.7720E-03
6.1	4.3178E-03
7.21	8.6356E-04
8	<i>3.9926E-04</i>
9	<i>1.3601E-04</i>
10	<i>4.6331E-05</i>
11	<i>1.5783E-05</i>
12	<i>5.3764E-06</i>
13	<i>1.8315E-06</i>

Source: DTN: MO0109SPAFIE10.006

NOTE: Extrapolated data are in italics.

Table 7. CCDF of Uncorrected Fracture Intensity of Fractures with Length < 1 m (TSw35 unit)

Uncorrected Fracture Intensity (m/m <sup>2</sup> )	CCDF	Uncorrected Fracture Intensity (m/m <sup>2</sup> )	CCDF
0.29	9.286E-01	8	5.854E-02
2.774	8.571E-01	9	3.534E-02
2.984	7.857E-01	10	2.133E-02
3.053	7.143E-01	11	1.288E-02
3.855	6.429E-01	12	7.772E-03
4.21	5.714E-01	13	4.692E-03
4.525	5.000E-01	14	2.832E-03
4.55	4.286E-01	15	1.709E-03
4.64	3.571E-01	16	1.032E-03
4.963	2.857E-01	17	6.229E-04
5.19	2.143E-01	18	3.760E-04
6.56	1.429E-01	19	2.269E-04
7.415	7.143E-02	20	1.370E-04

Source: DTN: MO0109SPAFIE10.006

NOTE: Extrapolated data are in italics

Table 8. Correction Factor for Fracture Intensity for Fractures < 1 m

	TSw34	TSw35	TSw36
Survey bias	1.18	1.12	1.18
Survey area	1/0.6	1/0.6	1/0.6
Smaller fractures (< 0.3 m)	1.33	N/A (1.0)	1.4
<b><i>u<sub>ACC2</sub></i></b> (product of individual correction factors)	<b>2.616</b>	<b>1.867</b>	<b>2.753</b>

Source: DTN: MO0109SPAFIE10.006

From a numerical value of fracture intensity, the number of composite fractures to be used in the criticality calculations is determined. Some small and long fractures are assumed to combine to make an ideal composite vertical plane. The process is repeated to make another ideal plane parallel to the first one. If two sets of fractures are present, the process produces two sets of ideal parallel planes. Because the fracture intensity was calculated for 1 m<sup>3</sup> of rock, each of these ideal planes has a surface of 1 m<sup>2</sup>. This in turn yields the numerical correspondence between fracture intensity and number of composite fractures (a fracture intensity of 10 m/m<sup>2</sup> yields 10 composite fractures since each fracture plane has a surface of 1 m<sup>2</sup>).

Table 9 summarizes the previous results for fracture intensity. It will be used to stochastically generate fracture intensity to obtain a final probability of high fracture intensity in the software fracpc2.c (BSC 2001j). In essence, two random numbers between 0 and 1, *rdn1* and *rdn2*, need to be generated. Taking TSw34 as an example, also valid for TSw36, *rdn1* will provide the

fracture intensity due to fractures > 1 m sampled from Table 4 (find *rdn1* in column 2 and then the corresponding value of the fracture frequency in column 1). This value needs to be corrected as described above. The correction factor is 1.726 as read from Table 5. The random number *rdn2* will initiate the sampling of the uncorrected fracture intensity due to fractures < 1 m. The value is read from Table 6. It also needs to be corrected by the multiplying factor of 2.616 as read in Table 8. Because those two distributions are independent (BSC 2001k, Section 6.9.8), the resulting total fracture intensity is the sum of the fracture intensities of fractures > 1 m and fractures < 1 m.

In the case of the TSw35 unit, because fracture intensities of fractures > 1 m and fractures < 1 m cannot be proven independent, the relationship is multiplicative instead of additive (as showed in Table 9). For the TSw35 unit, the uncorrected fracture intensity for fractures < 1 m is sampled from Table 7 and corrected by the coefficient of 1.867 read in Table 8. Unlike units TSw34 and TSw36, the TSw35 unit uncorrected fracture intensity for fractures < 1 m needs to be further corrected by multiplying by the fracture frequency for fractures > 1 m. This is equivalent to having fracture intensity for both types of fractures increasing in a constant ratio (instead of being independent as in units TSw34 and TSw36). The rest of the calculation proceeds as in the TSw34 and TSw36 cases by adding that fracture intensity due to fractures > 1 m (fracture frequency value read from Table 4 and coefficient of 1.232 read from Table 5, their product gives the fracture intensity due to fractures > 1 m).

Table 9. Summary of Fracture Intensity for Stochastic Sampling

	Fracture Intensity (m/m <sup>2</sup> )
TSw34	1.726×"Table 4" + 2.616×"Table 6"
TSw35	1.232×"Table 4"+1.867×" Table 7"×"Table 4"
TSw36	1.817×"Table 4" + 2.753×"Table 6"

Source DTN: MO0109SPAFIE10.006

NOTE: "Table 4", "Table 6" and "Table 7" stand for the sampled table numbers. The coefficients are given in Table 5 and Table 8.

### 6.3.4 Equivalent Fracture Intensity

This section treats the lithophysae solely as an additional surface area for deposition and neglects mixing time constraints and kinetics (BSC 2001l, Section 5.4.1). When a single fracture intersects a lithophysal cavity along its diameter, the surface area available to water flow and deposition increases from a plane to a sphere. This case is relevant when the lithophysae are small (smaller than the fracture spacing) and when few fractures intersect the lithophysae. When numerous fractures intersect the same lithophysal cavity, there is a net loss of surface area.

A small parametric study determines the fracture intensity at which the change in surface area becomes a net loss. One fracture can intersect a spherical lithophysal cavity through its center. In this case, the change in surface area can be expressed by the ratio of the surface area of a sphere to the surface area of two circles:  $4\pi R^2 / (2\pi R^2) = 2$ , that is a ratio of the planar surface area to the spherical surface area of 0.5. Similarly, if the fracture plane is tangent to the sphere, the ratio of the planar surface area to the spherical surface area is 0. The same calculation can be done for more than one plane. BSC 2001l (Section 5.4.4) suggests that in the case of spherical

cavities, the total surface area increases only if the fracture intensity of fractures from the same orientation set is less than  $3/\text{diameter}$ . For a master plane including the center of the sphere of radius  $R$ , the increase in surface area is  $4\pi R^2 - 2(\pi R^2) = 2\pi R^2$ . This translates into an equivalent increase in fracture intensity expressed in  $\text{m}/\text{m}^2$  of  $\pi R^2$  (fracture intensity does not take into account the two walls of the fracture but only considers fractures as immaterial planes, hence adding a fracture with a surface area of  $2\pi R^2$  adds only  $\pi R^2$  to the fracture intensity).

To derive an equation for the maximum equivalent fracture intensity, it is assumed that all lithophysae have a fracture through their center (Assumption 5.17) and that all have the same radius  $r$ . In Equation 1, the number of lithophysae in a volume of rock,  $N$ , is set equal to the lithophysae porosity,  $\eta$ , (void volume per volume of rock) multiplied by the rock volume  $V$  and divided by the volume of one spherical lithophysae, with a radius of  $r$ , that has a void volume equal to a sphere:  $(4/3)\pi r^3$ . If  $V$  is set equal to  $1 \text{ m}^3$ , then  $V$  in Equation 1 is eliminated. The number  $N$  of lithophysae is expressed by:

$$N = \frac{\eta V}{4/3\pi r^3} = \frac{\eta}{4/3\pi r^3} \quad (\text{Eq. 1})$$

If each lithophysal cavity is intersected by one single fracture, the increase in fracture intensity  $F.I._{add}$  is the number of lithophysae times the increase in fracture intensity for one lithophysae. A sphere surface area is  $4\pi r^2$ , the initial surface area of the fracture at the location of the sphere is  $2\pi r^2$ , hence the increase in surface area is  $4\pi r^2 - 2\pi r^2$ . The factor 0.5 takes into account the fact that a single fracture is considered as an immaterial plane for the  $F.I.$  computations, not as 2 closely-spaced parallel planes.

$$F.I._{add} = 0.5N(4\pi r^2 - 2\pi r^2) = \pi r^2 \quad (\text{Eq. 2})$$

Hence:

$$F.I._{add} = \frac{3\eta}{4r} \quad (\text{Eq. 3})$$

Equation (Eq. 3) shows that the smaller the lithophysal cavity, the greater the added fracture intensity. However, the lithophysae radius must be large enough to be intersected by fractures. It is conservatively assumed that the radius is  $1/4$  of the fracture spacing (average distance between two successive parallel fractures)  $sp$  but still that all lithophysae are cut by fractures (Assumption 5.17). Equation (Eq. 3) becomes:

$$F.I._{add} = \frac{3\eta}{sp} \quad (\text{Eq. 4})$$

The same derivation can be done for a cube of side  $a_c$ , then a box of cross-section  $a_b$  and length  $L$ . In the case of a cube, the number  $N$  of lithophysae is (with Assumption 5.17):

$$N = \frac{\eta}{a_c^3} \quad (\text{Eq. 5})$$

A cube surface area is  $6a_c^2$ , the initial surface area of the fracture at the location of the cube is  $2a_c^2$ , hence the increase in surface area is  $6a_c^2 - 2a_c^2$ . The factor 0.5 takes into account the fact that a single fracture is considered as an immaterial plane for the *F.I.* computations, not as 2 closely-spaced parallel planes.

$$F.I._{add} = 0.5N(6a_c^2 - 2a_c^2) = 2Na_c^2 \quad (\text{Eq. 6})$$

Hence

$$F.I._{add} = 2 \frac{\eta}{a_c} \quad (\text{Eq. 7})$$

If it is assumed again that half the cube side is 1/4 of the fracture spacing:

$$F.I._{add} = 4 \frac{\eta}{sp} \quad (\text{Eq. 8})$$

The box of dimensions  $L \times a_B \times a_B$  (representing a lithophysal cavity) is assumed to be lying flat on its longer side perpendicular to the mostly vertical fractures. The box surface area is  $4a_B L + 2a_B^2$ , the initial surface area of the fracture at the location of the box is  $2a_B^2$ , hence the increase in surface area is  $4a_B L + 2a_B^2 - 2a_B^2$ . The factor 0.5 takes into account the fact that a single fracture is considered as an immaterial plane for the *F.I.* computations, not as 2 closely-spaced parallel planes. Therefore,  $N = \frac{\eta}{a_B^2 L}$ :

$$F.I._{add} = 0.5 \left( \frac{\eta}{a_B^2 L} \right) (4a_B L + 2a_B^2 - 2a_B^2) = \frac{2\eta}{a_B} \quad (\text{Eq. 9})$$

Next, the shape ratio is introduced:  $r_s$  ( $r_s = L/a_B$ ) and assuming, similarly to the sphere and cube, that half the longest box side is 1/4<sup>th</sup> of the fracture spacing (Assumption 5.17):

$$F.I._{add} = \frac{4r_s \eta}{sp} \quad (\text{Eq. 10})$$

Because many lithophysae, especially those of medium size, are elliptic or even gash-like, a value of 2 is retained for  $r_s$ . The value of 2 was chosen as a compromise between the spherical and elliptical cavities. The true value is likely to be smaller than 2 because most lithophysae especially small ones are spherical. The box shape is assumed to include the shape irregularities:

$$F.I._{add} = \frac{8\eta}{sp} \quad (\text{Eq. 11})$$

The inverse of the average fracture spacing (equivalent to the number of fractures in a given fracture orientation set over 1 m) is conservatively taken as the maximum of the number of fractures in the three orientation sets (2 vertical and 1 horizontal). This choice yields the highest fracture intensity, i.e. the highest accumulation space.

Some results are displayed in Table 10 for three different cases: worst case, 95<sup>th</sup> percentile and median. The worst case represents a combination of extreme values, all observable in the field (Exploratory Studies Facility and ECRB tunnels). It is possible to come up with worse cases with the extrapolation of Section 6.3.3. Column 3 gives the average angle between the two vertical sets of fractures. Column 7 gives the fracture intensity for each unit or sub-unit. Columns 4, 5 and 6 give the relative importance of each direction set. Their sum equals the value in Column 7. Column 8 gives the fracture aperture. The largest fracture apertures are used in the worst case while the median fracture apertures are used in the median case. The product of columns 7 and 8 yields the fracture porosity. Column 10 gives the lithophysae porosity. The same conventions as in the fracture aperture are used. The worst case assumes the largest measured lithophysae porosity while the median assumes the median lithophysae porosity. Column 11 gives the extra fracture intensity obtained with (Eq. 11). The spacing is given by only the most abundant set. Column 12 gives the corresponding diameter (not used in this analysis). Column 13 represents the sum of columns 7 and 11. The methodology can be extended to any fracture intensity, obtained in Section 6.3.3, by still using the relative importance of the different direction sets.

Table 10. Equivalent Fracture Intensity (that includes lithophysae)

1	2	3	4	5	6	7	8	9	10	11	12	13
Unit	Fraction [-]	Angle	# of fract. / m in			Tot. F.I. m/m <sup>2</sup>	Aper. (mm)	Fract. Por. [-]	Lith. Por. [-]	Add. F.I. m/m <sup>2</sup>	Lith. Diam. (cm)	Equ. F.I. m/m <sup>2</sup>
			Set 1	Set 2	Set 3							
WORST CASE												
TSw34	0.085	70°	18	9	1	28	0.99	2.7%	N/A	N/A	N/A	28
TSw35(1)		74°	13	4	1	18	1.12	2%	27%	28.1	3.85	46
TSw35(2)		74°	31	9	3	43	0.94	4.1%	N/A	N/A	N/A	43
TSw36	0.111	64°	37	29	7	73	0.89	6.5%	N/A	N/A	N/A	73
95 <sup>th</sup> PERCENTILE												
TSw34	0.085	70°	8	4	1	13	0.92	1.2%	N/A	N/A	N/A	13
TSw35	0.804	74°	8	3	1	12	1.02	1.3%	18%	13.0	5.6	25
TSw36	0.111	64°	16	13	3	32	0.88	2.8%	N/A	N/A	N/A	32
50 <sup>th</sup> PERCENTILE (MEDIAN)												
TSw34	0.085	70°	3	2	0	5	0.74	0.4%	N/A	N/A	N/A	5
TSw35	0.804	74°	8	3	1	12	0.74	0.9%	7.1%	5.1	5.6	17
TSw36	0.111	64°	5	4	1	10	0.74	0.8%	N/A	N/A	N/A	10

Source: DTN: MO0109SPAFIE10.006 (worksheet "porosity")

NOTE: Fraction = fraction of repository occupied by the unit  
 Tot. F.I. = Total fracture intensity (m/m<sup>2</sup> - 1 fracture corresponds to 1 plane and not 2)  
 Add. F.I. = Additional fracture intensity  
 Aper. = Fracture aperture  
 Lith. Diam = 1/2 minimum fracture spacing

#### 6.4 GEOMETRIC CHARACTERISTICS OF THE DILUTION-MIXING ZONE

The dilution-mixing zone below the drift is cone-shaped (Assumption 5.8). A cone is fully described by its base diameter and height, which is a function of:

- Characteristics of the media (Van Genuchten parameter *m*) that relates to the depth of the shadow zone. Section 6.4.1 gives details on the constant value of 10 meters chosen for the cone height. However, a possible change in that value does not invalidate the model.
- Ratio of total flux to the flux going through the WP (so-called dilution factor).
- Saturation of the fractures. The volume of the mixing zone increases with decreasing saturation (the smaller the saturation the larger size is required to reach a given dilution). It should be noted that the saturation present during accumulation does not have to match the saturation used for criticality calculations. A higher saturation can occur in an episodic event after the accumulation has occurred. A conservative value of 10% is used but values of saturation of 50% and 100% are also examined.

#### 6.4.1 Size of the Dilution-Mixing Zone

The mechanism of dilution is consistent with an analytical approach used by Philip et al. (1989) that describes flow perturbation induced by a cylindrical cavity in a uniform unsaturated flow field. Philip et al. (1989) determined the depth of the down gradient zone beyond which the flow field is back to its undisturbed condition (i.e., shadow zone). Similarly BSC 2001i (Section 11) presents results from numerical experiments. To approximate the depth of influence by Philip's equation it was necessary to determine relative permeability for the fracture system surrounding the drift. It was assumed that the relationship between fracture saturation and relative permeability follows the Van Genuchten formulation (Assumption 5.19). The Van Genuchten fracture parameters are used to calculate the geometric characteristics of the shadow zone following the procedure described in CRWMS M&O 2000f (Section 2.1). Results are presented in BSC 2001i (Table 5-25). A minimum depth of 22 meters was found. In a similar fashion, results from BSC 2001i (Figure 11.3.1-3) show that the shadow zone extends to at least 3 or 4 drift diameters for an infiltration rate of 10 mm/year. This is also corroborated by CRWMS M&O 2000c (Figures 6 and 7) where an infiltration rate of 500 mm/year was used although the shadow zone depth is in this case smaller than in the lower infiltration rate case. To take into account the heterogeneity of the media and the variability in flow rates, a final depth of 10 meters was selected (Assumption 5.10). This number was chosen as reasonably conservative. Clearly, further studies are needed. Eventually, a probabilistic distribution of the shadow zone length (for a given flow rate) will be used.

#### 6.4.2 Dilution

In this model, dilution is controlled by the total water flux and the water flux through the WP. The total water flux is the local infiltration rate, i.e., the average infiltration rate times the local focusing multiplier. Water moving downward in the UZ may be focused into preferential pathways with increased seepage in certain locations. The flow focusing multiplier is the ratio of local flux to average percolation flux. Dilution is equated to the ratio ( $> 1$ ) of those two fluxes. In other words, the dilution factor is the ratio of the volume of water that would flow through the same area if the drift were not there, to the volume of water that flows into the WP. The dilution factor is different from the mixing ratio defined as the constant fraction of resident water added to a PHREEQC cell. The partial dilution factor at cell  $i$  is the dilution level at that particular cell. The partial dilution factor in the last considered cell is the dilution factor as defined above. Each cell (at end of scaling) has about 10% more water than the previous cell. The progression is exponential. The final dilution factor is high in the cases of interest for criticality (in the thousands), i.e., there is a tremendous increase in the volume of water. The exponential increase is the most consistent with the cavity (drift opening) effect. The cavity effect brings more and more water to dilute the WP effluent (very little or even none at the beginning and then plenty when the flow is almost back to what it was above the drift opening).

##### 6.4.2.1 Infiltration and Seepage Rates

Information from this section is not directly used by the model but is eventually part of the final criticality probability. This section provides the probability that the flow through the WP is in the vicinity of 1 liter/year and the probability of a given dilution factor. Higher flow rates result in WP effluent with concentrations too low to generate significant accumulations of radionuclides. The software *SeepageFlow\_macro* is used to combine all seepage-related distributions into one single distribution. All seepage rates between 1 and 20 liter/year are

assumed to correspond to 1.5 or 15 liter/year respectively, through the WP (Assumption 5.14). The seepage rate is defined as the amount of water entering the drift from any location on the crown and walls in a 5.23 meter interval (21PWR or 44BWR WP length + 2 semi-intervals CRWMS M&O 2001d). Most of the seepage flows from the crown area, so it is conservatively assumed that 100% of the seepage rate flows from the crown area (Assumption 5.13).

Infiltration and seepage rates used to compute the bounding probability of final dilutions are given in DTN: SN0012T0511599.003. Seepage fraction (the fraction of the total number of WPs contacted by seepage into the drift, CRWMS M&O 2001d, Section 6.3.1), mean of seep flow rate (i.e., seepage rate), and standard deviation of seep flow rate are uncertain and follow a triangular distribution whose minimum, peak, and maximum are given in Table 11. The seepage rate itself follows a beta distribution whose parameters  $\alpha$  and  $\beta$  can be computed from the mean and standard deviation and whose lower and upper bounds are 0 and 10 standard deviations, respectively.

Table 11. Distribution of Seepage Versus Infiltration Flux

Infiltration Flux $q$ (mm/yr)	Seepage Fraction $F_s$ [-]			Mean of Seep Flow Rate (Seepage Rate) $Q_s$ (m <sup>3</sup> /yr)			Std.Dev of Seep Flow Rate $Q_s$ (m <sup>3</sup> /yr)		
	Min	Peak	Max	Min	Peak	Max	Min	Peak	Max
2.4	0	0	0	0	0	0	0	0	0
5	0	0	0.0831	0	0	0.0857	0	0	0.0395
14.6	0	0	0.0831	0	0	0.401	0	0	0.0955
60.0	0	0	0.31	0	0	0.701	0	0	0.815
73.2	0.0066	0.0541	0.376	0.365	0.365	0.788	0.0799	0.0799	1.02
213	0.0066	0.0541	0.452	3.99	4.24	4.24	0.21	0.21	2.34
500	0.0765	0.129	0.512	1.56	6.2	12.1	3.94	5.39	6.89
1000	0.261	0.303	0.609	27.1	30.9	35.6	16.1	17.3	18.5
3000	1	1	1	129	129	129	64.7	64.7	64.7

Source: DTN: SN0012T0511599.003

Table 12 presents the mountain-wide infiltration flux as a function of the climate. The local infiltration rate, however, could be increased by a flow focusing multiplier that follows a log-uniform distribution as given in Table 13. (Local infiltration rate is infiltration rate times the focusing multiplier).

Table 12. Average Infiltration Rates

Climate	Lower Bound (mm/year)	Mean (mm/year)	Upper Bound (mm/year)
Modern	1.3	4.6	11.1
Monsoon	4.6	12.2	19.8
Glacial Transition	2.5	17.8	33.0
Probability <sup>a</sup>	0.17	0.48	0.35

Source: CRWMS M&O 2000h, Table 3.5-4

NOTE: <sup>a</sup> Values given in CRWMS M&O 2000h (Section 3.5.3.2).

Table 13. Flow Focusing Multipliers

	Low Infiltration	Base Infiltration	High Infiltration
Min	1	1	1
Max	47.3	22.4	9.7

Source: DTN: SN0012T0511599.003

Using information from both Table 12 and Table 13, the highest local infiltration rate is approximately 400 mm/year (17.8 mm/year) × (22.4). Table 14 gives the current probability of the relevant seepage rates. The range of 1 to 20 liter/year was retained as relevant since the aqueous concentration of actinides in the WP effluent stream is high enough only for small flow rates (1.5 liter/year). Higher WP fluxes typically do not yield as much accumulation as lower fluxes although the total mass released from the WP may be higher than in a small flow rate case. However, the aqueous actinide concentration is then too small to lead to significant actinide accumulations. The upper bound of 20 liters accounts for the fact that some water is diverted from flowing into the WP by the DS and WP itself.

Table 14. Probability of Seepage Rate into Drift Being Between 1 and 20 liter/year

Climate	Probability
Modern	21.9% - 22.1%
Monsoon	11.6% - 12.2%
Glacial Transition	9.5% - 9.2%

Source: BSC 2001I, Table 5-21

NOTE: Results are from two Monte-Carlo runs (10,000 trials).

Dilution factors are obtained by calculating the ratio of the local infiltration rate (product of mountain scale infiltration rate and focusing multiplier) to the seepage rate. The percentiles of the distribution of the dilution factors are given in Table 15.

Table 15. Percentiles of Dilution Factor for the 3 Climates (seepage rate between 1 and 20 liter/year)

Climate	Minimum	5 <sup>th</sup> Perc.	25 <sup>th</sup> Perc.	Median	75 <sup>th</sup> Perc	95 <sup>th</sup> Perc.	Maximum
Modern	6.2 - 6.1	10.8 - 10.9	22.0 - 21.6	45.9 - 44.4	101.1 - 105.5	374.3 - 358.3	1518.1 - 1601.7
Monsoon	8.4 - 8.2	16.0 - 15.5	44.4 - 46.8	112.2 - 117.1	239.3 - 239.2	621.2 - 634.6	1196.5 - 1289.9
Glacial Transition	8.3 - 6.8	12.0 - 12.2	30.1 - 31.3	74.6 - 73.6	194.0 - 198.6	851.2 - 823.9	1513.1 - 1339.1

Source: BSC 2001I, Table 5-22

NOTE: Results are from two Monte-Carlo runs.

The connection between the result files (spreadsheet files "xxxx\_CritIn.xls" where xxxx stands for the source term name) and the dilution factors is given by Table 16:

Table 16. Correspondence between Local Infiltration Rate and Dilution Factor

Local Infiltration Rate (liter/year)	Dilution Factor for Effluent Flux = 1.5 liter/year	Dilution Factor for Effluent Flux = 15 liter/year
10,000	6667	667
1,000	667	66.7
500	333	33.3
100	66.7	6.7
50	33.3	3.3

The probability of each dilution factor can be computed by linear interpolation of Table 15. Dilution factors larger than the maximum of Table 15 can be assigned a CCDF of  $10^{-4}$ . This value is obtained by noting that the maximum values obtained during 10,000 Monte-Carlo trials do not change much between runs; this value is thus an upper bound for the probability.

#### 6.4.2.2 Thorough Mixing

In the model described in this document, the maximum accumulation can only be attained if there is a thorough mixing of the effluent and resident waters. The longitudinal dispersivity of 10% was assumed for a fractured medium (Assumption 5.15). BSC 20011 (Section 5.3.5) describes the approach used to compute the conditions favorable to thorough mixing.

Table 17 summarizes the results.

Table 17. Fracture Intensity needed for Thorough Mixing under Different Conditions

Ground Water Velocity (mm/year)	Under Molecular Diffusion Only	Under Dispersion		
		Sat=10%	Sat=50%	Sat=100%
1	4.3 m/m <sup>2</sup>	30 m/m <sup>2</sup>	83.6 m/m <sup>2</sup>	300 m/m <sup>2</sup>
10	43 m/m <sup>2</sup>	30 m/m <sup>2</sup>	83.6 m/m <sup>2</sup>	300 m/m <sup>2</sup>
100	430 m/m <sup>2</sup>	30 m/m <sup>2</sup>	83.6 m/m <sup>2</sup>	300 m/m <sup>2</sup>

Source: BSC 20011, Table 5-34

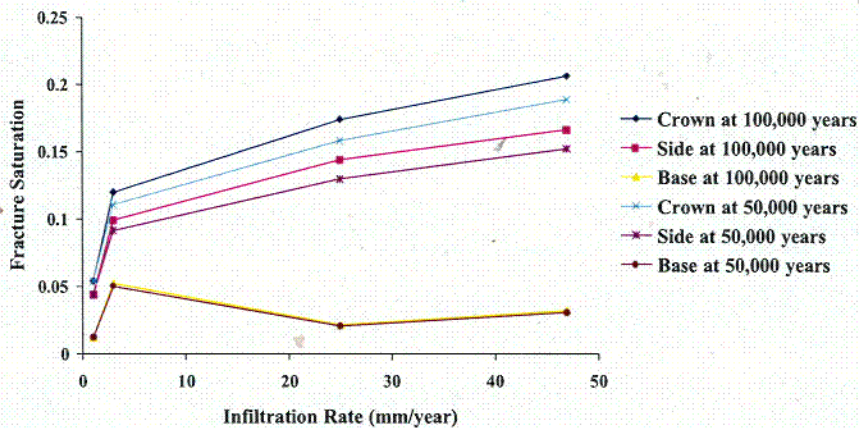
#### 6.4.3 Fracture Saturation

Fracture saturation is an important parameter because it has a very strong impact on the final accumulation density. Values of fracture saturation underneath the WP were obtained from the drift-scale Thermal Hydrological Chemical (THC) model with permeability homogeneous by layer (DTN: LB991200DSTTHC.002) and from the seepage model with a fully heterogeneous permeability field (CRWMS M&O 2000c, Figures 6 and 7). A high saturation could be produced by a low permeability, a high flow rate, or a partial plugging (through a drop in permeability). The full plugging case is of limited interest because it prevents mixing, and thus precipitation, from happening. The following development considers the increase of saturation mainly from the standpoint of increase in flow rate.

### 6.4.3.1 Homogeneity by Layer Permeability Model

In the homogeneous case, fracture saturation below the drift is slightly above or at residual saturation (1%). Host rocks saturation at the crown and on the side is between 10 and 20% depending on the infiltration rate (Figure 5). The saturation at the crown is a bounding value for the average saturation. It is expected to be higher at this location because of capillary barrier effects. A value of 10% saturation is used as an upper bound in the actinide accumulation result spreadsheets.

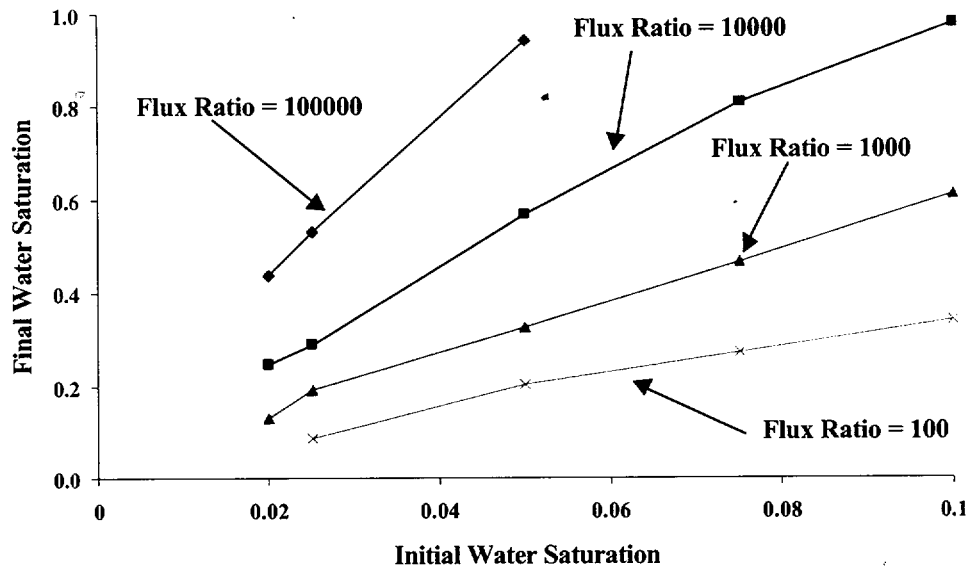
A simplistic linear extrapolation from the last 2 points of the "Base at 50,000 years" and "Base at 100,000 years" in Figure 5 (BSC 2001I, Section 5.3.6.1) suggests that at the highest infiltration rate (400 mm/year - Section 6.4.2) the saturation at the base of the drift would be in the vicinity of 20%.



Source: BSC 2001I, Figure 5-12

Figure 5. Fracture Saturation around the Drift at Different Infiltration Rates

This paragraph is to show that the assumption of linear extrapolation used in the previous paragraph is conservative and that a saturation of 20% is an upper bound. The simplistic model of Figure 6 plots, as a function of the initial saturation, the final saturation that would result from an increase in flux. It shows that the fracture system in its current saturation state can sustain a flux much larger than the current flux. An eight-fold increase of the infiltration rate (from 50 to 400 mm/year) generates an increase in drift seepage by less than a factor of 8. A flux ratio of 100 yields only an increase in saturation by a factor of 3 to 4. This would lead to a smaller increase in saturation than derived in the previous paragraph.



Source: BSC 2001I, Figure 5-13

NOTE: Flux ratio = ratio of final to initial flux.

Figure 6. Saturation Response to a Flux Increase in Fractures

#### 6.4.3.2 Stochastic Permeability Model

If it is hard to increase the saturation to high levels in the homogeneous case, heterogeneity can always provide cases when this is possible. TOUGH2 modeling runs done for the seepage model (CRWMS M&O 2000c) use a stochastic permeability field. Results (CRWMS M&O 2000c, Figures 6 and 7) show that the base of the drift is at residual fracture saturation or slightly above, consistent with the THC model results. The value of 10% saturation as an upper bound is also retained as in Section 6.4.3.1. It is, however, possible to imagine zones with lower permeability where local saturation would be higher. To account for this, actinide accumulation results are also calculated for saturation of 50% and 100%. The 100% saturation case is actually a saturated case whose flow dynamics would be different from the unsaturated case. It is nevertheless considered as a limit to unsaturated cases rather than as a true saturated case.

#### 6.4.3.3 Probability of a Given Saturation

Four saturation cases are typically used in this model: the typical case with a saturation of 10% (or sometimes 5% in the low flow rate cases) and more extreme cases with a saturation of 50% and 100%. An upper bound of the probability of those two cases can be estimated by noting that high saturation would be created by a combination of high seepage rates and low permeability. It should be noted that low permeability does not preclude high fracture intensity. Seepage rates are dominated by the focusing multipliers that follow a loguniform distribution. Although seepage rates do not follow a loguniform distribution, they can be approximated that way. Permeability is typically modeled as a lognormal distribution. Although lognormal and loguniform distributions are quite different, they do suggest that the saturation distribution is related to the order of magnitude of the saturation. In most circumstances, the saturation would be residual (1%) or slightly higher; in less common instances, the saturation can go up to 10%;

and in a few extreme cases, the saturation can reach 100%. A saturation of 10% has been conservatively applied to all cases with a lower saturation in this model.

Current conditions and computer simulations with modern climate show fractures at almost residual saturation in the shadow zone. An increase in the infiltration rate (by still keeping the seepage rate at 1.5 or 15 liter/year - only for cases of concern in this report) will produce an increase in the dilution factor. The dilution factor can then be considered as a surrogate for the saturation according to information from Figure 4 (increase in saturation for a given increase in flow rate). Table 18 displays the CCDF of high dilution factors for the different climates.

Table 18. CCDF of High Dilution Factors

<b>Dilution Factor</b>	<b>Modern Climate</b>	<b>Monsoon Climate</b>	<b>Glacial Climate</b>
1000	0.00525	0.00820	0.02536
2000	1.30E-04	3.35E-05	1.55E-04
5000	1.96E-09	2.29E-12	3.50E-11
10000	1.81E-17	2.61E-24	2.95E-22

Source: BSC 2001, Table 5-35

## 6.5 STAND-ALONE LITHOPHYSAE

In the stand-alone lithophysal cavity submodel, the maximum accumulation in a lithophysal cavity is also directly linked to the amount of dilution that can take place in the cavity. If it is assumed that each fracture carries about the same amount of water (Assumption 5.18), the maximum accumulation is a function of the number of fractures connected to the lithophysae. In the case of small lithophysae (Section 6.3.4), it is assumed that the mineralization is uniformly distributed over all the available surface area when precipitation is possible. In this section, it is assumed that the accumulation is at the bottom of the lithophysae but in such a way that it does not hinder outflow. Reasonableness of this assumption is presented in BSC 2001l (Section 5.4.1).

The number of composite fractures in a given surface area is determined in BSC 2001l (Section 5.4.5) and reproduced in Table 20. It can be extrapolated to any number of fractures as given in Table 20 according to the following equation and Table 19. BSC 2001k (Section 6.9.8) determined that the tail of the fracture distributions (i.e., at higher fracture frequency or intensity) follows an exponential distribution. Parameters from Eq. 12 are derived by plotting on a semi-log plot the number of fractures within a given length interval (0.25 m, 0.5 m and 1 m) vs. their field frequency (BSC 2001k, Fig. 6-30), fitting the results to straight lines.

$$\text{Pr (Av. \# of composite fractures in lithophysae diameter } > n) = \exp (a \times n / c + b) \quad (\text{Eq. 12})$$

Table 19. Parameters for Equation 12

Lithophysae Diameter (m)	a	b	c
1.0	-1.3546	-0.1084	5.33
0.5	-2.0026	+0.0029	2.665
0.25	-2.7928	+0.0803	1.3325

Source: BSC 2001l, Table 5-38

Table 20. CCDF for the Number of Composite Fracture Intersections for Selected Lithophysal Cavity Size

Lithophysae Diameter = 1 m							
Number of Fractures	9.3	10.7	16.0	21.3	26.7	32.0	37.3
CCDF	2.344E-01	4.807E-02	1.650E-02	3.697E-03	1.138E-03	2.649E-04	6.837E-05
Lithophysae Diameter = 0.5 m							
Number of Fractures	4.6	5.3	8.0	10.7	13.3	16.0	18.7
CCDF	1.317E-01	1.664E-02	3.271E-03	2.844E-04	4.494E-05	6.067E-06	8.189E-07
Lithophysae Diameter = 0.25 m							
Number of Fractures	2.3	2.7	4.0	5.3	6.7	8.0	9.3
CCDF	7.122E-02	4.494E-03	2.275E-04	1.525E-05	9.341E-07	5.721E-08	3.504E-09

Source: BSC 2001l, Table 5-39

## 6.6 PHREEQC POSTPROCESSING

Once the PHREEQC runs have been executed, the output needs to be postprocessed. The first step is to scale the results from the 1 kilogram of water used in the simulations to the true volume of water. The volume of water increases with mixing. The volume of water in cell  $i$  is  $(1/0.9)^i$  where 0.9 represents the fraction of the resident water in the mixing process. The second step is to combine results from all individual runs into the total actinide accumulation through time. This is done with the *Acc\_with\_decay* software program. Detailed explanations are given in the software (BSC 2001g). Enrichment (mole ratio of fissile U to total U) through time of the source term is included at this point. The third step is to tie together accumulation mass and the different parameters of the dilution zone to yield the final product usable in criticality calculations (see files "xxx\_CritIn.xls" in Attachment II where xxx represents the source term).

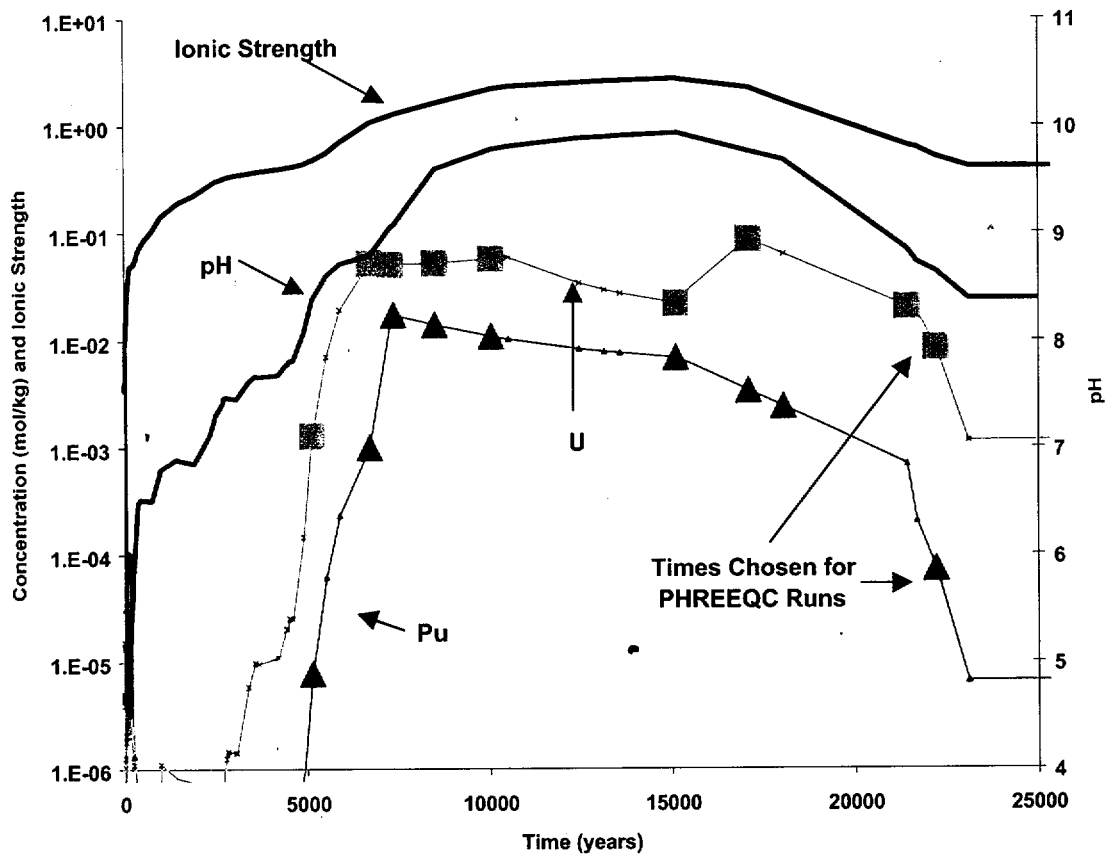
## 6.7 MODEL IMPLEMENTATION

### 6.7.1 Step-By-Step Model Description

As mentioned earlier, the external accumulation model considers accumulation in three different geometries within the tuff: fractures, fractures with small lithophysae, and large stand-alone lithophysae. The first step in the model for all three geometries is running PHREEQC to determine the amount of U and Pu minerals that precipitate in the rock. The subsequent steps involve using Microsoft Excel to make further calculations to yield results of total accumulation (moles) and accumulation density ( $\text{mol}/\text{m}^3$ ). In addition, the model calculates the volume of the accumulation zone. The steps involved in running the model for the fractures-only and the fractures-with-lithophysae geometries are presented first, followed by the steps to run the model for the stand-alone lithophysae. The step-by step description provides in parenthesis the names of example files located in Attachment II that demonstrate each step. The example files come from the external accumulation calculation for a Pu ceramic waste form (BSC 2001c and BSC 20011).

#### 6.7.1.1 Fractures-Only and Fractures-With-Small-Lithophysae Geometries

**Step 1**—In this step, the source term from an EQ6 run is identified as input for PHREEQC. Figure 7 shows the example source term. Data from selected times on the source term curve (referred to as EQ6 output times) are chosen for PHREEQC simulations as indicated by the squares and triangles in Figure 7. PHREEQC is run at each selected EQ6 output time to determine the transport and accumulation of U and Pu in a system containing minerals similar to those found in the tuff at Yucca Mountain.



Source: BSC 2001I, Attachment IV, files on electronic media, "p52rLx41\_SourceTerm.xls", original data from BSC 2001c, Section 6.8.2.

Figure 7. Source Term for Run p52rLx41 From EQ6

Input:

Parameter	Value	Source
Drip rate	1.5 or 15 l/year	Must match source term
Waste Package Effluent Composition (referred to as source term) at each selected EQ6 output time	Varies (moles/kg)	EQ6 calculation
Minerals in Tuff: Identify types, volumes, dissolution rates	See input file P52rLx41_20_10_10k.dat	Section 5.3.2 (CRWMS M&O 2000g)
Fraction of diluted Waste Package effluent (remaining is Mixing Water fraction) for each cell	0.9 for base case, 0.8 and 0.95 for sensitivity studies	N/A
Mixing Water Composition	J-13 water composition, or pore water	See Section 6.7.2
List of minerals that may form based on EQ6 runs	See input file P52rLx41_20_10_10k.dat	EQ6 Run
Number of cells for simulation	100 for base case, higher for sensitivities	N/A
Length of Run	200 steps	N/A

Calculations:

Run PHREEQC at each selected EQ6 output time.

*(Example: "P52rLx41\_20\_10\_10k.dat" is the input file for  $t = 10,000$  years. The source term for the example is "P52rLx41\_SourceTerm.xls").*

Output:

Accumulation of U and Pu minerals per cell for each selected EQ6 output time

*(Example: "P52rLx41\_20\_10\_10k.xls" is the output file for  $t = 10,000$  years).*

(Cell is a volume of rock that contains 1 liter of water. The actual volume of the rock depends on the porosity in the rock and is calculated in Step 7. In a PHREEQC run, all cells have the same volume, the PHREEQC cell results are then scaled differently as described in Step 3).

**Step 2**—This step calculates the U and Pu accumulated per year per liter in each cell from the U and Pu-containing minerals that were precipitated in PHREEQC. (The example is given for U only.)

Input:

Parameter	Value	Source
Moles U minerals accumulated at step 200 for each cell	Varies	PHREEQC output file
Moles U minerals accumulated at step 190 for each cell	Varies	PHREEQC output file
Moles of U per mole of U-bearing minerals	Boltwoodite-Na: 1 Uranophane: 2 Schoepite: 1	Formula of minerals in current thermodynamic database
PHREEQC time step	0.67 or 0.067 years	Inverse of drip rate from Step 1

Calculations:

For each cell, calculate U accumulated per year per liter of solution:

$$\text{U accumulated per year per liter of solution} = \frac{[ (\text{U-minerals accumulated at PHREEQC step 200}) - (\text{U-minerals accumulated at PHREEQC step 190}) ] \times (\text{moles U per mole of U-mineral})}{(10 \text{ steps} \times \text{PHREEQC time step})}$$

(Example: column D, sheet "P52rLx41\_20\_10\_10k", of "P52rLx41\_J13\_Base\_Cases\_SUMMARY.xls").

Output:

Moles of U accumulated per year per liter of solution in each cell. (This has not yet been scaled to account for the increase in volume that occurs in each cell due to mixing water that is added.)

**Step 3**—This step calculates the U accumulated per year per cell based on the total volume of water affected by each cell. For example, in each cell approximately 10% additional water mixes in with the water flowing in from the cell above, but PHREEQC only reports the accumulation occurring in one liter of solution. Therefore at each cell, the actual U accumulation is greater than the value reported in the PHREEQC output file by the partial dilution factor (Section 6.4.2).

Input:

Parameter	Value	Source
Moles U accumulated per year per liter of solution per cell	Varies	Step 2
Fraction of diluted Waste Package effluent (remaining is Mixing Water fraction) for each cell	0.9 for base case, 0.8 and 0.95 for sensitivity studies	N/A

Calculations:

Calculate the Partial dilution factor for cell  $i$  (where  $i$  = cell number).

$$\text{Partial dilution factor for cell } i = \frac{1}{1 - \text{Fraction of diluted Waste Package effluent}}$$

Calculate the Moles U accumulated per year based on total water volume.

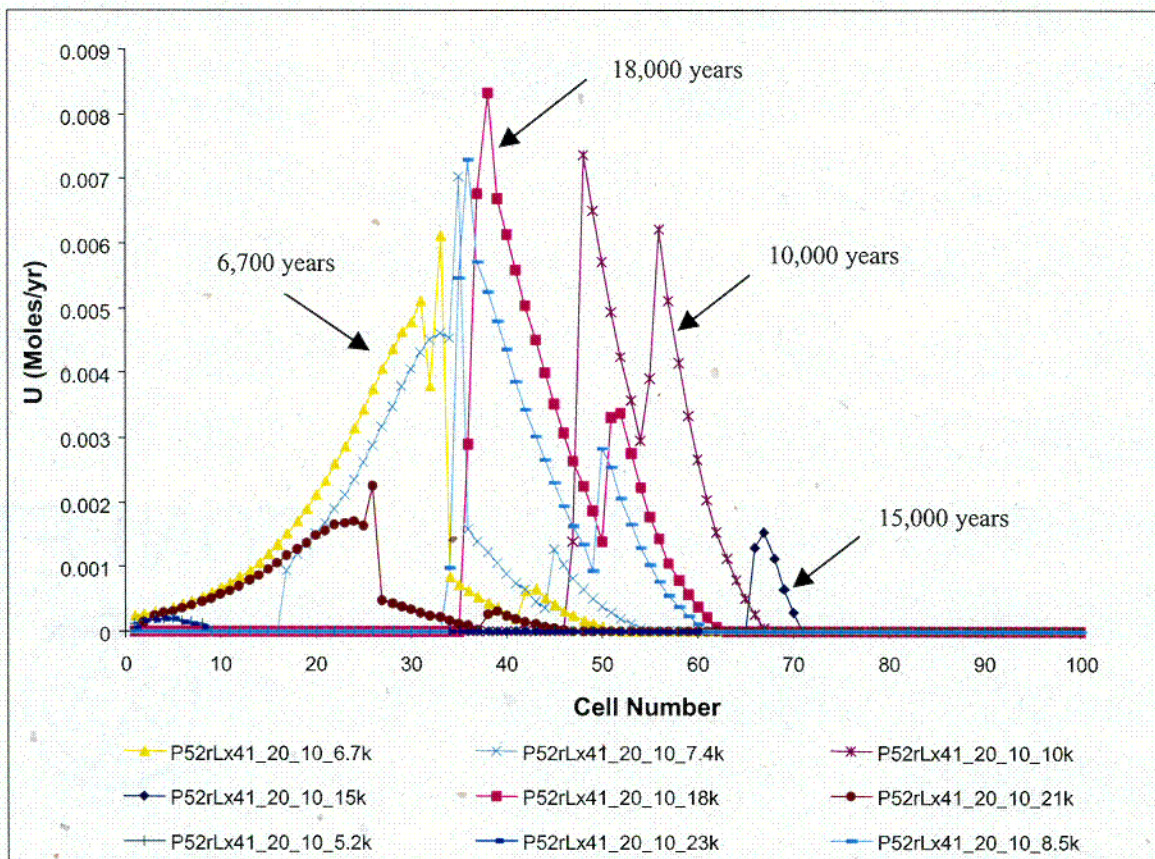
$$\text{Moles U accumulated per year based on total water volume} = \text{moles U accumulated per year per liter of solution per cell} \times \text{partial dilution factor for cell } i$$

(Example: column E, sheet "P52rLx41\_20\_10\_10k", of "P52rLx41\_J13\_Base\_Cases\_SUMMARY.xls").

Output:

Partial dilution factor per cell, Total U and Pu accumulation per year per cell for each selected EQ6 output time

Figure 8 provides a plot of the moles of U accumulated per year versus cell number for each PHREEQC run, which represents a single EQ6 output time. The legend provides the name of the file for each run. Each cell has a depth of 0.12 m for the highest local infiltration rate of 10,000 l/year. Figure 9 provides a similar plot for Pu accumulation.

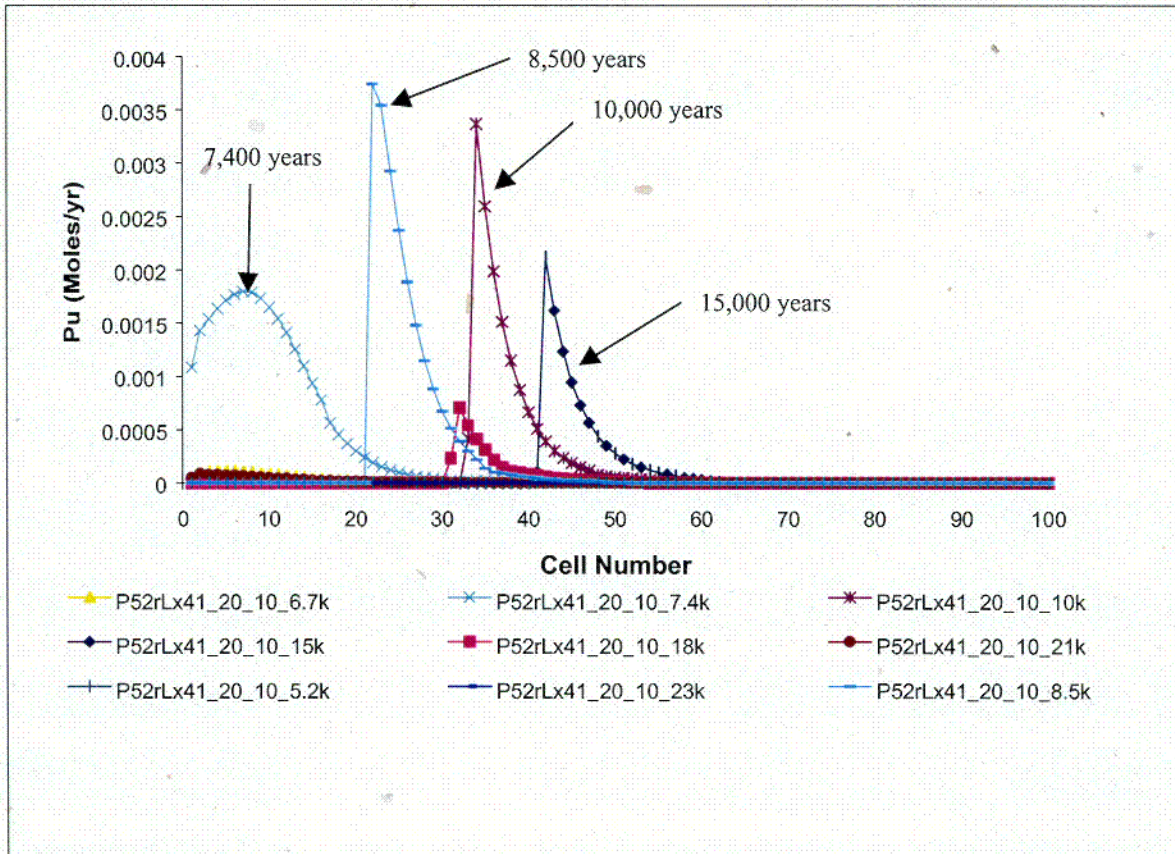


Source: BSC 2001I, Attachment VII, Folder "p52rLx41", file "p52rLx41\_J13\_Base\_Cases\_SUMMARY.xls, provided in this AMR in Attachment II

NOTES: Water flows from cell 1 (top) to cell 100 (bottom). Each line corresponds to a PHREEQC run executed with a single EQ6 output time aqueous concentrations. Plot shows the accumulation in moles in one year around the time given on the plot and in the key.

Figure 8. Moles U Accumulated per Cell in One Year

CO6



Source: BSC 2001I, Attachment VII, Folder "p52rLx41", file "p52rLx41\_J13\_Base\_Cases\_SUMMARY.xls", provided in this AMR in Attachment II.

NOTES: Water flows from cell 1 (top) to cell 100 (bottom).

Each line corresponds to a PHREEQC run executed with a single EQ6 output time aqueous concentrations.

Plot shows the accumulation in moles in one year around the time given on the plot and in the key.

Figure 9. Moles Pu Accumulated in One Year Versus Cell Number

C07

**Step 4**—This step calculates the total cumulative accumulation over the entire time of interest.

Input:

Parameter	Value	Source
Accumulation per cell layer for each EQ6 output time	Varies	Step 3

Calculations:

Calculate the Time cumulative U accumulation (moles) for each cell.

$$\text{Time cumulative U accumulation (moles) for each cell} = \frac{1}{2} \times \left( \begin{array}{c} \text{U accumulated at } t_1 \\ + \\ \text{U accumulated at } t_2 \end{array} \right) \times (t_2 - t_1) + \frac{1}{2} \times \left( \begin{array}{c} \text{U accumulated at } t_2 \\ + \\ \text{U accumulated at } t_3 \end{array} \right) \times (t_3 - t_2) + \text{etc.}$$

(Example: Column T and U, sheet "p52rLx41", of "P52rLx41\_CritIn.xls").

Calculate the Total U accumulated.

$$\text{Total U accumulated} = \text{sum over all cells}$$

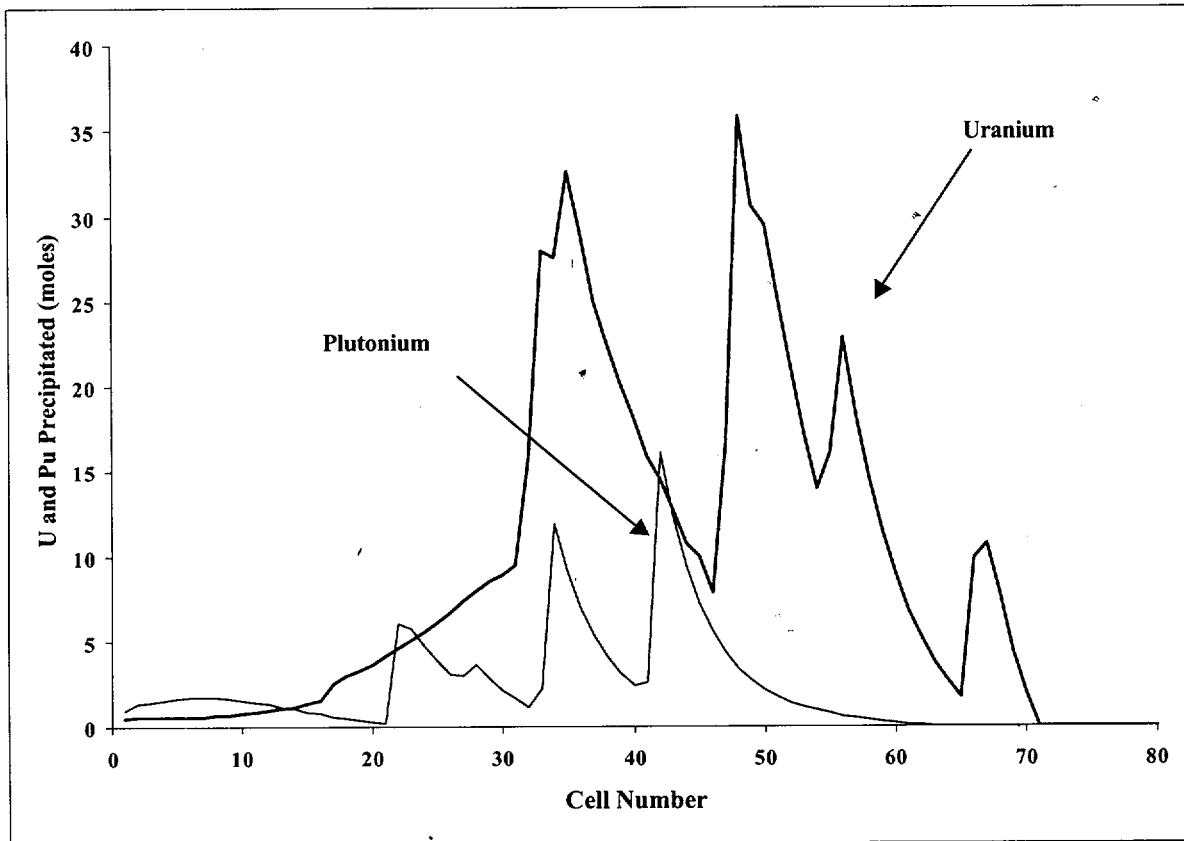
(Example: Row 107, sheet "p52rLx41", of "P52rLx41\_CritIn.xls").

Output:

Total accumulation per cell, Total accumulation

Figure 10 shows the total accumulation calculated versus cell number. The total accumulation summed over all cells was calculated to be 727 moles of U and 180 moles of Pu at 23,000 years after breach (Cells T107 and U108 in sheet "p52rLx41" in file "p52rLx41\_CritIn.xls". The total amount of U and Pu contained in the source term was 1186 moles and 160 moles, respectively. The calculated Pu accumulation was higher than the amount in the source term due to the approximations in estimating the accumulation with only 9 different EQ6 output times rather than a larger number. In future documents, the number of EQ6 output times used will be in the vicinity of 50.

Figure 10 presents the final accumulation in space at the end of the precipitation period. The jagged aspect of the plot is due to the summation on a limited number of EQ6 output times (9 output times), each producing its own accumulation peak. Using more EQ6 output times would yield a smoother curve. Each peak corresponds to a single EQ6 output time. Because PHREEQC runs yield yearly accumulation (step 3), a peak height depends on the period of time this particular EQ6 output time is deemed representative and on the actual yearly accumulation itself. The accumulation peak location is a function of the dilution needed to precipitate actinide minerals. The height of the peak depends on how long a given set of EQ6 output time aqueous concentrations is applied and how much actinides precipitate. Assuming that the annual accumulation is the same, if the EQ6 output time is chosen when the EQ6 time stepping is fast, that particular set of concentrations will not be applied for long, and will result in a smaller peak. On the other hand, if the EQ6 output time is in a period when the EQ6 has large time steps and little changes in the aqueous concentration, the peak will be taller.



Source: BSC 2001i, Figure 6-23

Figure 10. Cumulative Mass of Solids at 23,000 Years After Breach (No Decay)

**Step 5**—This step calculates the total accumulation over the entire time of interest when radioactive decay of Pu is considered.

Input:

Parameter	Value	Source
Accumulation per cell layer for each EQ6 output time	Varies	Step 3

Calculations:

Run the software “Acc\_with\_decay”. Values of total accumulation per cell are printed to the Microsoft Excel spreadsheet. Calculate the Total U accumulated.

$$\text{Total U accumulated} = \text{sum over all cells}$$

(Example: Columns V and W, sheet “p52rLx41”, of “p52rLx41\_CritIn.xls”).

Output:

Total accumulation per cell and total accumulation with decay of Pu considered.

**Step 6**—This step calculates the mixing volume for each cell layer.

Input:

Parameter	Value	Source
Drip rate	1.5 or 15 l/year	Must match source term
Partial dilution factor per cell	Varies	Formula in Step 3

Calculations:

Calculate the Mixing volume.

$$\text{Mixing volume} = \text{Drip Rate} \times \text{partial dilution factor per cell}$$

(Example: Column E, sheet "Density at 23K (no lith)", of "p52rLx41\_CritIn.xls").

Output:

Mixing volume for each cell

**Step 7a (fractures-only)**—In this step, the rock volume at each cell layer is calculated.

Input:

Parameter	Value	Source
fracture porosity	6.5%, but varied for sensitivity	Table 10, worst case value
fracture saturation	0.1, with sensitivities at 0.05, 0.5 and 1.0	Assumed
mixing volume for each cell	Varies	Step 6

Calculations:

Calculate the Rock volume.

$$\text{Rock volume} = \frac{\text{Mixing volume}}{(\text{fracture porosity} \times \text{fracture saturation})}$$

Note: fracture saturations are varied from 10% to 100%

(Example: Column F, sheet "Density at 23K (no lith)", of "p52rLx41\_CritIn.xls").

Output:

Rock volume for each cell layer

**Step 7b (fractures-with-lithophysae)**—This step calculates the rock volume and dimensions for the fracture-with-lithophysae geometry.

Input:

Parameter	Value	Source
Mixing volume	Varies	Formula in Step 6
fracture porosity	2%, but varied for sensitivity	Table 10, worst case for zone which contains small lithophysae
fracture saturation	0.1, with 0.05, 0.5 and 1.0 for sensitivity	Assumed
fracture aperture	1.12, but varied for sensitivity	Table 10
lithophysae porosity, $\eta$	27%, but varied for sensitivity	Table 10
Inverse of fracture spacing, $1/sp$	13	Taken to be maximum number of fractures in the 3 sets for worst case, Unit TSw35(1), Table 10, (see discussion in Section 6.3.4)

Calculations:

Calculate additional fracture intensity ( $F.I_{.add}$ ) (Eq. 11).

$$F.I_{.add} = 8\eta \times (1/sp)$$

Calculate the Rock Volume.

$$\text{Rock Volume} = \frac{\text{fracture porosity} \times \text{fracture saturation} + F.I_{.add} \times \text{fracture aperture} \times \text{fracture saturation}}{\text{Mixing volume}}$$

(Example: Column E and F, sheet "Density at 23K (with lith)", of "p52rLx41\_CritIn.xls").

Output:

Rock volume

**Step 8**—This step calculates the depth of each cell.

Input:

Parameter	Value	Source
Drip rate	1.5 or 15 l/year	Must match source term
Fraction of diluted Waste Package effluent (remaining is mixing water fraction) for each cell	0.9 for base case, 0.8 and 0.95 for sensitivity studies	N/A
Shadow zone	10 m	Conservative, See Section 6.4.1
local infiltration rate <sup>a</sup>	Ranges from 10,000 to 50 l/year	See Section 6.4.2.1

NOTE: <sup>a</sup> Local infiltration rate is infiltration rate x focusing multiplier.  
Seepage rate is the rate of water seeping into the drift subjected to the local infiltration rate.

Calculations:

Solve for the total number of cells in shadow zone,  $n$ . This represents the number of cells required to get from the drip rate to the local infiltration rate, based on adding approximately 10% mixing water at each cell.

$$\text{Local infiltration rate} = \frac{\text{Drip rate}}{(1 - \text{mixing ratio})^n}$$

$$\text{Depth of the midpoint of each cell} = \frac{\text{shadow zone}}{\text{total number of cells in shadow zone} \times (\text{cell number} - 0.5)}$$

(Example: Cell C9 and Column B, sheet "Density at 23K (with lith)", of "p52rLx41\_CritIn.xls").

Output:

Depth of each cell

**Step 9**—This step calculates the density of accumulation.

Input:

Parameter	Value	Source
U and Pu accumulated in each cell	Varies	Calculated in Step 4
rock volume in each cell	Varies	Calculated in Steps 7a and 7b

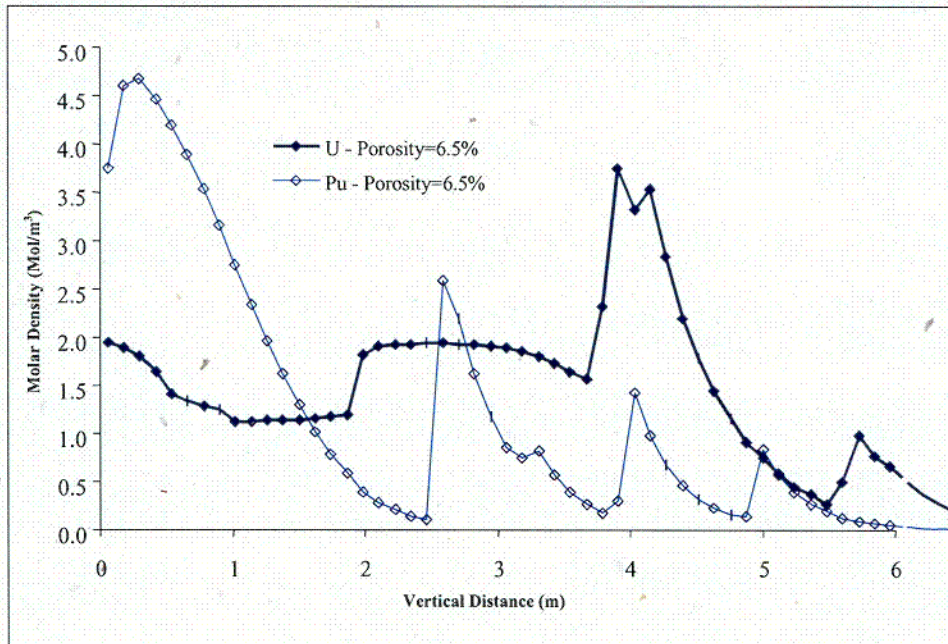
Calculations:

Calculate for each cell

$$\text{Accumulation density} = \text{Accumulation} + \text{rock volume}$$

(Example: Column I and J, sheet "Density at 23K (with lith)", of "p52rLx41\_CritIn.xls").

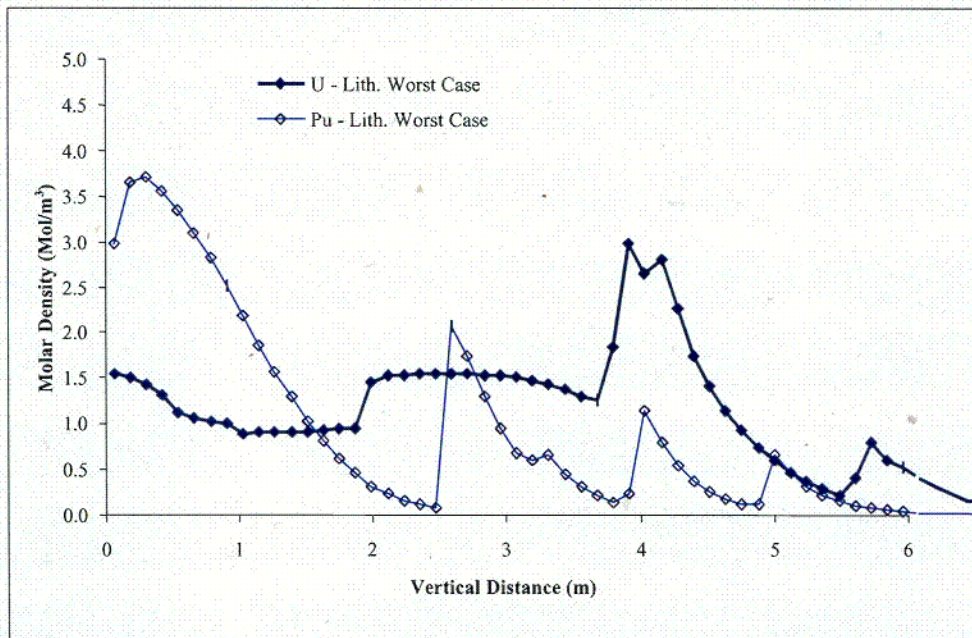
Figure 11 shows the accumulation density versus depth for the fractures-only geometry and Figure 12 shows the results for the fractures-with-lithophysae geometry.



Source: BSC 20011, Figure 6-25[JPN47]

NOTE: The molar density is given in moles of solids per cubic meters of bulk rock.

Figure 11. Cumulative Molar Density at Final Time for Fractures Only



Source: BSC 20011, Figure 6-26

NOTE: The molar density is given in moles of solids per cubic meters of bulk rock.

Figure 12. Cumulative Molar Density at Final Time for Fractures with Small Lithophysae

008

### 6.7.1.2 Large Stand-Alone Lithophysae

**Step 1**—In this step, PHREEQC calculates the accumulation (without transport) in a large lithophysae for the source term as used in Step 1 of the fractures-only and fractures-with-lithophysae geometries.

#### Input:

Parameter	Value	Source
Source term at selected EQ6 output times	Varies (moles/kg)	EQ6 calculation
Mixing Water Composition	J-13 water composition, or pore water	See Section 6.7.2
List of minerals that may form based on EQ6 runs	See input file P52rLx41_mix_10k.dat	EQ6 Run
A range of volume of mixing water that is mixed with 1 liter WP effluent in the lithophysae	Ranges from 0.001 to 2000	N/A

#### Calculations:

Run PHREEQC using the source term at selected EQ6 output times.

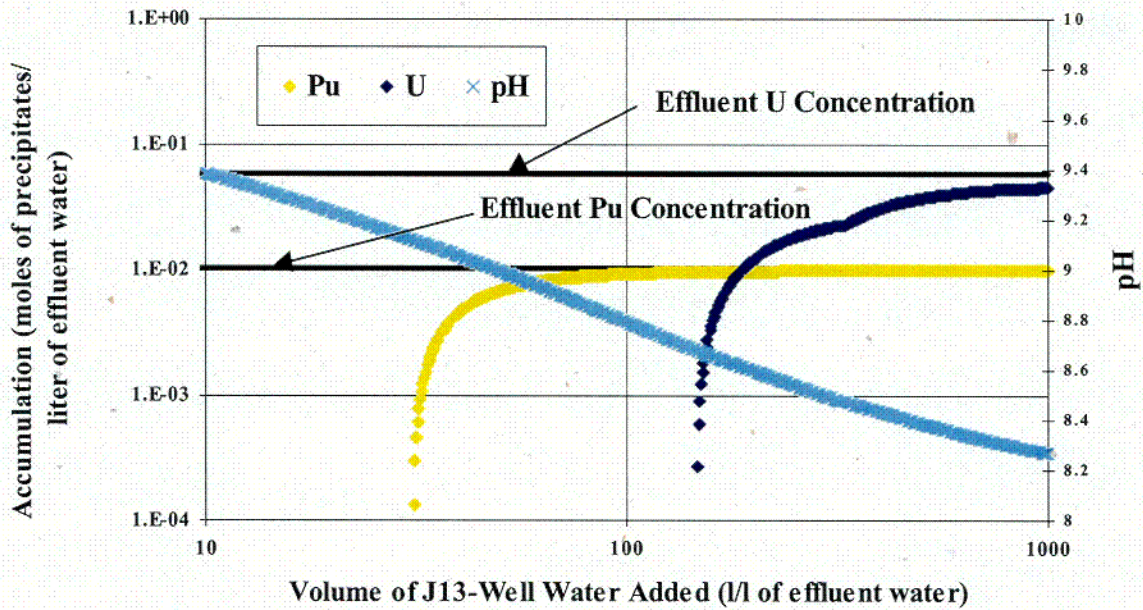
#### Output:

Moles of U and Pu accumulated for selected volumes of mixing water added to one liter of WP effluent

A plot of accumulation as a function of the volume of mixing water added for one EQ6 output time (10,000 years) is provided in sheet "all(2)" in file "p52rLx41\_mix\_10k\_calcul.xls".

*(Example: input file "p52rLx41\_mix\_10k.dat", output file "p52rLx41\_mix\_10k.xls", and sheet "all(2)", of "p52rLx41\_mix\_10k\_calcul.xls").*

Figure 13 shows the calculated accumulation of U and Pu versus volume of mixing water added using the source term at 10,000 years after breach. The figure shows that accumulation occurs for Pu when at least 30 liters of mixing water (J-13 well water) are mixed with 1 liter of effluent water. For U, at least 150 liters of mixing water are required.



Source: BSC 2001I, Figure 6-22

NOTE: This plot presents the cumulative amount of actinides (in moles) precipitating from 1 liter of effluent water as J13-well water is incrementally added. This amount asymptotically tends to the initial actinide mass contained in the aqueous solution. This means that all the actinides can virtually precipitate by dilution provided that there is enough dilution water.

Figure 13. Accumulation in a Large Stand-Alone Lithophysae at 10,000 Years After Breach

**Step 2**—In this step the U and Pu accumulated per year for a subset of volumes of mixing water added to 1 liter of WP effluent is calculated.

Input:

Parameter	Value	Source
Moles U and Pu minerals accumulated for a subset of volume of mixing water that is mixed with 1 liter WP effluent in the lithophysae	Varies (moles/liter of WP effluent))	Calculated in Step 1 (highlighted values in sheet "all(2)" in file "p52rLx41_mix_10k_calcul.xls")
Drip rate	1.5 or 15 l/year	Must match source term

Calculations:

$$U \text{ accumulated (moles/year)} = U \text{ accumulated (moles/liter)} \times \text{Drip rate (liters/year)}$$

(Example: Column K and L, sheet "p52rLx41", of "p52rLx41\_CritIn\_lith.xls").

Output:

U and Pu accumulated per year for a subset of volume of mixing water that is mixed with 1 liter WP effluent

209

**Step 3**—In this step, the total U and Pu accumulated over the whole time period of interest is calculated for each selected volume of mixing water that is mixed with 1 liter WP effluent.

Input:

Parameter	Value	Source
Moles U and Pu accumulated per year for a subset of the volume of mixing water that is mixed with 1 liter WP effluent	Varies (moles/year)	Calculated in Step 2

Calculations:

$$\text{Total U accumulated (moles)} = \frac{1}{2} \times \left( \begin{matrix} \text{U accumulated at } t_1 \\ \text{U accumulated at } t_2 \end{matrix} \right) \times (t_2 - t_1) + \frac{1}{2} \times \left( \begin{matrix} \text{U accumulated at } t_2 \\ \text{U accumulated at } t_3 \end{matrix} \right) \times (t_3 - t_2) + \text{etc.}$$

(Example: Column U and V, sheet “p52rLx41”, of “p52rLx41\_CritIn\_lith.xls”).

Output:

Total U accumulated in lithophysae with different volumes of mixing water that are mixed with 1 liter WP effluent. These volumes correspond to the number of fractures intersecting the lithophysae. For example a volume of mixing water of 85 corresponds to a lithophysae with 85 fractures transporting mixing water and intersecting the lithophysae and one fracture transporting waste package effluent water and intersecting with the lithophysae. Each fracture carries an equal volume of water and the water is well mixed in the lithophysae.

**Step 4**—This step determines the total accumulation when radioactive decay of Pu is considered.

Input:

Parameter	Value	Source
Moles U and Pu accumulated per year for a subset of the volume of mixing water that is mixed with 1 liter WP effluent	Varies (moles/year)	Calculated in Step 2

Calculations:

Run the software “Acc\_with\_decay”. Results are printed to the Microsoft Excel spreadsheet.

(Example: Columns V and W, sheet “p52rLx41\_2”, of “p52rLx41\_CritIn\_lith.xls”).

Output:

Total U and Pu accumulated in lithophysae with different volumes of mixing water that is mixed with 1-liter WP effluent with decay of Pu considered.

**Step 5**—This step determines the percentage of the lithophysae filled with Pu and U minerals.

Input:

Parameter	Value	Source
Total U and Pu accumulated for each volume of mixing water that is mixed with 1 liter WP effluent	Varies (moles)	Calculated in Steps 3 and 4
Molar volumes of U- and Pu-bearing mineral	Varies (cm <sup>3</sup> /mole)	Current thermodynamic database
Number of moles of U and Pu per mole of mineral	Varies (for example 1 mole Pu per mole PuO <sub>2</sub> )	Formula for the mineral from the thermodynamic database
Diameter of lithophysae assuming spherical shape	1, 0.5, and 0.25 m	N/A

Calculations (example for U only):

Calculate the Volume of minerals.

$$\text{Volume of minerals} = \frac{\text{Moles U accumulated}}{\text{Moles U per mole U-bearing mineral} \times \text{molar volume (cm}^3\text{/mole)}}$$

Calculate the Volume of lithophysae.

$$\text{Volume of lithophysae} = \frac{4}{3} \times \pi \times \left( \frac{\text{Diameter of Lithophysae}}{2} \right)^3$$

Calculate the Percentage of Lithophysae filled with minerals.

$$\text{Percentage of Lithophysae filled with minerals} = \frac{\text{volume of minerals}}{\text{volume of lithophysae} \times 100}$$

(Example: Rows 83-124, sheet "p52rLx41", of "p52rLx41\_CritIn\_lith.xls").

Output:

Percentage of Lithophysae filled with U- and Pu-bearing minerals.

### 6.7.1.3 Example Results

Table 21 shows the results of the External Accumulation Model for four source terms with fractures only geometry. The results are documented in BSC 20011 (Section 6.6.1).

Table 21. Example Results for Four Source Terms

Source Term (Time Frame)	Moles in Source Term		Accumulation No decay		Accumulation with Decay			Highest Density <sup>a</sup> (with Cell Number) at Saturation of 10%	
	U (mol)	Pu (mol)	U (mol)	Pu (mol)	U (mol)		Pu (mol)	U (mol/m <sup>3</sup> )	Pu (mol/m <sup>3</sup> )
					Non-Fissile	Fissile			
P51_1131 (50k - 63k)	1000.7	14.0	NC	10.3	NC		NC	6.55 (1) - ND	4.69 (1) - ND
P52{rs}L241 (0.7k - 14k)	833.6	115.9	851.9	113.7	632.0	234.8	96.3	3.49 (32) - ND	3.19 (26) - ND
P52rLx41 (5k - 23k))	1186.3	159.7	727.0	180.0	481.0	183.2	137.9	3.75 (31) - ND	4.67 (1) - ND
P51_1132 (40k - 85k)	973.7	12.4	298.3	5.4	NC		NC	8.60 (1) - ND	0.45 (1) - ND

Source: BSC 20011, Table 6-4

NOTES: <sup>a</sup> For "worst case" with fracture porosity=6.5% and high dilution

NC: Not computed; ND: No decay

Table 22 presents the accumulation calculated in a 1-meter diameter lithophysal cavity for a dilution ratio of 85, which is equivalent to assuming a high fracture intensity of 85 m/m<sup>2</sup>. The results of the calculations are documented in BSC 20011 (Section 6.6.2).

Table 22. Accumulation in 1 meter-Diameter Lithophysal Cavity with High Fracture Intensity

Source Term (Time Frame)	Total U (mole)		Total Pu (mole)
	Non-Fissile	Fissile	
P51_1131 (50k - 63k)	NC		10.29 - ND
P52{rs}L241 (0.7k - 14k)	352.8	132.5	64.9 - DC
P52rLx41 (5k - 23k))	214.5	86.4	93.0 - DC
P51_1132 (40k - 85k)	NC		5.21 - ND

Source: BSC 20011, Table 6-5

NOTES: All results for fracture intensity of 85 m/m<sup>2</sup>.

NC: Not computed; ND: No decay; DC: Decay

### 6.7.2 WP Source Terms

The source term is typically provided by the geochemical code EQ6. An EQ6 output consists of tens to hundreds of snapshots of the effluent composition through time. EQ6 can automatically adapt the time-stepping of its numerical algorithm to reduce the time step when the chemistry

changes rapidly or to increase it when the chemistry is more stable. PHREEQC does not have this flexibility and this precludes using the entirety of the EQ6 output as a variable source term. The solution to the problem is to use only selected EQ6 output times. More steps should be selected at actinide concentration peaks which have the greatest impact on the final total accumulation (see Section 6.6). The more EQ6 output times used, the more accurate the total accumulation is relative to the source term. Because each EQ6 output time is modeled by a PHREEQC run, the parameters described in the following sections do not have to be constant throughout the period of interest but can vary to better match the local environment (e.g., the resident water composition can change with time).

### 6.7.3 Water Composition

The chemical composition of the resident water has an effect on the results (BSC 20011, Section 6.5.1). Because a drop in pH is the driving force in actinide precipitation, the pH of the resident water is important. The resident water can be J-13 well water, current pore water, pore waters developed in the Thermal-Hydrological-Chemical (THC) simulations or any other water that will be deemed appropriate (e.g., basalt water after intrusion). J-13 well water and current pore water composition are given by DTN: MO0006J13WTRCM.000 and DTN: LB0101DSTTHCR1.001, respectively. The expected composition of the water impinging the DS and WP through time is given by the THC model (BSC 2001b, Section 6.3.5 and DTN: LB0011DSTTHCR1.001). The period of interest is the extended cool-down period (that goes from 2,000 to 100,000 years). During that long period the water composition changes gradually back to the initial system composition. The THC model chooses to use as a starting point of its calculation a pore water rather than the J-13 well water (BSC 2001b, Sections 4.1.3, 5.A.3, and 6.1.2). One has to remember to use a resident water consistent with the EQ6 source term, in particular relative to the temperature and CO<sub>2</sub> partial pressure.

### 6.7.4 Drip Rates

The drip rate is usually either 1.5 or 15 liter/year consistent with the input conditions of the source term. These drip rates correspond to the actual flow rate through the WP and not to the seepage rate or infiltration rate, both greater than the drip rate. The relationship of infiltration rate to drip rate is investigated in Section 6.4.2 and is part of the dilution mechanism.

### 6.7.5 Mineral Dissolution at the Fracture Surface

Rate laws are used to characterize the slow dissolution of the tuff minerals making up the fracture walls and the invert. The dissolution rate laws follow the transition-state theory (TST) formalism by measuring changes in moles of the surface minerals as a function of time (CRWMS M&O 2000g, Section 4.3.2). Therefore mineral composition, the surface area, and the volume of the fractures in the tuff had to be calculated. Sensitivity studies revealed that surface areas had little influence on the total amount of deposited fissile materials except for cases in which no dilution of WP effluent with resident J-13 water occurred (BSC 20011, Section 6.4.3.2). The net effect of increased surface area is to increase the total volume of minerals precipitated. The surface area is assumed to be independent of the fracture aperture (Assumption 5.7). It is also assumed to be constant as the tuff dissolves (Assumption 5.12).

The tuff minerals dissolve and produce alteration minerals such as clays, zeolites and chalcedony (CRWMS M&O 2000f, Figure 6-10). It should be noted that if the solution becomes

supersaturated with respect to some of the tuff minerals (feldspars and micas) they are not allowed to precipitate in the simulations since they normally would not form at low temperatures. The tuff alteration minerals take up more volume than the initial minerals and thus could eventually plug the voids in the host rock.

#### **6.7.6 Precipitation of Minerals**

Unlike EQ6 that senses the phases that should precipitate, PHREEQC requires the user to specify them. They are given in the "EQUILIBRIUM\_PHASES" field of the PHREEQC input file. Selection of minerals was based on the results of EQ6 calculations for chemical degradation of Pu-ceramic waste packages (CRWMS M&O 2000g). In PHREEQC runs, precipitation of quartz is not allowed because it is less soluble than cristobalite, which is the most common silica phase in the rock. Instead, chalcedony was chosen as the precipitated SiO<sub>2</sub> phase (CRWMS M&O 2000g, Section 6.2). Dolomite precipitation was also not allowed because of slow kinetics at 25°C. Magnesium was allowed to precipitate as the carbonate mineral magnesite. Only one of the phases of the goethite/hematite couple was allowed to precipitate. Runs with similar source terms showed that the system is not very sensitive to these minerals (CRWMS M&O 2000f, Section 5.1.6). Solid solutions typically used in EQ6 are approximated by their components in PHREEQC. The different phases of beidellite, nontronite and saponite represent an approximation of the smectite solid solution used in the EQ6 runs.

#### **6.7.7 Thermodynamic Database**

The most current EQ6 thermodynamic database "data0.ymp" was used (DTN: MO0009THERMODYN.001) as input to *transl*, the software that translates the EQ6-formatted database to a PHREEQC-formatted database.

#### **6.7.8 Number of PHREEQC Time Steps**

To avoid unproductive use of computer resources and time, most of the runs were not allowed to run to completion (that is to the time where the next EQ6 output time aqueous concentrations should start being used), but were stopped after a few hundred simulated years. Early termination is justified because the system quickly reaches steady-state conditions as all the inputs are constant (concentrations, flow rates, surface area). As illustrated in CRWMS M&O 2000f (Section 6.1.1), the masses of most species within a given cell are approximately linear functions of simulated time and, therefore, simple multiplicative factors can be applied.

#### **6.7.9 Number of Cells in Mixing-Dilution Zone**

Phillip et al. (1989) investigated the groundwater diversion around an opening in a homogenous porous rock in unsaturated conditions. In the UZ, groundwater flow is diverted when it encounters an opening like a tunnel or a waste emplacement drift. The primary mechanism in diversion of groundwater flow is the capillary action of pores open to the atmosphere. The capillary force in the rock pores prevents water entry into the drift unless gravitational forces acting on the pore water overcome the atmospheric pressure (capillary barrier). Therefore, groundwater tends to be diverted from the drift and travels laterally. As time passes, the rock surrounding the drift becomes more saturated, and due to gravitational forces, water flows around the drift. The footprint created by emplacement of the drift in the UZ creates a shadow

zone underneath the drift. The depth of the shadow zone influences mixing of the WP effluent with the resident water.

The PHREEQC run discretizes the shadow zone in 100 cells with a uniform dilution usually set at 10% at each advection step. The advection step is defined in the PHREEQC input files and is taken as the flux through the WP, usually 1.5 l/year expressed as 1 liter in 0.667 year; the water velocity is irrelevant when no diffusion is modeled because the cell volume can take up any desired shape. It should be noted that the mixing proportions of 90% - 10% have only a weak effect on the results. Mixing proportions of 95% - 5% and 80% - 20% were also examined (BSC 20011, Section 5.3.7). The results in each cell are certainly different when different mixing proportions are used. However, when the scaling of the PHREEQC results to the true geometry of the system is done, they all map to approximately the same accumulation density. The choice of the appropriate mixing proportions is a trade-off between spatial resolution (the faster the mixing, the less resolution) and assurance that the maximum accumulation has been reached (very little accumulation results from no mixing and it progressively increases from there as displayed in BSC 20011, Figure 6-7).

The maximum dilution factor that can be attained in the 100 cells of the PHREEQC runs is  $(1/0.9)^{100} \sim 37650$ . This value assumes that the typical mixing proportions of 90% already mixed water and 10% fresh water is used (mixing ratio of 10% as defined in the PHREEQC runs) and that the mixing ratio is constant (that is, more and more water is added to the increasing mass of water). The number of cells  $n$  for a given dilution factor and mixing ratio can be computed from:

$$DilutionFactor = \frac{q_{eff}}{Inf.} = (1 / (1 - MixingRatio))^n$$

$$n = \ln\left(\frac{q_{eff}}{Inf.}\right) / \ln(1 / (1 - MixingRatio)) \quad (Eq. 13)$$

where  $q_{eff}$  is the effluent flow rate and  $Inf.$  is the local infiltration rate. The following example shows how to use Equation 13. If the dilution factor is 100 and the mixing ratio 10%, the relevant number of PHREEQC cells that need to be considered is 43 ( $(1/0.9)^{43} \sim 100$ ), i.e., any accumulation occurring in cells beyond cell 43 will not count toward accumulation with this particular dilution factor.

#### 6.7.10 Stand-Alone Lithophysae Runs

In the stand-alone lithophysae case, only mixing is considered, there is no PHREEQC advection. The degree of mixing is a function of the number of fractures connected to the lithophysal cavity.

### 6.8 MODEL VALIDATION

The objective of this model is to predict external accumulation of fissile materials as seepage water flows through the breached WP. In this model, "external" is considered to be the rock beneath the drift's invert. The risks of criticality will depend on the amount of fissile materials per unit volume that could be accumulated in fracture networks and lithophysae. Although this model was evaluated with a WP containing Pu-ceramic waste form, it can be used with any other spent nuclear fuel type.

This model is an abstraction and simplification of major processes and features that control accumulation of fissile materials external to the WP. In this process conservative assumptions were made to select the most efficient method (mixing WP effluent with resident water) for precipitating fissile materials in the fractured tuff below the drift. In this model transport of radionuclides was assumed to be limited to dissolved species in water flowing through the failed WP. Other mechanisms like sorption, reducing zones, and colloidal transport, including transport by microbial communities, were not included in the model. In addition, conservative assumptions were made on the effects of parameters for which reliable information on the amount, type, or quality of data was inadequate. Finally, the significance of each process that affects accumulation was evaluated through sensitivity analyses.

The approach taken in validation of this model is in three parts. First, PHREEQC's prediction of the precipitated minerals was compared to experimentally observed minerals from degrading HLW glass (Section 6.8.1). Second, it is emphasized that all of the important features that describe the fracture system at the repository have been characterized based on field measurements made at the repository itself (Section 6.8.2). Third, the potential of several other mechanisms causing precipitation of radionuclides, besides dilution, are evaluated (Section 6.8.3). It is important to remember that most mechanisms that are evaluated in this section could play important roles in the fate and transport of radionuclides. However, the criterion is to choose a mechanism that could precipitate a sufficient quantity of radionuclides in the host rock beneath the invert, such that the calculated accumulation is the most conservative with respect to criticality.

### **6.8.1 Comparison of PHREEQC Performance with Experimental Results**

PHREEQC was validated against experimental data (Bruton and Shaw 1988). The comparison criterion is based on the nature of the precipitates. The experiment consisted of observing the minerals that precipitated after immersing Defense Waste Product Facility (DWPF) glass and West Valley glass in J-13 well water at 90°C. The results of the comparison are presented in Table 23 and Table 24, respectively. In general all the major phases observed to precipitate in the experiment are also predicted by PHREEQC. (The formulas for the predicted minerals are provided in Attachment II, folder "transl", subfolder "Starting\_Point", file data0.ymp\*.txt.)

The current "data0.ymp" thermodynamic database contains thermodynamic data for all minerals at 25°C, but does not include data for higher temperatures (such as 90°C) for some of the minerals (Assumption 5.20). The database includes temperature coefficients for all the predicted phases in the HLW glass degradation cases, except  $\text{Co}_2\text{SiO}_4$ ,  $\text{MnO}_2$ ,  $\text{NpO}_2$ ,  $\text{AmO}_2$ ,  $\text{PuO}_2$ , weeksite, boltwoodite,  $\text{EuPO}_4 \cdot 10\text{H}_2\text{O}$  and  $\text{AmPO}_4(\text{am})$ . However, temperature effects (for 90°C versus 25°C) are not expected to be large. A study that looked at the simulation of the reaction between spent fuel and J-13 water at 25°C and 90°C showed that the increase in temperature did not greatly impact the identity of precipitated phases or solution composition, except in the case of U (Bruton and Shaw 1988). For U, one of the U minerals ( $\text{Na}_2\text{U}_2\text{O}_7$ ) only formed at 90°C; whereas the minerals haiweeite, soddyite, and schoepite formed at both temperatures (Bruton and Shaw 1988). This does not impact the results because the database used in the glass degradation simulations includes log K values for  $\text{Na}_2\text{U}_2\text{O}_7$  up to 100°C (Attachment II, folder "transl", subfolder "Starting\_Point", file data0.ymp\*.txt).

Table 23. Comparison of Experimentally Observed and Predicted Precipitates in Reaction of DWPF Glass with J-13 Well Water at 90°C

Experimentally Observed Precipitates	Predicted Precipitates	Amount of Glass Dissolved (g/liter)				
		10	0.942	0.105	1.08E-02	2.95E-03
		Predicted Mass of Precipitates (moles of solids/liter of solution)				
<b>Smectites</b>	Nontronite	3.19E-03	6.01E-05			
	Saponite-Na <sup>3</sup>	8.43E-04				
<b>Mg-silicates</b>	Talc (Mg <sub>3</sub> Si <sub>4</sub> O <sub>10</sub> (OH) <sub>2</sub> )					8.05E-06
<b>Fe-bearing phases:</b> Fe-silicates, Ferrihydrite, maghemite, magnetite, Fe-oxide or hydroxide	Hematite	5.13E-04	2.06E-04			1.15E-06
<b>Ni-bearing phases:</b> Ni-silicates, Ni-Fe silicates	Bunsenite (NiO)	1.22E-03	1.14E-04	1.20E-05	5.82E-07	
eucryptite (LiAlSiO <sub>4</sub> )	Petalite (LiAlSi <sub>4</sub> O <sub>10</sub> )	1.79E-02	1.75E-03			
<b>Zeolites:</b> Garronite, analcime/pollucite, thomsonite, Na-zeolite	Mesolite			9.50E-05	5.08E-06	
<b>Ca-bearing silicates:</b> Gyrolite, tobermorite, truscottite/reyerite, Ca-silicates	Saponite-Ca		1.03E-04	3.49E-05	2.72E-05	1.85E-05
	Andradite (Ca <sub>3</sub> Fe <sub>2</sub> O <sub>12</sub> Si <sub>3</sub> )		8.24E-05		4.07E-06	
<b>U-bearing minerals:</b> weeksite Ca-U silicate	CaUO <sub>4</sub>	7.32E-04	7.08E-05	7.87E-06	8.14E-07	2.21E-07
Ba-bearing phase						
Zn-Si phase -- willemite						
borosilicates						
aragonite (CaCO <sub>3</sub> )	Calcite			9.91E-05	2.61E-04	2.77E-04
	Strontianite	4.09E-05	4.02E-06	2.54E-07		
arsenate apatite (Ca(P,As)O <sub>4</sub> - OH, F, or Cl)						
	MnO <sub>2</sub> (gamma)	2.15E-03	2.02E-04	2.25E-05	2.33E-06	6.34E-07
	Cassiterite (SnO <sub>2</sub> )	2.54E-06	7.87E-08	3.88E-05		
	NpO <sub>2</sub>	5.72E-07	3.58E-08			
	Thorianite (ThO <sub>2</sub> )	1.05E-07	9.89E-09	1.10E-09	1.14E-10	3.10E-11
	AmO <sub>2</sub>	5.04E-09	4.95E-10	2.57E-11		
	PuO <sub>2</sub>		6.15E-08			

Source: Bruton and Shaw 1988 and FILE: **case2\_df\_calcul.xls**; worksheet: sheet2, Att. II, folder "Glass Valid".

Table 24. Comparison of Experimentally Observed and Predicted Precipitates in Reaction of West Valley Glass with J-13 Well Water at 90°C

Experimentally Observed Precipitates	Predicted Precipitates	Amount of Glass Dissolved (g/liter)			
		10	1.30E+00	1.59E-01	1.17E-02
		Predicted Mass of Precipitates (moles of solids/liter of solution)			
<b>Smectites</b>	Nontronite	7.85E-03	1.02E-03	6.51E-05	0.00E+00
	Saponite-Na				
<b>Mg-silicates</b>	Talc ( $Mg_3Si_4O_{10}(OH)_2$ )	1.13E-03	1.70E-04		6.18E-06
<b>Fe-bearing phases:</b> Fe-silicates, Ferrihydrite, maghemite, magnetite, Fe-oxide or hydroxide	Hematite				
	Co <sub>2</sub> SiO <sub>4</sub>	1.39E-07			
	Spinel-Co		1.20E-08	1.46E-09	8.98E-11
<b>Ni-bearing phases:</b> Ni-silicates, Ni-Fe silicates	Bunsenite (NiO)	4.60E-04	5.92E-05	6.59E-06	0.00E+00
	eucryptite (LiAlSiO <sub>4</sub> )	Petalite (LiAlSi <sub>4</sub> O <sub>10</sub> )	3.08E-03	4.01E-04	
<b>Zeolites:</b> Garronite, analcime / pollucite, thomsonite, Na-zeolite	Mesolite			2.70E-05	
<b>Ca-bearing silicates:</b> Gyrolite, tobermorite, truscottite/reyerite, Ca-silicates	Saponite-Ca			4.39E-05	2.14E-05
	Andradite (Ca <sub>3</sub> Fe <sub>2</sub> O <sub>12</sub> Si <sub>3</sub> )			5.97E-05	9.24E-06
<b>U-bearing minerals:</b> weeksite Ca-U silicate	Weeksite-Na	1.05E-04			
	CaUO <sub>4</sub>		2.04E-05	3.37E-06	2.47E-07
	Boltwoodit		5.61E-06		
Ba-bearing phase	Witherite (BaCO <sub>3</sub> )	3.60E-05	4.68E-06	5.67E-07	3.51E-08
Zn-Si phase – willemite					
borosilicates					
aragonite (CaCO <sub>3</sub> )	Calcite				2.44E-04
	Strontianite	2.67E-05	3.56E-06	2.90E-07	
arsenate apatite (Ca(P,As)O <sub>4</sub> - OH, F, or Cl)	Hydroxylapatite	1.64E-04			
	Fluorapatite	1.16E-04	8.67E-05	1.92E-05	1.41E-06
	EuPO <sub>4</sub> ·10H <sub>2</sub> O	8.11E-07	1.06E-07	6.56E-09	
	AmPO <sub>4</sub> (am)	6.85E-07	8.91E-08		
	MnO <sub>2</sub> (gamma)	1.54E-03	2.00E-04	2.45E-05	1.80E-06
	Cassiterite (SnO <sub>2</sub> )	2.09E-06	1.17E-07		
	NpO <sub>2</sub>	3.35E-06	4.13E-07	3.24E-08	
	Thorianite (ThO <sub>2</sub> )	1.39E-03	1.81E-04	2.21E-05	1.63E-06
	AmO <sub>2</sub>			1.09E-08	7.65E-10
	PuO <sub>2</sub>	4.98E-08	9.98E-08		
	SiO <sub>2</sub> (am)	7.05E-03			
	RuO <sub>2</sub>	5.81E-05	7.51E-06	8.68E-07	1.07E-08

Source: Bruton and Shaw 1988 and FILE: case2\_wv\_calcul.xls; worksheet: sheet2, Att. II, folder "Glass Valid".

The PHREEQC database, used in the glass degradation runs was created using the software “transl” (Section 3.1.3). For the current application, it was necessary to run transl to generate a PHREEQC database with thermodynamic data at 90°C. The files associated with running transl are located in Attachment II, folder “transl”. The resulting database, phreeqc.ymp\_90, is located in Attachment II, folder “Glass Valid”. The PHREEQC input files (\*.dat), the output files (\*.out and \*.xls), and the files in which the glass degradation results were calculated (\*.calcul.xls) are provided in Attachment II, folder “Glass Valid”.

### **6.8.2 Description of the Fracture System**

An important feature of the External Accumulation Model is the description of the fracture system in the vicinity of the repository. Running PHREEQC provides the quantity of fissile material that precipitates; but, the description of the fractures provides the geometry in which it precipitates, which is very important for criticality calculations. The maximum accumulation density of material depends primarily on fracture porosity (volume of voids per volume of rock), which is a combination of fracture aperture, and fracture intensity (total length of fractures per volume of rock). However, the fracture porosity itself is not sufficient to characterize the potential for accumulation of a fracture system. The fracture aperture is also important because it controls both the flow through the fracture and the potential plugging of the system. Other features contributing to the void space such as lithophysae are also investigated.

All of the important features that describe the fracture system at the repository (porosity, fracture intensity, fracture aperture, lithophysae occurrences) have been characterized based on field measurements made at the repository itself. The details are provided in BSC 20011. In order to be conservative, higher values of fracture intensity, aperture, and porosity than were measured in the field are also used in the calculations.

### **6.8.3 Evaluation of Mechanisms for Fissile Accumulation**

Following is a list of major mechanisms for accumulation of materials in the UZ:

- Microbial Communities
- Reducing zone
- Colloidal filtering
- Diffusion and adsorption

Although all these mechanisms are viable, only dilution and mixing of WP effluent with resident water could cause a rapid decrease in the pH leading to significant precipitation of fissile materials. In order to assess the risk of external criticality the selected mechanisms should be able to support significant precipitation of fissile materials in a relatively small volume of the host rock.

#### **6.8.3.1 Bio-accumulation**

The accumulation of biomaterials, particularly bacteria and fungi, could enhance accumulation of fissile materials in two ways. First, the bodies of the bacteria or fungi could serve as colloidal particles, and might transport U and Pu into the tuff. Second, the bodies could serve as

reductants, either directly absorbing actinides, or causing precipitation via reduction from the VI to IV oxidation state. To determine the impact of bio-accumulation, it is necessary to estimate the amount of biomass that may be present in the tuff walls of the drift, particularly in the conical volume described in Assumption 5.8.

The microbial communities model was developed to predict total biomass produced from degradation of the EBS and contributions from the natural environment. The model was designed based on constraints of nutrient availability, chemical energy released from oxidation-reduction reactions, pH, temperature, and relative humidity on microbial growth. Although during the high temperature and high radiation period microbial communities will not be viable in the drift, they will be reintroduced as microbial growth factors become more favorable. The results of the microbial communities model show that during the first 10,000 years a maximum of eight grams of microbial mass per linear meter of repository will be produced annually from the materials used in the construction of the ground support and the WP (CRWMS M&O 2000i, page 124). This amounts to production of a maximum of 14.96 grams of microbial mass per year from 7145.5 kg of material (mass was calculated from a 21-PWR WP in non-lithophysal host rock) (CRWMS M&O 2000i, page 124). Based on this small mass or abundance of microbes being generated, effects on the bulk chemistry in the drift are expected to be negligible. However, the effects and impact of other aspects of biological activities such as production of gaseous products due to respiration, colloidal transport, and microbially-induced corrosion on longevity of the WP components was not addressed.

The microbial communities could influence fate and transport of radionuclides by increasing the quantity of CO<sub>2</sub> gas (CRWMS M&O 2000i). Formation of CO<sub>2</sub> gas could influence waste dissolution due to changes in aqueous carbonate speciation and pH. The External Accumulation Model has been run using values of CO<sub>2</sub> partial pressure equal to 10<sup>-3</sup> and 10<sup>-2</sup> bar, which are conditions likely to be found at the repository. The results indicate that higher values of CO<sub>2</sub> partial pressure are less conservative, since less accumulation occurs (BSC 20011, Section 6.5.3). Due to the small amount of microbes produced and as mentioned in the colloidal transport section (6.8.3.3), this mode of radionuclide transport compared to the amount of solid forming from dilution/mixing would be negligible for criticality evaluation and less conservative.

### 6.8.3.2 Reducing Zone

A study of oil and gas exploration near Yucca Mountain (Grow et al. 1994) concluded that Cambrian through Triassic rocks in the vicinity of the mountain experienced temperatures that were too high to allow oil generation. Geochemical samples from Tertiary lacustrine deposits do show potential for gas production; however, because of extensive late Tertiary faulting in the area, the seal might not be adequate to retain gases. The same study concludes that oil and gas resources beneath Yucca Mountain would most likely be less than 1.0 million barrel of oil, which is very low for oil production (Grow et al. 1994). The source regions for these reduced materials (if they exist at all) are well below the current repository level.

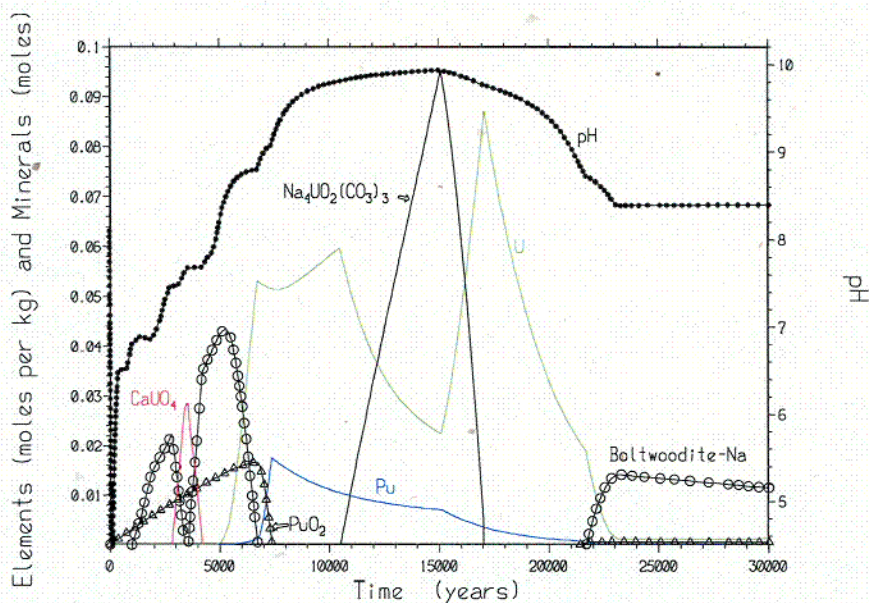
Overall, the existence of hydrocarbons could contribute to formation of a reducing zone that influences precipitation and mobility of ions. Adler (1974) attributes formation of uranium ore in sandstone and other sediments to chemical reduction. Uranium's mobility depends on the solubility of the U(VI) species in groundwater, and precipitation of the metal as ore is governed almost exclusively in sandstone by chemical reduction. However, such ore deposits form below

the water table, where gases diffuse more slowly and advective gas mixing is minimal, allowing the buildup of H<sub>2</sub>S and methane from organic decomposition. It is extremely unlikely that similar reducing conditions could form in the UZ. Since this model is developed for precipitation in the UZ, the possibility of reducing zones, below the water table, is not considered.

### 6.8.3.3 Colloidal transport and filtering

Colloids may contribute to accumulation if they are formed within the WP, carry a significant radionuclide load, and subsequently are filtered out in the rock below the drift. The sources for generation of colloids within the Yucca Mountain repository are degradation of the (1) waste form, (2) steel within the WP, and (3) concrete components in the drift. In general, colloidal concentration is influenced by factors such as ionic strength, temperature, pH, solubility, and size of the particle (CRWMS M&O 2001c, Section 6.1.1.1).

In order to quantify the aspects of colloidal transport that affect criticality, one needs to examine chemical conditions that were selected to maximize dissolution of fissile materials in water flowing through the failed WP. For example in BSC 2001c an early precipitation of Pu as PuO<sub>2</sub> was followed by rapid dissolution (about 14,000 years) of PuO<sub>2</sub> in the WP (Figure 13).



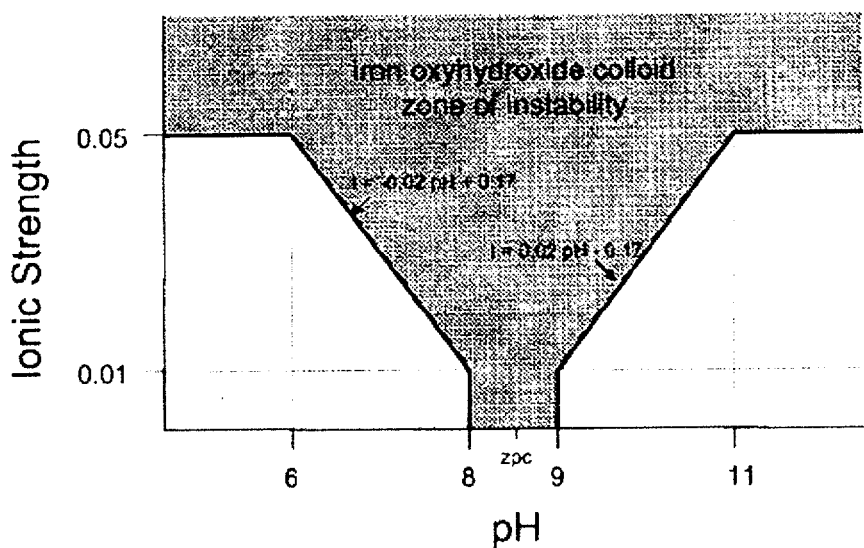
Source: BSC 2001c, Figure 6-26

Figure 14. Case s5: Minerals and Aqueous U and Pu

During this period pH increased from 8.5 to 9.5 and solution ionic strength had values up to 3.0. Actually, during dissolution of Pu, the ionic strength of the aqueous system was always higher than 0.05 (Figure 7) Figure 15 shows that iron-(hydro)oxide colloids are unstable in solutions with ionic strength above 0.05. Smectite colloids, that form from degrading HLW glass and SNF, are also unstable in solutions with ionic strengths above 0.05 (CRWMS M&O 2001c, Figure 12).

In a more recent study (CRWMS M&O 2001c, Section 6.1.1.1), the concentration limit of Pu in the SNF leach tests (as both colloids and aqueous species) was found to be close to the solubility limit of Pu in J-13 water. The study analyzed colloid generation from SNF for over 4 years. The solubility limit of Pu in J-13 was determined to be about  $1 \times 10^{-7}$  moles/L. Given the concentrations from the SNF leach test, and the highest drip rate used for this study (15 L/y), no more than  $1.5 \cdot 10^{-2}$  moles of Pu would be deposited as colloids in  $10^4$  years.

The combination of extreme ionic strength, pH, drip rate and limited solubility of radionuclides will not produce enough colloidal particles to influence external criticality quantitatively. Thus while colloidal transport could be an important mechanism for performance assessment dose calculations, colloids probably do not produce sufficient accumulation to be considered for criticality calculations.



NOTE: Schematic representation (used in abstraction) of iron-(hydr)oxide colloidal stability as a function of ionic strength and pH. At and near the ZPC colloids are unstable, even at low ionic strengths. At higher ionic strengths the pH range at which colloids are unstable is greater. Above ionic strength 0.05 colloids are assumed to be unstable for all pH (Abstracted from Liang and Morgan 1990, Figure 1).

Source: CRWMS M&O 2001c, Figure 11, p. 53

Figure 15. Schematic Representation of Iron-(Hydro)oxide Colloid Stability as a Function of pH and Ionic Strength

### 6.8.3.4 Sorption

At first glance, sorption might appear to be an effective mechanism for accumulating Pu. Formal  $K_d$ 's (Table 25) for Pu may be as high as 200 mL/g on vitric tuff; thus a solution containing  $10^{-4}$  M Pu ( $\sim 2.4 \cdot 10^{-5}$  g/mL), could yield  $\sim 4.8$  g of sorbed Pu / kg of rock. However, the  $K_d$ 's are typically obtained from experiments with much lower actinide concentrations and masses. In reality, sorption gives way to precipitation when the solution exceeds the solubility limits, and the amount of mass that can be deposited by sorption is less than the amount that can be deposited by simple precipitation of an actinide-rich phase (e.g., Langmuir (1997, Figure 10.7, p. 355)).

Azaroual and Fouillac (1997) compared the experimental results for distilled water-granite interaction at 180°C and 14 bars with the results of numerical simulation (EQ3/6 with fluid centered flow-through calculation mode). They confirmed that surface area is the most important factor in comparison of results from geochemical modeling (EQ3/6) versus experimental observations. They found that the effective surface area of a mineral is much smaller than the measured BET surface area.

Sorption requires a large surface area to be an effective means of accumulation; once the surface coverage exceeds  $\sim$ one monolayer of actinide species in thickness, the accumulation mechanism is effectively precipitation, not sorption. The surface areas of the fractures themselves are small, but if the matrix were involved (with BET surface areas  $\sim 1$  m<sup>2</sup>/g [Oversby 1985]), sorption might become significant. However, <sup>36</sup>Cl evidence in the *Yucca Mountain Science and Engineering Report* (DOE 2001, Section 4.2.1.2.9) suggests that there is very little interaction between the fractures and matrix. A study of actinide diffusion in tuff (McKeegan et al. 1989) suggests an effective diffusion coefficient of actinides, into the matrix, of only  $10^{-13}$  cm<sup>2</sup>/s. If the effective sorption distance is taken as (time-diffusion coefficient)<sup>(1/2)</sup>,  $10^5$  years would yield a diffusion zone only  $\sim 0.6$  cm thick. Thus sorption in the matrix is not considered to be an effective accumulation mechanism.

Table 25. Sorption Coefficient Distributions for UZ Unit

Element	Rock type	Min $K_d$ (mL/g)	Max $K_d$ (mL/g)
Pu	Devitrified	5	70
	Vitric	30	200
	Zeolitic	30	200
	Iron Oxide	1000	5000
U	Devitrified	0	2
	Vitric	0	1
	Zeolitic	0	10
	Iron Oxide	100	1000

Source: Adapted from CRWMS M&O 2000h, Table 3.11-1, p. 236

## 7. CONCLUSIONS

The External Accumulation Model predicts accumulation of fissile materials in fractures and lithophysae in the rock beneath the drift containing a degrading waste package. The model begins with a source term generated by EQ6. PHREEQC simulates the transport of the effluent water downward through the fractured tuff. During transport, resident water mixes with the effluent water, lowering the pH and causing precipitation of U and Pu minerals. The accumulation zone is assumed to have a cone shape, with the actual dimensions of the cone determined by the fracture characteristics, such as porosity, and by the local infiltration rate. The model can be used to determine the external accumulation for source terms coming from degrading waste packages that contain Pu-ceramic (the example for this report), DOE SNF, and commercial SNF. The model does not consider accumulation in the invert or in the pore matrix of the rock.

The model validation includes comparisons with experimental and field data. PHREEQC simulations of glass degradation were compared to experimental results and found to match favorably (Section 6.8.1). The description of the fracture system was developed using field data collected from the proposed repository site (Section 6.3). Data important to calculating accumulation density (fracture porosity, intensity, and aperture) were extrapolated to higher values than found in the field to enhance the conditions for criticality. Selection of the inputs and the range of parameters were based on the criteria of being the most conservative selection for external criticality risk calculations. The mechanism of mixing to cause accumulation proved to be quite effective in the example cases presented. The total accumulations calculated by the model for four example cases were compared to the quantity in the source term (Table 21). In case p52{rs}L241 for U and in case p52rLx41 for Pu, all of the material was predicted to precipitate in the fractures.

This document may be affected by technical product information that requires confirmation. Any changes to the document that may occur as a result of completing the confirmation activities will be reflected in subsequent revisions. The status of the technical product input information quality may be confirmed by review of the DIRS database.

## 8. INPUTS AND REFERENCES

### 8.1 DOCUMENTS CITED

Adler, H.H. 1974. "Concepts of Uranium-Ore Formation in Reducing Environments in Sandstones and Other Sediments." *Formation of Uranium Ore Deposits, Proceedings of a Symposium, Athens, Greece, 6-10 May 1974*. IAEA-SM-183/43. Pages 141-168. Vienna, Austria: International Atomic Energy Agency. TIC: 219174.

Azaroual, M. and Fouillac, C. 1997. "Experimental Study and Modelling of Granite-Distilled Water Interactions at 180 [degrees] C and 14 Bars." *Applied Geochemistry*, 12, 55-73. Oxford, United Kingdom: Elsevier Science. TIC: 246576.

Bruton, C.J. and Shaw, H.F. 1988. "Geochemical Simulation of Reaction Between Spent Fuel Waste Form and J-13 Water at 25°C and 90°C." *Scientific Basis for Nuclear Waste Management XI, Symposium held November 30-December 3, 1987, Boston, Massachusetts*. Apted, M.J. and Westerman, R.E., eds. 112, 485-504. Pittsburgh, Pennsylvania: Materials Research Society. TIC: 203662.

BSC 2001a. *Software Code: Acc\_with\_Decay*. V1.0. PC Windows98. 10499-1.0-00.

BSC (Bechtel SAIC Company) 2001b. *Drift-Scale Coupled Processes (DST and THC Seepage) Models*. MDL-NBS-HS-000001 REV 01 ICN 01. Las Vegas, Nevada: Bechtel SAIC Company. ACC: MOL.20010418.0010.

BSC (Bechtel SAIC Company) 2001c. *EQ6 Calculation for Chemical Degradation of Pu-Ceramic Waste Packages: Effects Updated Waste Package Design and Rates*. CAL-EDC-MD-000009 REV 00. Las Vegas, Nevada: Bechtel SAIC Company. ACC: MOL.20010606.0284.

BSC (Bechtel SAIC Company) 2001d. *Technical Work Plan for: Waste Package Design Description for LA*. TWP-EBS-MD-000004 REV 01. Las Vegas, Nevada: Bechtel SAIC Company. ACC: MOL.20010702.0152.

BSC 2001e. *Software Code: transl*. V2.0. PC Windows98. 10251-2.0-00.

BSC 2001f. *Software Code: SeepageFlow\_macro*. V1.0. PC Windows98. 10497-1.0-00.

BSC (Bechtel SAIC Company) 2001g. *Software Management Report (SMR) for Excel Marco "Acc\_with\_Decay"*. SDN: 10499-SMR-1.0.00. Las Vegas, Nevada: Bechtel SAIC Company. ACC: MOL.20010702.0051.

BSC (Bechtel SAIC Company) 2001h. *Site Recommendation Subsurface Layout*. ANL-SFS-MG-000001 REV 00 ICN 02. Las Vegas, Nevada: Bechtel SAIC Company. ACC: MOL.20010411.0131.

BSC (Bechtel SAIC Company) 2001i. *FY 01 Supplemental Science and Performance Analyses, Volume 1: Scientific Bases and Analyses*. TDR-MGR-MD-000007 REV 00 ICN 01. Las Vegas, Nevada: Bechtel SAIC Company. ACC: MOL.20010801.0404.

BSC (Bechtel SAIC Company) 2001j. *Software Code: fracspc2*. V1.0. HP. 10554-1.0-00.

BSC (Bechtel SAIC Company) 2001k. *Description of Fracture Systems for External Criticality Reports*. ANL-NBS-GS-000010 REV 00. Las Vegas, Nevada: Bechtel SAIC Company. Submit to RPC URN-0931

BSC (Bechtel SAIC Company) 2001l. *External Accumulation of Fissile Material from Waste Packages Containing Plutonium Ceramics*. CAL-EDC-GS-000004 REV 00. Las Vegas, Nevada: Bechtel SAIC Company. ACC: TBD. URN-0932

CRWMS M&O 1998. *Software Code: EQ3/6*. V7.2b. LLNL: UCRL-MA-110662.

CRWMS M&O 1999a. *Software User's Manual (UM) for PHREEQC Version 2.0 (beta)*. SDN: 10068-UM-2.0-00. Las Vegas, Nevada: CRWMS M&O. ACC: MOL.20000114.0118.

CRWMS M&O 1999b. *Software Validation Test Report (VTR) for PHREEQC Version 2.0 (beta)*. SDN: 10068-VTR-2.0-00. Las Vegas, Nevada: CRWMS M&O. ACC: MOL.20000113.0408.

CRWMS M&O 1999c. *Software Code: PHREEQC*. V2.0. PC. 10068-2.0-00.

CRWMS M&O 1999d. *User's Manual for EQ6 V7.2bLV*. SDN: 10075-ITP-7.2bLV-00. Las Vegas, Nevada: CRWMS M&O. ACC: MOL.20000126.0158.

CRWMS M&O 1999e. *Software Code: EQ6, Version 7.2bLV*. V7.2bLV. 10075-7.2bLV-00.

CRWMS M&O 2000a. *Total System Performance Assessment for the Site Recommendation*. TDR-WIS-PA-000001 REV 00 ICN 01. Las Vegas, Nevada: CRWMS M&O. ACC: MOL.20001220.0045.

CRWMS M&O 2000b. *Analysis of Base-Case Particle Tracking Results of the Base-Case Flow Fields (ID: U0160)*. ANL-NBS-HS-000024 REV 00. Las Vegas, Nevada: CRWMS M&O. ACC: MOL.20000207.0690.

CRWMS M&O 2000c. *Seepage Model for PA Including Drift Collapse*. MDL-NBS-HS-000002 REV 01. Las Vegas, Nevada: CRWMS M&O. ACC: MOL.20010221.0147.

CRWMS M&O 2000d. *Design Analysis for UCF Waste Packages*. ANL-UDC-MD-000001 REV 00. Las Vegas, Nevada: CRWMS M&O. ACC: MOL.20000526.0336.

CRWMS M&O 2000e. *Validation Test Report for EQ6 V7.2bLV*. SDN: 10075-VTR-7.2bLV-00. Las Vegas, Nevada: CRWMS M&O. ACC: MOL.20000124.0135.

CRWMS M&O 2000f. *Far-Field Accumulation of Fissile Material from Waste Packages Containing Plutonium Disposition Waste Forms*. CAL-EDC-GS-000002 REV 00. Las Vegas, Nevada: CRWMS M&O. ACC: MOL.20000929.0219.

CRWMS M&O 2000g. *In-Drift Accumulation of Fissile Material from Waste Packages Containing Plutonium Disposition Waste Forms*. CAL-EDC-GS-000001 REV 00. Las Vegas, Nevada: CRWMS M&O. ACC: MOL.20001016.0008.

CRWMS M&O 2000h. *Unsaturated Zone Flow and Transport Model Process Model Report*. TDR-NBS-HS-000002 REV 00 ICN 02. Las Vegas, Nevada: CRWMS M&O. ACC: MOL.20000831.0280.

CRWMS M&O 2000i. *In-Drift Microbial Communities*. ANL-EBS-MD-000038 REV 00 ICN 01. Las Vegas, Nevada: CRWMS M&O. ACC: MOL.20001213.0066.

CRWMS M&O 2001a. Not used.

CRWMS M&O 2001b. Not used.

CRWMS M&O 2001c. *Waste Form Colloid-Associated Concentrations Limits: Abstraction and Summary*. ANL-WIS-MD-000012 REV 00 ICN 01. Las Vegas, Nevada: CRWMS M&O. ACC: MOL.20010130.0002.

CRWMS M&O 2001d. *Abstraction of Drift Seepage*. ANL-NBS-MD-000005 REV 01. Las Vegas, Nevada: CRWMS M&O. ACC: MOL.20010309.0019.

Daveler, S.A. and Wolery, T.J. 1992. *EQPT, A Data File Preprocessor for the EQ3/6 Software Package: User's Guide and Related Documentation (Version 7.0)*. UCRL-MA-110662 PT II. Livermore, California: Lawrence Livermore National Laboratory. TIC: 205240.

DOE (U.S. Department of Energy) 1998. *Total System Performance Assessment*. Volume 3 of *Viability Assessment of a Repository at Yucca Mountain*. DOE/RW-0508. Washington, D.C.: U.S. Department of Energy, Office of Civilian Radioactive Waste Management. ACC: MOL.19981007.0030.

DOE (U.S. Department of Energy) 2000. *Quality Assurance Requirements and Description*. DOE/RW-0333P, Rev. 10. Washington, D.C.: U.S. Department of Energy, Office of Civilian Radioactive Waste Management. ACC: MOL.20000427.0422.

DOE (U.S. Department of Energy) 2001. *Yucca Mountain Science and Engineering Report*. DOE/RW-0539. [Washington, D.C.]: U.S. Department of Energy, Office of Civilian Radioactive Waste Management. ACC: MOL.20010524.0272.

Domenico, P.A. and Schwartz, F.W. 1990. *Physical and Chemical Hydrogeology*. New York, New York: John Wiley & Sons. TIC: 234782.

Grow, J.A.; Barker, C.E.; and Harris, A.G. 1994. "Oil and Gas Exploration Near Yucca Mountain, Southern Nevada." High Level Radioactive Waste Management, Proceedings of the Fifth Annual International Conference, Las Vegas, Nevada, May 22-26, 1994. 3, 1298-1315. La Grange Park, Illinois: American Nuclear Society. TIC: **210984**.

Langmuir, D. 1997. *Aqueous Environmental Geochemistry*. Upper Saddle River, New Jersey: Prentice Hall. TIC: 237107.

McClure, J.A. and Alsaed, A.A. 2001. *External Criticality Risk of Immobilized Plutonium Waste Form in a Geologic Repository*. TDR-EBS-MD-000019 REV 00. Las Vegas, Nevada: Bechtel SAIC Company. ACC: MOL.20010314.0001.

McKeegan, K.D.; Phinney, D.; Oversby, V.M.; Brink, M.B.; and Smith, D.K. 1989. "Uranium Transport in Topopah Spring Tuff: An Ion-Microscope Investigation." *Scientific Basis for Nuclear Waste Management XII, Symposium held October 10-13, 1988, Berlin, Germany*. Lutze, W. and Ewing, R.C., eds.. 127, 813-821. Pittsburgh, Pennsylvania: Materials Research Society. TIC: 203660.

Oversby, V.M. 1985. Results of BET Surface Area Measurements for the Topopah Spring Tuff Sample. Letter from V.M. Oversby (LLNL) to Dr. D. Kelmers (ORNL), August 28, 1985, WP: 123-85, with enclosures. ACC: MOL.19980210.0935.

Parrington, J.R.; Knox, H.D.; Breneman, S.L.; Baum, E.M.; and Feiner, F. 1996. *Nuclides and Isotopes, Chart of the Nuclides*. 15th Edition. San Jose, California: General Electric Company and KAPL, Inc. TIC: 233705.

Philip, J.R.; Knight, J.H.; and Waechter, R.T. 1989. "Unsaturated Seepage and Subterranean Holes: Conspectus, and Exclusion Problem for Circular Cylindrical Cavities." *Water Resources Research*, 25, (1), 16-28. Washington, D.C.: American Geophysical Union. TIC: 239117.

## 8.2 CODES, STANDARDS, REGULATIONS, AND PROCEDURES

AP-2.21Q, Rev. 1, ICN 0, BSCN 001. *Quality Determinations and Planning for Scientific, Engineering, and Regulatory Compliance Activities*. Washington, D.C.: U.S. Department of Energy, Office of Civilian Radioactive Waste Management. ACC: MOL.20010212.0018.

AP-3.10Q, Rev. 2, ICN 4. *Analyses and Models*. Washington, D.C.: U.S. Department of Energy, Office of Civilian Radioactive Waste Management. ACC: MOL.20010405.0009.

AP-SI.1Q, Rev. 3, ICN 1, ECN 1. *Software Management*. Washington, D.C.: U.S. Department of Energy, Office of Civilian Radioactive Waste Management. ACC: MOL.20010705.0239.

AP-SV.1Q, Rev. 0, ICN 2. *Control of the Electronic Management of Information*. Washington, D.C.: U.S. Department of Energy, Office of Civilian Radioactive Waste Management. ACC: MOL.20000831.0065.

## 8.3 SOURCE DATA

GS990408314224.001. Detailed Line Survey Data for Stations 00+00.89 to 14+95.18, ECRB Cross Drift. Submittal date: 09/09/1999.

GS990408314224.002. Detailed Line Survey Data for Stations 15+00.85 to 26+63.85, ECRB Cross Drift. Submittal date: 09/09/1999.

LB0011DSTTHCR1.001. Tables Showing Geochemical and Drift-Scale Seepage Model Data Which are Presented in AMR U0110/N0120, "Drift-Scale Coupled Processes (DST and THC Seepage) Models REV01". Submittal date: 12/19/2000.

LB0101DSTTHCR1.001. Pore Water Composition and CO<sub>2</sub> Partial Pressure Input to Thermal-Hydrological-Chemical (THC) Simulations: Table 3 of AMR N0120/U0110 Rev01, "Drift-Scale Coupled Processes (Drift-Scale Test and THC Seepage) Models". Submittal date: 01/26/2001.

LB990861233129.001. Drift Scale Calibrated 1-D Property Set, FY99. Submittal date: 08/06/1999.

LB990861233129.002. Drift Scale Calibrated 1-D Property Set, FY99. Submittal date: 08/06/1999.

LB990861233129.003. Drift Scale Calibrated 1-D Property Set, FY99. Submittal date: 08/06/1999.

LB991200DSTTHC.002. Model Input and Output Files, Excel Spreadsheets and Resultant Figures Which are Presented in AMR N0120/U0110, "Drift-Scale Coupled Processes (Drift-Scale Test and THC Seepage) Models". Submittal date: 03/11/2000.

MO0006J13WTRCM.000. Recommended Mean Values of Major Constituents in J-13 Well Water. Submittal date: 06/07/2000.

MO0009THERMODYN.001. Input Transmittal for Thermodynamic Data Input Files for Geochemical Calculations. Submittal date: 09/20/2000.

MO0102SPALIT10.001. Lithophysae Porosity and Diameter Distributions. Submittal date: 02/20/2001.

MO0105SPATHE04.005. Thermodynamic Data Input File in the PHREEQC Format for Geochemical Calculations. Submittal date: 05/30/2001.

MO0109SPAFIE10.006. Fracture Intensity for External Actinide Accumulation. Submittal date: 09/17/01.

SN0012T0511599.003. Results from Abstraction of Drift Seepage, Rev. 01. Submittal date: 12/20/2000.

## ATTACHMENT I. LIST OF FILES ON ATTACHED COMPACT DISKS (CDS)

This attachment contains the Microsoft-DOS directory for files placed on CD. The files are of these types:

- 1) Excel files (extension = xls), called out in the text and tables and contained on Disk 1, in folder "Excel".
- 2) PHREEQC input files (extensions = dat), can be read as a text file.
- 3) PHREEQC output files (extension = out), can be read as a text file.

Below are listed the contents of the files within the electronic attachment:

The first column is the DOS file name.

The second column lists <DIR> if it is a folder or gives the file size (bytes) if it is a file.

The third and fourth columns are the date and time of the last update.

The fifth column is the file name.

### Directory of Disk (extacc)

DOS FILE NAME	SIZE (IF A FILE)	DATE	TIME	FILE NAME
10K	<DIR>	08-07-01	11:56a	10k
15K	<DIR>	08-07-01	11:25a	15k
18K	<DIR>	08-07-01	11:28a	18k
21K	<DIR>	08-07-01	11:31a	21k
23K	<DIR>	08-07-01	11:35a	23k
5	2K <DIR>	08-07-01	11:39a	5.2k
6	7K <DIR>	08-07-01	11:42a	6.7k
7	4K <DIR>	08-07-01	11:46a	7.4k
8	5K <DIR>	08-07-01	11:49a	8.5k
GLASS~23	<DIR>	08-07-01	11:53a	Glass Valid
P52RL~26	XLS 3,193,344	07-12-01	2:36p	P52rLx41_CritIn.xls
P52RL~38	XLS 1,215,488	01-31-01	3:02p	P52rLx41_CritIn_lith.xls
P52RL~44	XLS 1,783,296	01-25-01	4:57p	
P52rLx41_J13_Base_Cases_SUMMARY.xls				
P52RL~50	XLS 4,621,312	07-25-01	2:58p	P52rLx41_SourceTerm.xls
PHREEQC	DAT 223,794	09-25-00	1:07p	phreeqc.dat
TRANSL	<DIR>	08-07-01	11:54a	transl
5 file(s)		11,037,234 bytes		

### Directory of F:\10k

.	<DIR>	09-25-00	1:07p	.
..	<DIR>	09-25-00	1:07p	..
P52RLX~6	DAT 9,441	01-04-01	2:34p	P52rLx41_20_10_10k.dat
P52RLX~8	OUT 148,859	01-05-01	5:16p	P52rLx41_20_10_10k.out
P52RL~12	XLS 4,826,400	01-05-01	5:16p	P52rLx41_20_10_10k.xls
P52RL~28	XLS 5,252,608	01-07-01	4:11p	P52rLx41_20_10_10k_calc.xls
P52RL~44	DAT 224,009	01-08-01	1:15p	P52rLx41_mix_10k.dat
P52RL~48	XLS 4,553,620	01-08-01	2:47p	P52rLx41_mix_10k.xls
P52RL~62	XLS 8,946,688	01-09-01	10:51a	P52rLx41_mix_10k_calcul.xls
7 file(s)		23,961,625 bytes		

### Directory of F:\15k

.	<DIR>	01-09-01	10:51a	.
---	-------	----------	--------	---

```

..                <DIR>                01-09-01 10:51a ..
P52RLX~6 DAT      9,439 01-04-01 2:32p P52rLx41_20_10_15k.dat
P52RLX~8 OUT      37,596 01-05-01 11:38a P52rLx41_20_10_15k.out
P52RL~10 XLS     4,826,400 01-05-01 11:38a P52rLx41_20_10_15k.xls
P52RL~26 XLS     5,226,496 01-07-01 4:34p P52rLx41_20_10_15k_calc.xls
P52RL~44 DAT      224,016 01-08-01 1:00p P52rLx41_mix_15k.dat
P52RL~46 XLS     4,553,620 01-08-01 2:26p P52rLx41_mix_15k.xls
P52RL~62 XLS     6,007,296 01-09-01 12:15a P52rLx41_mix_15k_calcul.xls
7 file(s)        20,884,863 bytes

```

Directory of F:\18k

```

.                <DIR>                01-09-01 12:15a .
..               <DIR>                01-09-01 12:15a ..
P52RLX~6 DAT      9,442 01-04-01 2:43p P52rLx41_20_10_18k.dat
P52RLX~8 OUT     46,843 01-05-01 3:18p P52rLx41_20_10_18k.out
P52RL~10 XLS     4,826,400 01-05-01 3:18p P52rLx41_20_10_18k.xls
P52RL~26 XLS     5,250,560 01-07-01 4:45p P52rLx41_20_10_18k_calc.xls
P52RL~44 DAT     224,009 01-08-01 1:02p P52rLx41_mix_18k.dat
P52RL~46 XLS     4,553,620 01-08-01 3:06p P52rLx41_mix_18k.xls
P52RL~62 XLS     6,114,304 01-09-01 12:08a P52rLx41_mix_18k_calcul.xls
7 file(s)        21,025,178 bytes

```

Directory of F:\21k

```

.                <DIR>                01-09-01 12:08a .
..               <DIR>                01-09-01 12:08a ..
P52RLX~6 DAT      9,440 01-04-01 2:51p P52rLx41_20_10_21k.dat
P52RLX~8 OUT     53,412 01-05-01 6:51p P52rLx41_20_10_21k.out
P52RL~10 XLS     4,826,400 01-05-01 6:51p P52rLx41_20_10_21k.xls
P52RL~26 XLS     5,254,144 01-07-01 4:57p P52rLx41_20_10_21k_calc.xls
P52RL~42 DAT     224,009 01-08-01 1:03p P52rLx41_mix_21k.dat
P52RL~46 XLS     4,553,620 01-08-01 2:57p P52rLx41_mix_21k.xls
P52RL~60 XLS     9,353,216 01-09-01 10:37a P52rLx41_mix_21k_calcul.xls
7 file(s)        24,274,241 bytes

```

Directory of F:\23k

```

.                <DIR>                01-09-01 10:37a .
..               <DIR>                01-09-01 10:37a ..
P52RLX~6 DAT      9,476 01-09-01 11:06a P52rLx41_20_10_23k.dat
P52RLX~8 OUT     229,089 01-09-01 8:55p P52rLx41_20_10_23k.out
P52RL~10 XLS     4,826,400 01-09-01 8:55p P52rLx41_20_10_23k.xls
P52RL~26 XLS     5,241,856 01-10-01 11:07a P52rLx41_20_10_23k_cal.xls
P52RL~44 DAT     223,985 01-08-01 5:48p P52rLx41_mix_23k.dat
P52RL~46 XLS     4,553,620 01-08-01 6:59p P52rLx41_mix_23k.xls
P52RL~62 XLS     9,555,456 01-09-01 10:38a P52rLx41_mix_23k_calcul.xls
7 file(s)        24,639,882 bytes

```

Directory of F:\5.2k

```

.                <DIR>                01-09-01 10:38a .
..               <DIR>                01-09-01 10:38a ..
P52RLX~6 DAT      9,503 01-09-01 11:12a P52rLx41_20_10_5.2k.dat
P52RLX~8 XLS     4,826,400 01-10-01 12:29a P52rLx41_20_10_5.2k.xls
P52RL~24 XLS     5,242,368 01-10-01 10:45a P52rLx41_20_10_5.2k_calc.xls
P52RL~42 OUT     284,692 01-10-01 12:29a P52rLx41_20_10_5.out

```

P52RL~44	DAT	224,010	01-08-01	5:48p	P52rLx41_mix_5.2k.dat
P52RL~48	XLS	4,553,620	01-08-01	6:55p	P52rLx41_mix_5.2k.xls
P52RL~62	XLS	9,342,464	01-09-01	10:40a	P52rLx41_mix_5.2k_calcul.xls
		7 file(s)	24,483,057 bytes		

Directory of F:\6.7k

.	<DIR>		01-09-01	10:40a	.
..	<DIR>		01-09-01	10:40a	..
P52RLX~6	DAT	9,443	01-04-01	2:36p	P52rLx41_20_10_6.7k.dat
P52RLX~8	OUT	78,725	01-05-01	7:04p	P52rLx41_20_10_6.7k.out
P52RL~10	XLS	4,826,400	01-05-01	7:04p	P52rLx41_20_10_6.7k.xls
P52RL~26	XLS	5,252,096	01-07-01	3:37p	P52rLx41_20_10_6.7k_calc.xls
P52RL~44	DAT	224,010	01-08-01	1:14p	P52rLx41_mix_6.7k.dat
P52RL~46	XLS	4,553,620	01-08-01	2:37p	P52rLx41_mix_6.7k.xls
P52RL~62	XLS	9,346,048	01-09-01	10:43a	P52rLx41_mix_6.7k_calcul.xls
		7 file(s)	24,290,342 bytes		

Directory of F:\7.4k

.	<DIR>		01-09-01	10:43a	.
..	<DIR>		01-09-01	10:43a	..
P52RLX~6	DAT	9,550	01-04-01	10:02a	P52rLx41_20_10_7.4k.dat
P52RLX~8	OUT	46,596	01-04-01	11:24a	P52rLx41_20_10_7.4k.out
P52RL~10	XLS	4,826,400	01-04-01	11:24a	P52rLx41_20_10_7.4k.xls
P52RL~28	XLS	5,261,312	01-07-01	4:01p	P52rLx41_20_10_7.4k_calc.xls
P52RL~44	DAT	224,048	01-08-01	9:58a	P52rLx41_mix_7.4k.dat
P52RL~48	XLS	4,553,620	01-08-01	10:46a	P52rLx41_mix_7.4k.xls
P52RL~62	XLS	6,208,000	01-10-01	4:07p	P52rLx41_mix_7.4k_calcul.xls
		7 file(s)	21,129,526 bytes		

Directory of F:\8.5k

.	<DIR>		01-10-01	4:07p	.
..	<DIR>		01-10-01	4:07p	..
P52RLX~6	OUT	41,886	01-25-01	4:52p	P52rLx41_20_10_8.5.out
P52RLX~8	DAT	9,325	01-25-01	11:34a	P52rLx41_20_10_8.5k.dat
P52RL~10	XLS	4,826,400	01-25-01	4:52p	P52rLx41_20_10_8.5k.xls
P52RL~26	XLS	5,258,752	01-25-01	4:00p	P52rLx41_20_10_8.5k_calc.xls
P52RL~44	DAT	223,790	01-09-01	1:29p	P52rLx41_mix_8.5k.dat
P52RL~46	XLS	4,549,518	01-09-01	2:22p	P52rLx41_mix_8.5k.xls
P52RL~62	XLS	6,359,552	01-09-01	4:39p	P52rLx41_mix_8.5k_calcul.xls
		7 file(s)	21,269,223 bytes		

Directory of F:\Glass Valid

.	<DIR>		01-09-01	4:39p	.
..	<DIR>		01-09-01	4:39p	..
CASE2_DF	DAT	6,991	06-19-01	1:09p	case2_df.dat
CASE2_DF	OUT	2,454,655	06-19-01	11:24a	case2_df.out
CASE2_DF	XLS	45,032	06-19-01	11:24a	case2_df.xls
CASE2~18	XLS	101,888	06-19-01	4:48p	case2_df_calcul.xls
CASE2_WV	DAT	7,011	06-19-01	1:09p	case2_wv.dat
CASE2_WV	OUT	3,392,827	06-19-01	1:11p	case2_wv.out
CASE2_WV	XLS	60,620	06-19-01	1:11p	case2_wv.xls
CASE2~36	XLS	170,496	06-19-01	4:47p	case2_wv_calcul.xls
PHREE~40	YMP	222,525	06-18-01	4:26p	phreeqc.ymp_90

9 file(s) 6,462,045 bytes

Directory of F:\transl

```
. <DIR> 06-18-01 4:26p .
.. <DIR> 06-18-01 4:26p ..
1_STAR~5 <DIR> 08-07-01 11:54a 1_Starting_Point
2_RUN~7 <DIR> 08-07-01 11:54a 2_Run_EQPT
3_CHEC~9 DAT <DIR> 08-07-01 11:55a 3_Check_watersys.dat
4_REM~11 <DIR> 08-07-01 11:55a 4_Remove_Org
5_RUN~13 <DIR> 08-07-01 11:55a 5_Run_transl
6_COR~15 <DIR> 08-07-01 11:55a 6_CorrectMANUALLY
0 file(s) 0 bytes
```

Directory of F:\transl\1\_Starting\_Point

```
. <DIR> 08-07-01 11:55a .
.. <DIR> 08-07-01 11:55a ..
DATA0Y~6 TXT 2,649,470 09-11-00 5:23p data0ymp_MO0009THRMODYN.001.txt
1 file(s) 2,649,470 bytes
```

Directory of F:\transl\2\_Run\_EQPT

```
. <DIR> 09-11-00 5:23p .
.. <DIR> 09-11-00 5:23p ..
DATA0 2,649,470 09-11-00 5:23p data0
DATA1 783,381 04-26-01 8:36a DATA1
DATA1F 1,044,199 04-26-01 8:36a DATA1F
OUTPUT 84,699 04-26-01 8:36a OUTPUT
SLIST 76,561 04-26-01 8:36a SLIST
5 file(s) 4,638,310 bytes
```

Directory of F:\transl\3\_Check\_watersys.dat

```
. <DIR> 04-26-01 8:36a .
.. <DIR> 04-26-01 8:36a ..
WATERSYS DAT 349 09-11-99 11:21a watersys.dat
1 file(s) 349 bytes
```

Directory of F:\transl\4\_Remove\_Org

```
. <DIR> 09-11-99 11:21a .
.. <DIR> 09-11-99 11:21a ..
DATA1F 1,044,199 04-26-01 8:36a DATA1F
DATA1F NUC 1,040,228 04-26-01 8:55a data1f.nuc
ORGSP~16 NUC 4,224 04-26-01 9:31a OrgSpecies.nuc
3 file(s) 2,088,651 bytes
```

Directory of F:\transl\5\_Run\_transl

```
. <DIR> 04-26-01 9:31a .
.. <DIR> 04-26-01 9:31a ..
DATA1F NUC 1,040,064 04-26-01 9:37a data1f.nuc
FIX_R~10 OUT 6,617 06-18-01 11:32a fix_redox.out
PHREE~12 NUC 222,186 06-18-01 11:32a phreeqc.nuc_90
S25 OUT 12,269 06-18-01 11:32a s25.out
TRANS~18 EXE 262,201 05-07-01 10:34p transl2.0.exe
```

WATERSYS DAT 349 09-11-99 11:21a watersys.dat  
6 file(s) 1,543,686 bytes

Directory of F:\transl\6\_CorrectMANUALLY

. <DIR> 09-11-99 11:21a .  
.. <DIR> 09-11-99 11:21a ..  
CHANGE~6 TXT 3,938 06-18-01 3:04p changemanually\_90.txt  
MANUAL~8 XLS 15,872 06-18-01 3:50p Manual\_Corrections.xls  
PHREE~10 YMP 222,525 06-18-01 4:26p phreeqc.ymp\_90  
3 file(s) 242,335 bytes

Total files listed:  
96 file(s) 234,620,017 bytes  
51 dir(s) 0 bytes free